In compliance with the
Canadian Privacy Legislation
some supporting forms
may have been removed from
this dissertation.

While these forms may be included
in the document page count,
their removal does not represent
any loss of content from the dissertation.

University of Alberta

NUMERICAL ANALYSIS OF BRINE TRANSPORT AT A POTASH MINE SITE IN SASKATCHEWAN

BY

M. DANIEL BORN

©

A thesis submitted to the Faculty of Graduate Studies and Research in partial fulfillment of the requirements for the degree of Master of Science

Department of Earth and Atmospheric Sciences

Edmonton, Alberta

Fall 2003

National Library of Canada
Acquisitions and Bibliographic Services
395 Wellington Street
Ottawa ON K1A 0N4
Canada

Bibliothèque nationale du Canada
Acquisitions et services bibliographiques
395, rue Wellington
Ottawa ON K1A 0N4
Canada

Your file Votre référence

Our file Notre référence

The author has granted a non-exclusive licence allowing the National Library of Canada to reproduce, loan, distribute or sell copies of this thesis in microform, paper or electronic formats.

L'auteur a accordé une licence non exclusive permettant à la Bibliothèque nationale du Canada de reproduire, prêter, distribuer ou vendre des copies de cette thèse sous la forme de microfiche/film, de reproduction sur papier ou sur format électronique.

The author retains ownership of the copyright in this thesis. Neither the thesis nor substantial extracts from it may be printed or otherwise reproduced without the author's permission.

L'auteur conserve la propriété du droit d'auteur qui protège cette thèse. Ni la thèse ni des extraits substantiels de celle-ci ne doivent être imprimés ou autrement reproduits sans son autorisation.

0-612-87724-8

Canada

University of Alberta

Library Release Form

Name of Author: **M. Daniel Born**

Title of Thesis: **Numerical analysis of brine transport at a potash mine site in Saskatchewan**

Degree: Master of Science

Year this Degree Granted: 2003

Permission is hereby granted to the University of Alberta Library to reproduce single copies of this thesis and to lend or sell such copies for private, scholarly or scientific purposes only.

The author reserves all other publication and other rights in association with the copyright in the thesis, and except as herein before provided, neither the thesis nor any substantial portion thereof may be printed or otherwise reproduced in any material form whatever without the author's prior written permission.

Oct 1, 2003

University of Alberta

Faculty of Graduate Studies and Research

The undersigned certify that they have read, and recommend to the Faculty of Graduate Studies and Research for acceptance, a thesis entitled Numerical Analysis of Brine Transport at a Potash Mine Site in Saskatchewan submitted by M. Daniel Born in partial fulfillment of the requirements for the degree of Master of Science.

Date: 30-Sept-2003

Abstract

Potash mining wastes include brine tailings and solid salt. These materials are stored on the land surface and represent a potential source of contamination to shallow groundwater resources in the vicinity of potash mine sites. This study analyzes brine migration at the Potash Corporation of Saskatchewan Patience Lake mine site, located 18 km east of Saskatoon.

A hydrogeological conceptual model for the mine site is developed using available data. The SUTRA code is used to simulate steady-state groundwater flow and transient, density-dependent groundwater flow and brine transport. 3D steady-state groundwater flow is calibrated to available data and detailed transient brine transport simulations are performed using a 2D cross section.

Base case simulation results indicate that vertical brine migration is enhanced by density-driven convection but brine does not reach the underlying Forestry Farm Aquifer after 72 years (2037). Sensitivity analyses suggest brine migration is sensitive to increased Patience Lake levels and Floral Sand permeability, which increases convective brine transport and impacts Forestry Farm Aquifer groundwater quality.

Dedication

For Rebecca and Leah

Preface

Thesis Format

This thesis is written in "paper" format, where each chapter is intended to function as a stand-alone manuscript. Chapter 1 provides background information and describes important hydrogeological considerations that directed the numerical modelling approach. The main body of the thesis, Chapters 2 and 3, consider brine transport from the potash mine site from different perspectives. Chapter 2 investigates hydrogeological uncertainties using an idealized 2D numerical model. Chapter 3 provides a more detailed characterization of brine transport at the mine site, utilizing the results from Chapter 2. The study results are summarized in Chapter 4. Supplementary information (maps, numerical model formulation and model verification) are attached in appendices.

The paper-based format is advantageous because it presents the ideas in each chapter in a concise, complete manner. As a consequence, however, a small amount of repetition is necessary to introduce ideas and information common to each chapter.

Acknowledgements

I sincerely thank my supervisor, Dr. Carl Mendoza, for his guidance and support throughout my graduate work. I enjoyed our discussions and learned more about hydrogeology each time we spoke. I truly appreciate your interest and commitment to this project.

Thank you to Dr. Ben Rostron and Dr. Malcolm Reeves for their assistance and advice throughout the modelling process.

Thank you to Brian Smerdon for reading and editing my thesis, and for the "philosophical" discussions over the years. Thank you to Andrew Davis for his help with the preparation of my thesis maps.

Thank you to Komex International Ltd. for their understanding and flexibility during the completion of my thesis.

Funding for this study was supported by an NSERC graduate scholarship to the author. Computing resources were made possible by the Province of Alberta Intellectual Infrastructure Partnership Program and an NSERC research grant to Dr. Ben Rostron. The Potash Corporation of Saskatchewan kindly made available the geologic and hydrogeologic data utilized in this study.

Finally, I would like to thank my family. The completion of this degree would not have been possible without Rebecca's continuous support, patience and belief in me. Thanks to my parents, Meb and Kay, Joan, Clarence, Dawn, Nikki, Randy, Loretto, Jonah, Sabrina, Tanner and Brandon for their love and support.

Table of Contents

Chapter 1
Introduction

1.1 Study Area 1
1.2 Objectives 3
1.3 Problem Description 3
1.3.1 Mining History 5
1.3.2 Patience Lake Elevations 6
1.3.3 Physical Properties of KCl-NaCl Brine 6
1.4 Geology 7
1.4.1 Bedrock Stratigraphy 8
1.4.1.1 Lea Park Formation 8
1.4.1.2 Judith River Formation 10
1.4.1.3 Bearpaw Formation 10
1.4.2 Quaternary Stratigraphy 10
1.4.2.1 Sutherland Group 11
1.4.2.2 Saskatoon Group 11
1.4.2.2.1 Floral Formation 11
1.4.2.2.2 Battleford Formation 12
1.4.2.2.3 Surficial Stratified Deposits 13
1.5 Hydrogeology 13
1.5.1 Hydrostratigraphy 13
1.5.2 Hydrogeologic Properties 14
1.5.2.1 Intrinsic Permeability 14
1.5.2.2 Porosity and Compressibility 16
1.5.3 Groundwater Flow 16
1.5.4 Geochemistry 18
1.6 Modelling Variable-Density Flow 19
1.6.1 Code Selection 20
1.6.2 Simplifying Assumptions 20
1.7 Summary 21
1.8 References 21

Chapter 2

Simulation of density-induced instabilities in heterogeneous media at a potash mine site in Saskatchewan

2.1 Introduction 24
2.2 Site Description 25
2.3 Modelling Methodology 27
2.3.1 Conceptual Model 29
2.3.2 The Numerical Model 29
2.3.3 Boundary and Initial Conditions 30
2.3.4 Spatial and Temporal Discretization 30
2.3.5 Model Parameters 31
2.3.6 Permeability Distributions of the Battleford Formation 31
2.3.6.1 Horizontal Correlation Length and Variance 32
2.3.6.2 Vertical Correlation Length and Mean Permeability 34
2.3.7 Unsaturated Flow 35
2.4 Model Results 35
2.4.1 Horizontal Correlation Length and Variance 36
2.4.2 Vertical Correlation Length 39
2.4.3 Reduced Mean Permeability 41
2.4.4 Comparisons With a Homogeneous Permeability Field 43
2.4.5 Unsaturated Flow 45
2.5 Discussion and Conclusions 47
2.6 References 49

Chapter 3

Groundwater flow and brine transport modelling at a potash mine site in Saskatchewan

3.1 Introduction 52
3.2 Site Description 55
3.2.1 Hydrostratigraphy 56
3.2.2 Hydrogeology 58
3.3 Modelling Methodology 59
3.4 Three-Dimensional Groundwater Flow Calibration 61
3.4.1 Conceptual Model 61
3.4.2 Model Domain and Discretization 61

3.4.3 Boundary Conditions 62
3.4.4 Three-Dimensional Flow Calibration 64
3.4.4.1 Calibrated Recharge Distribution 65
3.4.4.2 Calibrated Model Parameters 65
3.4.4.3 Steady State Model Calibration Results 67
3.4.4.3.1 Steady-State Groundwater Flow 69
3.5 Two-Dimensional Brine Transport Analysis 72
3.5.1 Conceptual Model 72
3.5.2 Boundary Conditions 73
3.5.3 Spatial and Temporal Discretization 76
3.5.4 Model Parameters 78
3.5.5 Transient Model Results 78
3.5.5.1 Analysis Locations and Methods 78
3.5.5.2 Transient Brine Transport 81
3.5.5.3 Evaluation 83
3.5.5.4 Discussion 84
3.6 Sensitivity Analysis 87
3.6.1 Floral Sand Permeability 87
3.6.2 Increased Dispersivity 90
3.6.3 Historical Patience Lake Elevations 92
3.6.4 Long-Term Patience Lake Elevation 93
3.6.5 Discussion 95
3.7 Conclusions 96
3.8 References 98

Chapter 4

Conclusions

4.1 Hydrogeological Assumptions 101
4.2 Hydrogeology and Brine Transport at the Patience Lake Mine Site 102
4.2.1 Groundwater Flow Calibration 103
4.2.2 Brine Transport 103
4.3 Future Work 104
4.3.1 Field Data 104
4.3.2 Numerical Modelling 105
4.4 References 105

List of Tables

Table		Page
1.1	Intrinsic permeability and porosity ranges for hydrostratigraphic units in the study area.	15
2.1	Hydrogeologic parameters used in numerical model.	29
2.2	Flow and transport parameters.	31
2.3	Group A numerical simulation statistical parameters.	34
2.4	Group B, C and D numerical simulation statistical parameters.	35
3.1	Calibrated model parameters.	66
3.2	Average errors calculated from calibration data.	69
3.3	Hydraulic heads from the 3D flow calibration used to determine specified pressure boundary conditions in the 2D numerical model.	73
3.4	Flow and transport parameters.	78

List of Figures

Figure		Page
1.1	Potash mine site locations in Saskatchewan.	2
1.2	Schematic cross section of the Patience Lake mine site.	4
1.3	Observed Patience Lake surface elevations from 1971 to 1993.	6
1.4	Fluid density as a function of solute concentration for a brine at 0°C and 1 atm.	7
1.5	Stratigraphy and hydrostratigraphy for the Patience Lake study area.	9
2.1	Potash mine site locations in Saskatchewan, Patience Lake mine site location and numerical model cross section.	26
2.2	Cross section A - A'. Conceptual model and boundary conditions for numerical simulations.	28
2.3	Simulated log permeability fields.	33
2.4	Simulated solute distribution for a stable system.	37
2.5	Simulated solute distribution for an unstable system.	38
2.6	Variance versus horizontal correlation length for Group A simulations after 1 year.	40
2.7	Simulated log permeability fields and velocity vectors at t = 18 days for different vertical correlation lengths.	42
2.8	Concentration distribution and velocity vectors beneath the brine source after 10 years.	44
2.9	Breakthrough curves of relative concentration for two points beneath the brine source.	46
2.10	Cross section of Battleford Formation deposits south of the Patience Lake mine site.	48
3.1	Site location and study area.	53
3.2	Hydrostratigraphy for an east-west cross section at the northern edge of Patience Lake.	57
3.3	Cut-away representation of spatial discretization and boundary conditions for the 3D numerical model.	63
3.4	Simulated versus observed hydraulic heads for calibrated 3D flow model.	68

Figure		Page
3.5	Calibrated steady-state hydraulic head distribution in the Forestry Farm Aquifer.	70
3.6	Groundwater velocity magnitude for the 3D calibrated flow model.	71
3.7	Boundary conditions for the 2D numerical model.	74
3.8	Simulated hydraulic head in the Forestry Farm Aquifer for both the 2D and 3D numerical models.	76
3.9	Transient solute source function applied to Patience Lake and the Waste Management Area.	77
3.10	Simulated 2D transient brine distribution beneath the Waste Management Area and Patience Lake.	79
3.11	Brine concentration breakthrough curves and simulated Patience Lake elevations.	82
3.12	Vertical brine concentration profiles after 72 yr (2037) for ***Connection*** and ***WMA*** analysis locations.	86
3.13	Brine concentration breakthrough curves at ***WMA***, ***Connection***, ***MidPL*** and ***NorthPL*** locations for Floral Sand permeability and dispersivity sensitivity analysis.	89
3.14	Simulated 2D transient brine distribution beneath the Waste Management Area and Patience Lake for the high Floral Sand permeability sensitivity simulation.	91
3.15	Brine concentration breakthrough curves at ***Connection*** and ***NorthPL*** illustrating the effect of simulating historical lake elevation changes.	93
3.16	Brine concentration breakthrough curves at ***NorthPL*** and simulated Patience Lake elevation illustrating the effect of long-term lake level changes.	94

Chapter 1

Introduction

Potash (KCl) is used primarily as a source of potassium fertilizer for agriculture. Approximately one third of the world's potash reserves are contained within the Prairie Evaporite Formation in Saskatchewan, between 1000 and 2500 m below the ground surface. By the 1980's, up to 1.2×10^7 tonne of potash was produced annually in Saskatchewan. For every tonne of refined potash, approximately two tonne of solid NaCl and 1 to 2 m^3 of NaCl brine tailings are produced as byproducts (Tallin et al., 1990).

The solid NaCl is typically stored on the land surface beside the mine site and the liquid brine is stored in unlined, dyked retention ponds (Tallin et al., 1990). At several mine sites, Waste Management Areas (WMA) are over 30 years old and several hundred hectares in size.

Migration of brine into the subsurface represents a potential source of contamination for shallow groundwater resources in the vicinity of potash mine sites. The Potash Corporation of Saskatchewan (PCS) is currently investigating the effectiveness of WMAs at its six mine sites in Saskatchewan. The objective is to reduce the potential for significant environmental impact resulting from long-term storage of mining wastes. An important aspect of this investigation is to be able to predict the long-term migration of brine from a WMA and evaluate the impact on groundwater quality.

1.1 Study Area

The PCS Patience Lake Mine site is located in central Saskatchewan, Canada, 18 km west of Saskatoon (Figure 1.1). The study area consists of approximately 400 km^2 around the mine site, encompassing Porter and Burke Lakes to the north and Cheviot and Crawford Lakes to the south (Map 1, Appendix A). The mine site, Patience Lake and other lakes in the study area are situated in a topographic low that extends from south to north. Cheviot and Crawford Lakes are located at an elevation of 517.5 and

518.5 metres above sea level (masl) respectively, Patience Lake (PL) is 514 masl, Burke Lake is 513 masl and Porter Lake is 510 masl. Local topographic highs to the east and west are 570 and 610 masl, respectively.

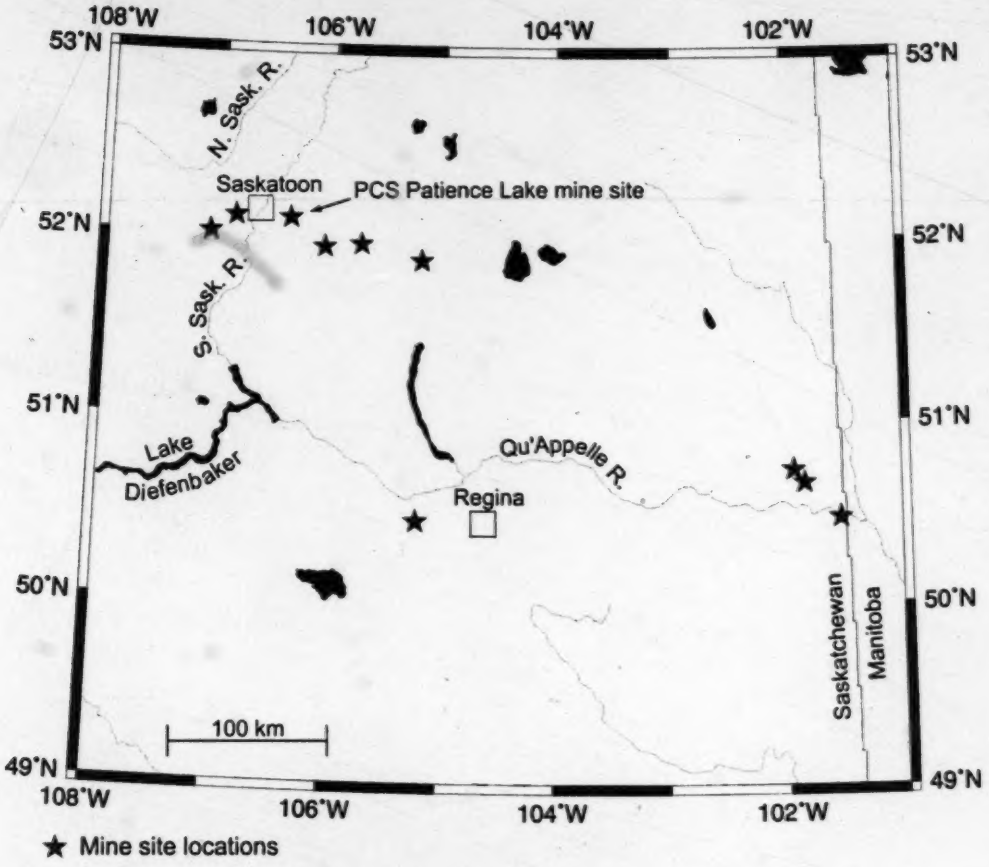

Figure 1.1. Potash mine site locations in Saskatchewan.

Saskatoon has a semi-arid climate that experiences a net water deficit with an average annual rainfall of 361 mm/year and a potential evaporation of 988 mm/year. The mean annual air temperature is 2°C, ranging between 18.4°C in July and –17.6°C in January (Wittrock and Wheaton, 1993). Average recharge to groundwater in the area is estimated to be 1 to 3 mm/yr (Hayashi et al., 1998).

The low topography likely places PL and the PCS mine site in a local groundwater discharge area. Depression-focused recharge at the topographic highs to the east and

west likely cause topographically driven groundwater flow downward and laterally through shallow deposits converging in low-lying regions (Tóth, 1962; Tóth, 1963). The lakes in the study area are naturally saline (primarily $NaSO_4$).

1.2 Objectives

The principal purpose of this thesis is to assess the primary mechanisms controlling solute transport from the PCS Patience Lake WMA into the groundwater system, and to predict long-term environmental impact of brine migration on local groundwater resources. Geologic and hydrogeologic information available for the study area was utilized to develop two- and three-dimensional (2D and 3D), variable-density, groundwater flow and solute transport numerical models. Specific objectives included:

1. Develop a 3D conceptual model of the groundwater flow system for the study area;
2. Assess and justify major hydrogeological assumptions;
3. Construct a numerical model based on the conceptual model;
4. Calibrate the 3D numerical model using existing groundwater monitoring data;
5. Simulate potential 2D transient brine migration from the WMA; and,
6. Assess the important processes and mechanisms affecting brine migration by completing a sensitivity analysis.

1.3 Problem Description

The PCS Patience Lake mine site and associated WMA are located at the south end of PL (Map 1, Appendix A). The geology immediately underlying the mine site and PL consists of low permeability glaciolacusterine and till deposits (Christiansen, 1999). These shallow deposits are underlain by a regional sand and gravel aquifer, approximately 25 to 40 m below ground surface (bgs). Geologic evidence suggests that a locally continuous glaciofluvial sand channel may be in direct contact with both the base of PL and the regional aquifer (Figure 1.2).

Natural vertical hydraulic gradients result in the upward flow of groundwater, discharging into PL, which is generally thought to hydrodynamically contain mine waste from the underlying aquifer (Clifton, 1993). However, if lake levels rise above the hydraulic head

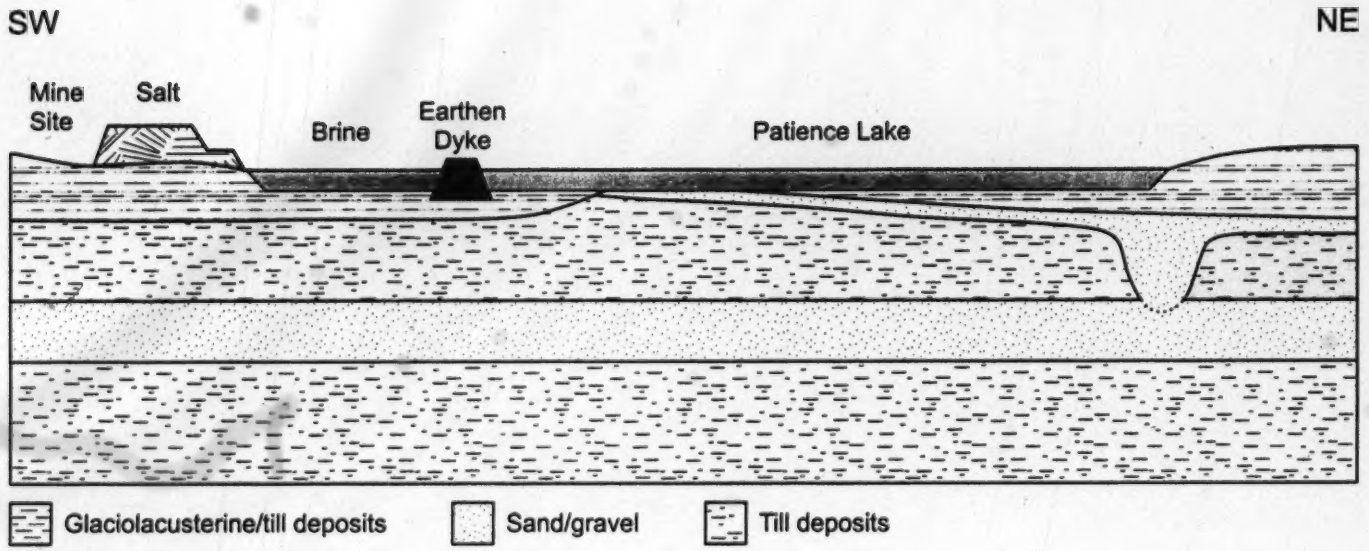

Figure 1.2. Schematic cross section of the Patience Lake mine site (not to scale).

of the underlying aquifer, the vertical hydraulic gradient may be reversed, resulting in recharge to the underlying aquifer from PL. Furthermore, the brine tailings and water in PL have dissolved solid concentrations and fluid densities much greater than underlying native groundwater. The concentration and density gradients could increase the tendency for the downward migration of these dense fluids, opposite to the direction of groundwater flow.

1.3.1 Mining History

Potash mining at the PL mine site began in 1958, but was halted within the first year due to flooding in the mine (Rutten, 2003). Mining operations resumed in 1965. A Waste Management Area (WMA) was established, shortly after flooding in 1958, to store solid salt tailings and saturated liquid brine tailings produced during the mining process. The solid salt tailings are stored on the land surface and the brine tailings are contained in unlined retention ponds at the south end of PL (Map 1, Appendix A).

A perimeter drain around the WMA was constructed in 1970 and an earthen dyke constructed between the brine retention ponds and PL in 1976. Additional mine flooding resulted in the abandonment of conventional mine operations in 1987, which marked the end of solid salt tailings production. The maximum areal extent of the salt pile and brine ponds, estimated from available air photos and maps, is approximately 60 and 50 ha, respectively (Map 1, Appendix A). The maximum height of the salt tailings pile was estimated at 36 m above the land surface. The dissolution/weathering rate of the salt pile has been estimated at 0.06 m/year (Rutten, 2003).

Solution mining operations began in 1988 and continue to present day. Heated brine tailings from the brine retention ponds are injected into the mined caverns to dissolve the KCl of the Prairie Evaporite Formation (Shaw, 1999). The KCl-brine solution is extracted to the surface and pumped back into the brine ponds. During the winter months, solid KCl preferentially precipitates and is dredged from the bottom of the brine ponds. Solid salt tailings are not produced in the solution mining process. In 1992, PL had chloride and total dissolved solids concentrations of 190,000 and 340,000 mg/L, respectively (Clifton, 1993).

1.3.2 Patience Lake Elevations

A hydrograph for PL from 1971 to 1993 is presented in Figure 1.3. In the early 1970s, near the beginning of mining operations, the PL elevation was 514 masl. The lake level increased in 1974 and ranged between 514.3 to 514.6 masl until 1983. A steady increase in lake level occurred from 1983 to 1987 and reached a maximum elevation of 515.6 masl on April 26, 1987 (Clifton, 1993). The increase in lake level corresponds with increased pumping of brine to control mine flooding before the conventional mine was abandoned in 1987. After solution mining commenced, the lake level receded to 514.7 masl.

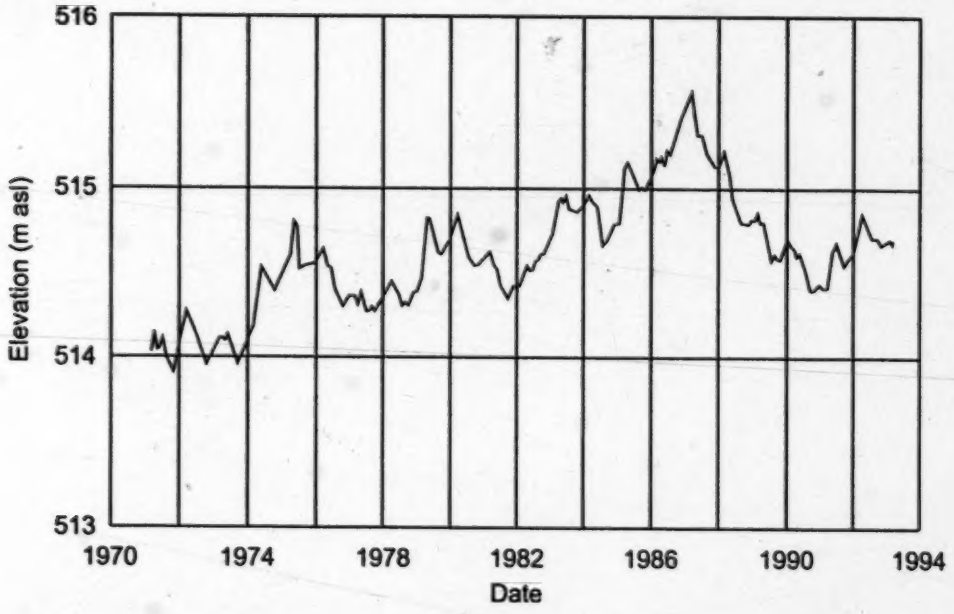

Figure 1.3. Observed Patience Lake surface elevations from 1971 to 1993 (data from Clifton, 1993).

1.3.3 Physical Properties of KCl-NaCl Brine

The brine stored in the retention ponds of the Patience Lake WMA is mutually saturated with KCl and NaCl as a result of the solution mining process. Braitsch (1971) describes a NaCl-KCl-H_2O system for temperatures ranging from 0 to 100°C. The mean annual

temperature for Saskatoon is 2°C (Wittrock and Wheaton, 1993) and shallow groundwater temperatures are less than 8°C (Uwiera, 1998). For a mutually saturated brine at 0°C, the chloride concentration would be approximately 122 mol Cl/1000 mol H_2O, which corresponds to a total dissolved solids concentration of approximately 0.294 kg/kg. The density of this saturated brine, estimated using an empirical formula for petroleum reservoir brines from McCain (1991), is 1235 kg/m^3. While the equation for brine density as a function of solute concentration of McCain (1991) is not linear, it is closely approximated by a linear function with a slope of 801.6 kg/m^3 (Figure 1.4). The average density of native groundwater at 8°C is 999.7 kg/m^3.

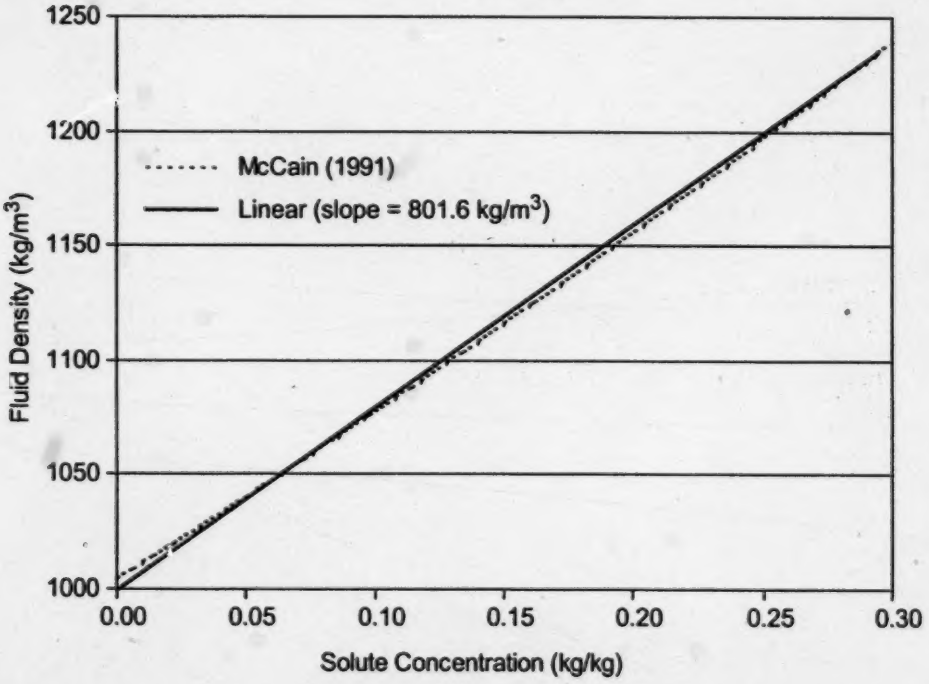

Figure 1.4. Fluid density as a function of solute concentration for a brine at 0°C and 1 atm.

1.4 Geology

The geology of the Saskatoon area has been described by Christiansen (1967a, 1967b, 1970,1992). More detailed geological investigations for the PL mine site area have been

performed by Clifton (1993), Golder (1996) and Christiansen (1999). Borehole logs, cross sections and geologic descriptions from the above sources were used to interpret the stratigraphic setting for the study area. Christiansen (1999) analyzed 114 borehole logs, which are accompanied by an electronic database of interpreted structural information, and was particularly useful in developing the geologic framework for the numerical model. This database was carefully checked against the borehole logs for accuracy and inconsistencies in geologic interpretation. The borehole locations from Christiansen (1999) are indicated on Map 2 (Appendix A). Additional field data were not collected for the purposes of this hydrogeologic interpretation, as this is beyond the scope of the current study.

1.4.1 Bedrock Stratigraphy

Bedrock consists of late Cretaceous age clastic sediments of the Lea Park, Judith River and Bearpaw formations, in ascending order (Figure 1.5). The most significant structural feature of the bedrock geology is a collapse feature (the Saskatoon Low) located 15 km south of Saskatoon. Selective dissolution of Devonian Elk Point Group evaporites resulted in the collapse of overlying Cretaceous and Pleistocene deposits (Christiansen, 1967a). The collapse feature extends to the west and south edges of the study area, where the topographic surface of the Lea Park and Judith River formations subside rapidly (Map 2, Appendix A).

1.4.1.1 Lea Park Formation

The Lea Park Formation comprises more than 240 m of marine silt and clay (Christiansen, 1970). It is a fine-grained, thick, laterally continuous unit over the entire study area, and is considered a barrier to groundwater flow. Therefore, it is the lowermost unit considered in the development of the conceptual model. The top of the Lea Park Formation dips slightly to the southwest over most the study area, ranging between 390 and 410 masl (Map 2, Appendix A). However, along the south and west edges of the study area, the Lea Park surface subsides to a minimum of 273 masl.

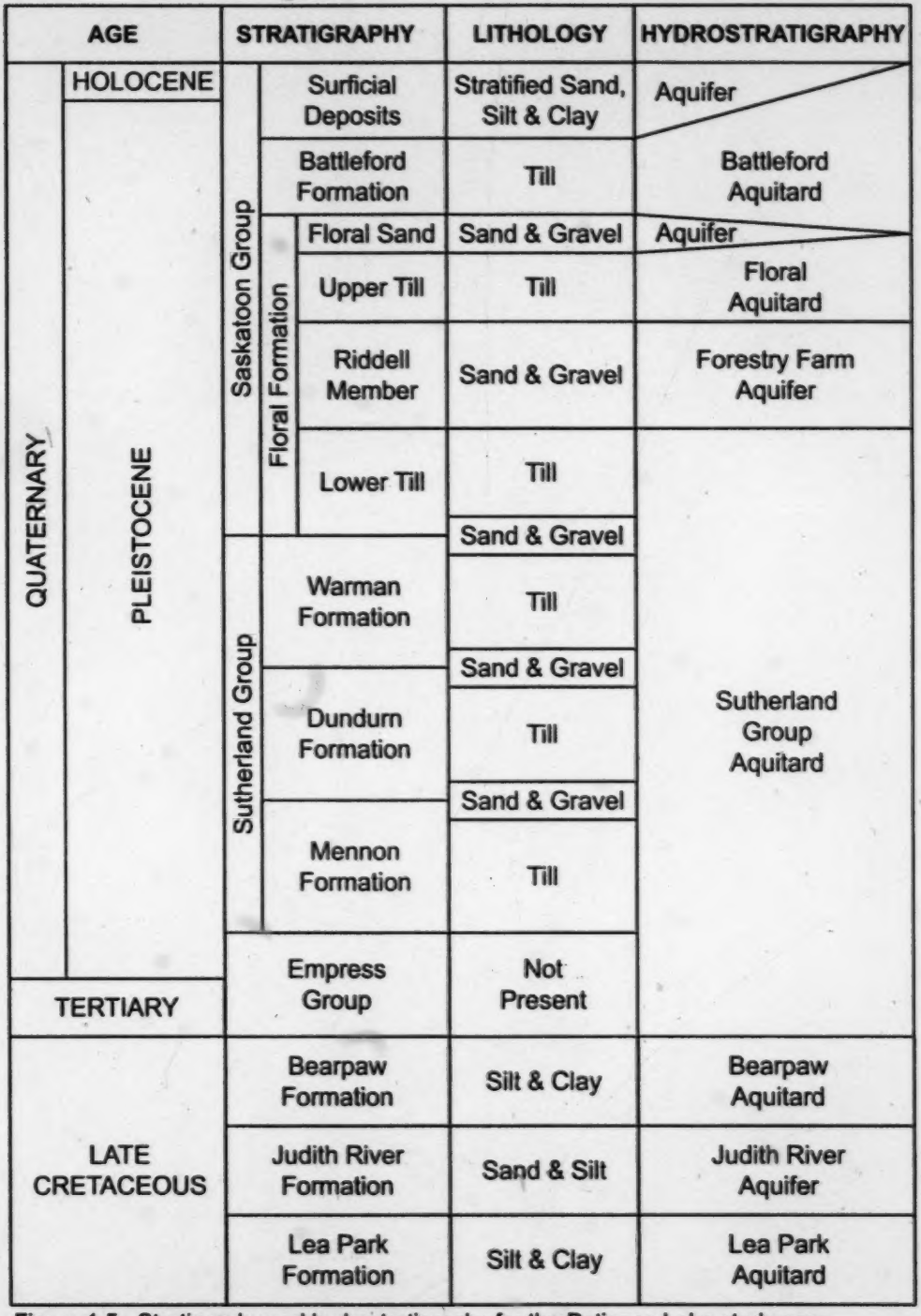

Figure 1.5. Stratigraphy and hydrostratigraphy for the Patience Lake study area (stratigraphy after Christiansen, 1999).

1.4.1.2 Judith River Formation

Overlying the Lea Park Formation is the Judith River Formation. It ranges from 8 to 36 m thick and is continuous over the study area. This unit is comprised of non-marine, fine-grained sand, silt and clay that is interbedded with carbonaceous concretionary zones (Christiansen, 1970) and forms the lower-most aquifer in the region. Its upper surface is relatively flat, except in the south and west where it is influenced by the Saskatoon Low collapse structure.

1.4.1.3 Bearpaw Formation

The upper-most bedrock unit is the Bearpaw Formation, which is composed of non-calcareous marine silt and clay (Cristiansen, 1967a). It is in direct contact with the Quaternary glacial deposits above and the surface is characterized by an erosional disconformity. Beneath PL, the top of the Bearpaw Formation surface ranges between 450 and 460 masl and ranges between 20 and 30 m thick. To the east of PL and in the southwest corner of the study area, fluvial channels are eroded into the bedrock surface (inferred from Christiansen, 1999) (Map 3, Appendix A). The eastern channel is filled with sand and gravel except at the north end of the study area where it is filled with till. The southwest channel is also filled with coarse-grained sediments, except at the south end of the study area. The Saskatoon Low collapse feature impacts the bedrock surface only at the extreme southwest corner of the study area, which is consistent with the findings of Christiansen (1967a).

1.4.2 Quaternary Stratigraphy

The Quaternary sequence of sediments consists of glacial, proglacial and nonglacial deposits. Because the Empress Group is not present in the study area, the Sutherland Group is in direct contact with the bedrock and is overlain by the younger Saskatoon Group (Figure 1.5). Christiansen (1992) defined the individual formations within each group based on lithologies, stratigraphic position, contacts of weathered zones/nonglacial stratified deposits and carbonate content.

1.4.2.1 Sutherland Group

The Sutherland Group is comprised primarily of till and is divided into the Mennon, Dundurn and Warman formations (Figure 1.5) which are differentiated based on carbonate content, clay content, Atterberg limits and electrical resistance (Christiansen, 1992). Each of the formations typically consists of a till and intertill sequence. The lower and upper contacts of the Sutherland Group are nonconformable due to erosion or nondeposition.

Within the study area, the The Mennon and Warman Formations are relatively thin and discontinuous. The Dundurn Formation is laterally extensive and is characterized as an unoxidized, dense, grey till with a lower carbonate content and higher clay content compared to the overlying Saskatoon Group deposits (Christiansen, 1992). The upper surface of the Sutherland Group deposits ranges from approximately 465 to 500 masl. Sutherland Group deposits are continuous over the entire study area (except south of the WMA) and generally range in thickness between 15 and 45 m. Where fluvial channels have been eroded into the bedrock surface, Sutherland Group deposits may consist of up to 70 m of interbedded till, sand and gravel deposits.

South of the WMA, at a local bedrock high (460 m contour on Map 3, Appendix A), Sutherland Group sediments have been eroded away, resulting in Saskatoon Group deposits lying in direct contact with the Bearpaw Formation.

1.4.2.2 Saskatoon Group

The Saskatoon Group lies between the Sutherland Group and the land surface and is separated into (in ascending order) the Floral Formation, Battleford Formation and Surficial Stratified Deposits (Christiansen, 1992).

1.4.2.2.1 Floral Formation

The Floral Formation lies directly over the Sutherland Group and is separated into a lower till, Riddell Member and upper till. Compositionally, the two tills are indistinguishable (Christiansen, 1992). They are only differentiated where the Riddell Member exists. The tills of the Floral Formation are typically described as grey, sandy

clay to clay with a higher carbonate content and electrical resistivity than the underlying Sutherland Group tills. The upper till is commonly oxidized and fractured, whereas the lower till is unoxidized. The Riddell Member consists of proglacial and nonglacial sand and gravel, constituting the regionally extensive Forestry Farm Aquifer.

The lower Floral Formation till is relatively thin and primarily limited to the west of PL, resulting in the Forestry Farm Aquifer (FFA) lying in direct contact with the underlying Sutherland Group deposits over much of the study area. North and south of PL, the upper Floral Formation is also absent, placing the top of the FFA in contact with the overlying Battleford Formation. The FFA ranges in thickness from 2 to 25 m and is commonly interbedded with thin silt and clay units (Map 4, Appendix A). It is laterally continuous over most of the study area, extending beyond the study area toward the South Saskatchewan River (to the northwest). Along the east edge of the study area, the FFA pinches out.

In the study area, the upper Floral Formation till is absent north and south of PL but attains a thickness up to approximately 35 m to the west and east. Directly beneath PL and the WMA, the upper till thins to approximately 10 m. An Upper Sand layer (Floral Sand) was identified at the at the top of the Floral Formation (Golder, 1996; Christiansen, 1999) and is interpreted to extend north-northeast from the east side of the brine pond approximately 2 km to the north end of Burke Lake (Map 5, Appendix A). The Floral Sand appears to be limited to the topographic low directly beneath PL and Burke Lake and ranges in thickness between 3 and 20 m. From the northern tip of PL to the southern edge of Burke Lake (boreholes 76, 77, 79 and 82 on Map 5, Appendix A), the upper Floral Formation till is absent, resulting in a direct connection between the Floral Sand and FFA. In addition, the Floral Sand appears to sub-crop beneath the western edge of PL, near borehole 65 (Map 5, Appendix A).

1.4.2.2.2 Battleford Formation

The Battleford Formation is a soft, massive till that lies between the Floral Formation and the surficial stratified deposits. Along the east and west sides of the study area, the Battleford Formation extends to the land surface. The basal contact between the Battleford and Floral Formations is nonconformable and often distinguished by a boulder

pavement. The upper contact with the surficial stratified deposits is conformable (Christiansen, 1992).

The Battleford Formation is continuous over the study area and ranges in thickness from 2 to 85 m. The thickest accumulations are glacial moraines to the east and west of PL, producing topographic highs in the area (Clifton, 1993).

1.4.2.2.3 Surficial Stratified Deposits

The surficial stratified deposits consist of glaciolacustrine and glaciofluvial sediments deposited during the most recent deglaciation (Christiansen (1979, 1992)). Localized glaciaofluvial sand and gravel deposits, ranging between 1 and 6 m thick, are present east and west of PL (Clifton, 1993) between the topographic highs (moraines) and the topographic low (Patience and Burke Lakes). Glaciolacustrine silt and clay deposits have accumulated in topographically low areas beneath and adjacent to Patience, Burke and Porter Lakes and in the southern portion of the study area (Cheviot and Crawford Lakes). The silt and clay deposits range in thickness from 1 to 5 m beneath Patience and Burke Lakes to 21 m west of Cheviot Lake.

1.5 Hydrogeology

The geologic information described in Section 1.4 and available hydrogeologic data were used to establish a 3D conceptual model for the hydrogeology of the study area. The hydrogeologic conceptualization was then used as the basis for 2D and 3D groundwater flow and solute transport numerical models.

1.5.1 Hydrostratigraphy

Based on their inferred hydrogeological properties, geologic formations present in the study area were subdivided or grouped into hydrostratigraphic units (Figure 1.5) to form a series of aquifers and aquitards.

The Lea Park Formation, considered a barrier to groundwater flow, forms the base of the conceptual model. The Judith River aquifer represents the Judith River Formation sand and silt and is the lowermost aquifer. The Cretaceous silt and clay deposits of the

Bearpaw Formation form the uppermost bedrock aquitard. The Sutherland Group aquitard is a combination of the Mennon, Dundurn and Warman Formations and the lower till of the Floral Formation (where present). Intertill sand and gravel deposits of the Sutherland Group are thin and discontinuous and therefore, not explicitly represented in the conceptual model. The Forestry Farm Aquifer represents the Riddell Member sand and gravel deposits. Upper till deposits of the Floral Formation form the Floral aquitard which is subdivided into the Floral Sand aquifer where upper Floral Formation sand deposits are present. The Battleford aquitard comprises the Battleford Formation till and surficial silt and clay deposits. Surficial sand deposits form the uppermost aquifer in the conceptual model.

1.5.2 Hydrogeologic Properties

Soil matrix and fluid properties relevant to groundwater flow were obtained from published and unpublished data. Information specific to the study area is limited, consisting of hydraulic conductivity estimates for the FFA at six piezometers and for the Judith River aquifer at one piezometer (Clifton, 1993). Aquitard properties were obtained from published sources (Shaw and Hendry, 1998; Maathuis and van der Kamp, 1994; Keller, et al., 1988, 1989;). When data specific to the Saskatoon region was unavailable, hydrogeologic properties reported in Domineco and Schwartz (1990) were used.

1.5.2.1 Intrinsic Permeability

Hydraulic conductivity ranges for the hydrostratigraphic units of the study area, compiled from various sources, were converted to intrinsic permeability and are summarized in Table 1.1. The permeability of aquifer units is estimated from unpublished aquifer test and slug test results (Clifton, 1993), where available. An aquifer test performed on the Judith River Aquifer at the PL mine site (Clifton, 1993) resulted in a permeability estimate of 3.1×10^{-12} m^2. Aquifer and slug tests performed on six piezometers completed in the FFA resulted in permeability estimates from 6.1×10^{-13} to 4.1×10^{-11} m^2. The permeability of the Floral and surficial aquifers were estimated from literature (Table 1.1).

Table 1.1. Intrinsic permeability and porosity ranges for hydrostratigraphic units in the study area.

Hydrostratigraphic Unit	Permeability (m^2)*	Porosity (-)
Surficial Deposits		
sand	$2x10^{-14}$ to $6x10^{-10}$ (f)	0.26 to 0.53 (f)
silt and clay	$1x10^{-18}$ to $2x10^{-12}$ (f)	0.40 to 0.50 (c)
Battleford Aquitard		0.31 (d)
oxidized	$1x10^{-15}$ to $1x10^{-14}$ (c) $6.6x10^{-16}$ to $1.3x10^{-15}$ (d)	
unoxidized	$1.3x10^{-18}$ to $8.6x10^{-18}$ (d)	
Floral Aquifer	$9x10^{-14}$ to $3x10^{-9}$ (f)	0.25 to 0.46 (f)
Floral Aquitard	$1x10^{-16}$ to $1x10^{-15}$ (a)	0.20 to 0.30 (c)
Forestry Farm Aquifer	$6.1x10^{-13}$ to $4.1x10^{-11}$ (e)	0.25 to 0.46 (f)
Sutherland Aquitard	$1x10^{-18}$ to $1x10^{-17}$ (b)	0.30 to 0.35 (c)
Bearpaw Aquitard	$4.5x10^{-19}$ to $5.4x10^{-19}$ (d)	0.37 to 0.44 (d)
Judith River Aquifer	$3.1x10^{-12}$ (e)	0.05 to 0.41 (f)
Lea Park Aquitard	$1x10^{-19}$ to $1x10^{-17}$ (c)	0.34 to 0.61 (f)

* Originally reported as hydraulic conductivity (K) in m/s. Permeability = $K\mu/\rho g$; $\mu = 0.001$ kg/ms, $\rho = 999.7$ kg/m^3, $g = 9.81$ m/s^2

(a) Keller et al. (1988)
(b) Keller et al. (1989)
(c) Maathuis and van der Kamp (1994)
(d) Shaw and Hendry (1998)
(e) Clifton (1993)
(f) Domenico and Schwartz (1990)

Where possible, the permeability of aquitard units was estimated from published studies that investigated the hydrogeology of till sequences in the Saskatoon region. Keller et al. (1988, 1989) estimated permeabilities of the Floral and Sutherland aquitards at two sites approximately 15 km north of Saskatoon, utilizing both small-scale laboratory and field methods and large-scale analysis of the downward propagation of seasonal water table fluctuations. Shaw and Hendry (1998) estimated the permeability of the Battleford and Bearpaw aquitards approximately 140 km south of Saskatoon using small-scale laboratory and field methods. Maathuis and van der Kamp (1994) reviewed the permeability of Saskatchewan tills with the specific objective of characterizing groundwater flow beneath potash WMAs.

Permeability values from the above sources ranged from $6.6x10^{-16}$ to $1x10^{-14}$ m^2 for an oxidized, shallow till, to $1x10^{-18}$ to $1x10^{-15}$ m^2 for an unoxidized till. Estimates for the

Cretaceous silt and clay units of the Bearpaw and Lea Park aquitards ranged from $1x10^{-19}$ to $1x10^{-17}$ m^2 (Table 1.1).

1.5.2.2 Porosity and Compressibility

Domenico and Schwartz (1990) is the primary source of porosity data (Table 1.1). Values for the unconsolidated Pleistocene sand and gravel deposits range from 0.25 to 0.53. The porosity of the semi-consolidated Judith River aquifer was estimated between 0.05 and 0.41. For till and surficial silt and clay deposits, porosity ranged from 0.20 to 0.50. The bedrock silt and clay porosity ranged from 0.34 to 0.61.

Domenico and Schwartz (1990) report soil matrix compressibilities ranging from $5.2x10^{-9}$ Pa^{-1} for dense, sandy gravel to $2x10^{-6}$ Pa^{-1} for plastic clay. At environmental temperatures, water compressibility is between $4.4x10^{-10}$ Pa^{-1} (Freeze and Cherry, 1979) and $4.6x10^{-10}$ Pa^{-1} (Fetter, 1994).

1.5.3 Groundwater Flow

A groundwater divide within the FFA, coinciding with the topographic high approximately 6 km west of PL, was interpreted by Clifton (1993) (Map 1 Appendix A). Shallow groundwater east of the topographic divide flows toward Patience, Burke and Porter Lakes, and toward the South Saskatchewan River west of the groundwater divide. A similar topographic groundwater divide is inferred approximately 9 km east of PL. The two topographic features combine to create a local groundwater flow system.

In the semi-arid climate of central Saskatchewan, groundwater recharge through clayey till deposits occurs primarily during spring snowmelt run-off and is focused at small depressions that collect surface water (Fortin et al., 1991). This depression-focused recharge, averaged over an entire catchment, is estimated between 1 and 3 mm/year on the Saskatchewan prairies (Hayashi et al., 1998).

Observed hydraulic heads in the FFA and interpreted potentiometric surface are provided on Map 6 (Appendix A). At the study site, it is expected that groundwater recharge in the topographically high regions to the east and west of PL flows vertically

through the low permeability till deposits toward the underlying FFA. Groundwater within the FFA flows laterally, converging along the topographic low and discharging into Patience, Burke and Porter Lakes. Beyond the southeast edge of the study area, regional groundwater flow within the FFA is toward the northwest (Golder, 1996), which also converges along the topographic low. Along the topographic low, groundwater flow in the FFA is toward the north-northeast.

There is a long-term imbalance between the annual average precipitation (361 mm/yr) and potential evaporation (988 mm/yr) in the central Saskatchewan climate (Wittrock and Wheaton, 1993). As a result, there is no surface water outlet and PL is in a hydrogeologically closed region (Duffy and Al-Hassan, 1988). Thus, groundwater discharge to PL must balance the surface water deficit in order to maintain a perennial lake system.

Observed hydraulic heads within the shallow till (Battleford Formation), Floral sand, FFA and Judith River aquifer are also indicated on Map 6 (Appendix A). Observation points are limited to the topographic low at the margins of PL and the PCS mine site. The negative vertical hydraulic gradient between deeper piezometers in the FFA, the shallower piezometers in the Floral sand and the elevation of PL support the argument that groundwater discharges into PL. At the piezometer nest along the west shore of PL (94-8/A-101 on Map 6) for example, the hydraulic head is 516.5 masl in the FFA, 515.2 masl in the overlying Floral sand and PL is at an elevation of approximately 514 masl. It is this negative vertical hydraulic gradient that promotes hydrodynamic containment of brine in PL.

The decrease in hydraulic head within the FFA in the north-northeast direction means there is a gradual decrease in the negative vertical hydraulic gradient between PL and the FFA in that direction. For example, the vertical hydraulic gradient between PL and the FFA along the west shore (A-101) is -0.08 m/m, whereas at the north end of the lake (94-2), it decreases to -0.04 m/m. An increase in lake elevation could decrease the vertical hydraulic gradient even further. Conversely, a decrease in hydraulic head within the FFA (due to groundwater extraction, for example) could decrease the vertical hydraulic gradient. Assuming the hydraulic head distribution in the FFA remained constant, a PL elevation greater than 515.3 masl would reverse the direction of the

vertical hydraulic gradient, resulting in recharge conditions at the north end of the lake. The maximum observed lake elevation was 515.6 masl, in 1987 (Figure 1.3).

The vertical gradient between the Judith River aquifer and the FFA ranges between 0.01 m/m and 0.1 m/m, indicating the downward leakage of groundwater through the Sutherland and Bearpaw aquitards. Given the 60 to 70 m thickness of low permeability till and shale bedrock between the two aquifers, it unlikely that leakage from the FFA contributes a significant flux of water to the Judith River aquifer.

East of Saskatoon, groundwater flow within bedrock aquifers generally flows toward the west-northwest (Meneley, 1970). Within the study area, the two piezometers completed within the Judith River aquifer are insufficient to establish a groundwater flow direction; however, the apparent lateral hydraulic gradient toward piezometer D6 (Map 6) is consistent with the regional groundwater flow direction.

1.5.4 Geochemistry

Geochemical data for the study area is summarized from Clifton, 1993. The geochemistry of the FFA is dominated by dissolved sulphate and bicarbonate with average concentrations of 1,200 and 500 mg/L, respectively. Dissolved chloride concentrations range from 20 to 250 mg/L. Dissolved cation concentrations are represented equally by calcium, magnesium and sodium with averages ranging from 140 to 280 mg/L. The total dissolved solids (TDS) concentration generally ranges between 2,000 and 3,000 mg/L (Clifton, 1993). The geochemical composition of the overlying Battleford and Floral Formation till deposits is consistent with the FFA. The TDS concentration is generally less than that of the FFA, ranging from 250 to 2,500 mg/L. The Judith River aquifer is dominated by sodium and chloride and has TDS concentrations typically ranging between 3,000 and 7,000 mg/L (Clifton, 1993).

Average chloride concentrations obtained from piezometers in the vicinity of the mine site and PL are summarized on Map 6 (Appendix A). Piezometers completed within the Battleford Formation till impacted with chloride are located immediately west of the salt pile (A9, A10 and A45) or south of the mine site proper (A11 and A39). The single piezometer completed within the Floral Sand is located along the west shore of PL and

has a chloride concentration exceeding 168,400 mg/L. All piezometers completed within the FFA appear to have background chloride concentrations except for 94-2 and 96-5, located at the north end of PL, which have concentrations of approximately 1,500 mg/L (~10 times background values).

1.6 Modelling Variable-Density Flow

Researchers have attempted to describe the relationship of fresh-water saline-water mixing processes mathematically since the late nineteenth century (Reilly and Goodman, 1985). Advances in technology have increased our ability to describe more complex systems; however, simplifying assumptions are still invariably required. An appropriate mathematical model must be selected at the onset of an investigation that simplifies the problem as much as possible while maintaining an appropriate level of accuracy.

2D and 3D density-dependent numerical models are now commonly used in the analysis of fresh-water saline-water mixing (Kolditz et al., 1998). The dependent variables of the groundwater flow mass balance equation (fluid pressure) and solute transport mass balance equation (concentration) need to be solved simultaneously since fluid pressure is a function of density, density is a function of solute concentration, and solute concentration/transport depends on density (through velocity). Density-dependent numerical models are computationally intensive as a result of this coupling of governing equations. The inclusion of unnecessary or insignificant levels of complexity can result in excessive computational effort. Therefore, the appropriate selection and justification of simplifying assumptions can be as important as the selection of the numerical model itself.

Reilly and Goodman (1985) group possible simplifications into three categories.

1. The physics of the mixing process. A sharp interface model is the simplest and allows one to estimate the position of the fresh-water saline-water interface but does not allow for the determination of solute concentrations. Density-dependent models allow for the determination of solute concentrations and increase in complexity as the dimensionality of the problem increases and when transient systems are considered.

2. Aquifer characteristics. The simplest configuration consists of a single, homogeneous hydrostratigraphic unit. Complexity increases when the fresh- saline-water interface occurs in more than one hydrostratigraphic unit or when heterogeneous and/or anisotropic media are incorporated.
3. Scale of analysis. Small-scale, local systems require fine spatial discretization and are therefore more computationally intensive than regional-scale problems.

1.6.1 Code Selection

The analysis of brine transport from the PL mine site warrants a high level of complexity in its treatment: there are large density contrasts; it is a heterogeneous environment; the brine plume is in a transient state; and, it is a small-scale, site-specific problem.

The groundwater model SUTRA (Saturated-Unsaturated TRAnsport) (Voss, 1984) was selected for the numerical analysis. SUTRA is capable of simulating density-dependent transient transport for a single, non-conservative, solute species in fully saturated or saturated-unsaturated, heterogeneous, anisotropic porous media. In its initial development, SUTRA was strictly a 2D numerical model (Voss, 1984). 3D capabilities have recently been incorporated into the SUTRA code (Voss and Provost, 2003). The numerical formulation of the SUTRA 2D and 2D3D code is summarized in Appendix B. 2D and 3D model verification results are presented in Appendix C.

1.6.2 Simplifying Assumptions

Brine geochemistry at the WMA is dominated by dissolved chloride, which is generally considered a conservative solute; therefore, sorption processes are assumed to be negligible. The influence of till heterogeneity and the unsaturated zone on brine transport from the WMA is investigated in Chapter 2 to provide justification for additional simplifications to the conceptual model.

Schincariol et al. (1997) demonstrated that the initiation and growth of instabilities in variable-density system are closely tied to the spatial correlation of high and low permeability materials. The impact of heterogeneity on brine transport stability is investigated using stochastically generated permeability distributions.

An investigation of brine transport from the PCS Cory mine site explicitly accounted for saturated-unsaturated flow (Uwiera, 1998) but did not examine the impact on solute transport or the sensitivity of model results to unsaturated soil parameters. Simulations are conducted in Chapter 2 to determine if the unsaturated zone has a significant influence on brine transport at the PL mine site.

1.7 Summary

The objective of this thesis is to assess the impact of long-term brine storage at the PCS Patience Lake potash mine site on local groundwater resources. Initially, in Chapter 2, key hydrogeological assumptions are investigated to determine their potential influence on brine transport at the mine site. Chapter 3 incorporates the initial results in a more detailed brine transport analysis involving a 3D hydrogeological conceptualization of the study area and a sensitivity analysis investigating important processes/uncertainties in brine migration. The results of the study are summarized in Chapter 4.

1.8 References

Braitsch, O., 1971. Salt Deposits: Their origin and composition. Springer-Verlag.

Christiansen, E.A., 1967a. Collapse structures near Saskatoon, Saskatchewan, Canada. Canadian Journal of Earth Sciences, 4: 757-767.

Christiansen, E.A., 1967b. Geology and groundwater resources of the Saskatoon area (73-B). Saskatchewan Resarch Council.

Christiansen, E.A., 1970. Geology. In: E.A. Christiansen (Editor), Physical environment of Saskatoon, Canada. National Research Council of Canada, 68 p.

Christiansen, E.A., 1979. The Wisconsinan deglaciation of southern Saskatchewan and adjacent areas. Canadian Journal of Earth Sciences, 16: 913-938.

Christiansen, E.A., 1992. Pleistocene stratigraphy of the Saskatoon area, Saskatchewan, Canada: an update. Canadian Journal of Earth Sciences, 29: 1767-1778.

Christiansen, E.A., 1999. Geology of the PCS Patience Lake mine area, Unpublished report prepared for the Potash Corporation of Saskatchewan, June 21, 1999.

Clifton Associates Ltd., 1993. Study of environmental impact potential of Patience Lake basin and Potash Company of America mine site Saskatoon, Saskatchewan. S551, Unpublished report prepared for the Potash Company of America. September 16, 1993.

Domenico, P.A. and Schwartz, F.W., 1990. Physical and Chemical Hydrogeology. John Wiley & Sons Inc., 824 p.

Duffy, C.J. and Al-Hassan, S., 1988. Groundwater circulation in a closed desert basin: Topographic scaling and climatic forcing. Water Resources Research, 24(10): 1675-1688.

Fetter, C.W., 1994. Applied hydrogeology, third edition. Prentice-Hall, Inc., 691 p.

Fortin, G., van der Kamp, G. and Cherry, J.A., 1991. Hydrogeology and hydrogeochemistry of an aquifer-aquitard system within glacial deposits, Saskatchewan, Canada. Journal of Hydrology, 126: 265-292.

Freeze, R.A. and Cherry, J.A., 1979. Groundwater. Prentice-Hall, Inc., 604 p.

Golder Associates, 1996. Regional groundwater flow and solute transport modelling: Potash Corporation of Saskatchewan Patience Lake and Allan divisions, Unpublished report prepared for the Potash Corporation of Saskatchewan Inc. July, 1996.

Hayashi, M., van der Kamp, G. and Rudolph, D.L., 1998. Water and solute transfer between a prairie wetland and adjacent uplands, 1. Water balance. Journal of Hydrology, 207: 42-55.

Keller, C.K., van der Kamp, G. and Cherry, J.A., 1988. Hydrogeology of two Saskatchewan tills, I. Fractures, bulk permeability, and spatial variability of downward flow. Journal of Hydrology, 101: 97-121.

Keller, C.K., van der Kamp, G. and Cherry, J.A., 1989. A multiscale study of the permeability of a thick clayey till. Water Resources Research, 25(11): 2299-2317.

Kolditz, O., Ratke, R., Diersch, H. and Zielke, W., 1998. Coupled groundwater flow and transport: 1. Verification of variable density flow and transport models. Advances in Water Resources, 21(1): 27-46.

Maathuis, H. and van der Kamp, G., 1994. Final Report: Subsurface brine migration at potash waste disposal sites in Saskatchewan. R-1220-10-E-94, Saskatchewan Research Council.

McCain Jr., W.D., 1991. Reservoir-fluid property correlations - state of the art. SPE Reservoir Engineering, 6: 266-272.

Meneley, W.A., 1970. Groundwater Resources. In: E.A. Christiansen (Editor), Physical environment of Saskatoon, Canada. National Research Council of Canada, 68 p.

Reilly, T.E. and Goodman, A.S., 1985. Quantitative analysis of saltwater-freshwater relationships in groundwater systems - a historical perspective. Jounal of Hydrology, 80: 125-160.

Rutten, K., 2003. Personal communication, MDH Engineered Solutions.

Schincariol, R.A., Schwartz, F.W. and Mendoza, C.A., 1997. Instabilities in variable density flows: Stability and sensitivity analyses for homogeneous and heterogeneous media. Water Resources Research, 33(1): 31-41.

Shaw, R.J., 1999. Personal communication, Potash Corporation of Saskatchewan.

Shaw, R.J. and Hendry, M.J., 1998. Hydrogeology of a thick clay till and Cretaceous clay sequence, Saskatchewan, Canada. Canadian Geotechnical Journal, 35: 1041-1052.

Tallin, J.E., Pufahl, D.E. and Barbour, S.L., 1990. Waste management schemes of potash mines in Saskatchewan. Canadian Journal of Civil Engineering, 17: 528-542.

Tóth, J., 1962. A theory of groundwater motion in small drainage basins in central Alberta, Canada. Journal of Geophysical Research, 67(11): 4375-4387.

Tóth, J., 1963. A theoretical analysis of groundwater flow in small drainage basins. Journal of Geophysical Research, 68(16): 4795-4812.

Uwiera, M., 1998. Numerical simulation of brine migration in the vicinity of a potash mine. M. Sc. Thesis, University of Saskatchewan, Saskatoon, 208 p.

Voss, C.I., 1984. SUTRA: a finite-element simulation model for saturated-unsaturated fluid-density-dependent ground-water flow with energy transport or chemically-reactive single-species solute transport. 84-4369, U. S. Geological Survey Water-Resources Investigations.

Voss, C.I. and Provost, A.M., 2003. SUTRA: a model for saturated-unsaturated, variable-density ground-water flow with solute or energy transport. 02-4231, U. S. Geological Survey Water-Resources Investigations.

Wittrock, V. and Wheaton, E.E., 1993. Saskatoon SRC Climatological Reference Station Annual Summary, 1992. E-2900-5-B-93, Saskatchewan Resarch Council.

Chapter 2

Simulation of density-induced instabilities in heterogeneous media at a potash mine site in Saskatchewan

2.1 Introduction

Approximately one third of the world's potash reserves are located in Saskatchewan, which are mined for use in potassium fertilizer. However, for every tonne of potash produced, two tonne of solid NaCl and 1 to 2 m^3 of brine tailings are produced (Tallin et al., 1990). These waste streams are commonly stored on the land surface or in unlined retention ponds, and represent a potential threat to groundwater resources in the vicinity of potash mine sites. The resultant dense brines overlie fresh groundwater, which may result in density-induced transport at rates much higher than dispersion or hydraulically-driven transport alone.

There are many instances where a more dense fluid overlying a less dense fluid, creates the potential for density-driven mixing of miscible fluids. Examples include: seawater intrusion into coastal aquifers (Huyakorn et al., 1987); migration of landfill leachates (Frind, 1982); infiltration of saline water from irrigation disposal basins (Simmons and Narayan, 1997); reflux dolomitization (Jones et al., 2003); and, concentration of solutes in evaporating salt lakes (Wooding et al., 1997). Density-driven convection in such horizontally stratified fluids can result in vertical lobes, or fingers, of downward flowing dense fluid, displacing the less dense fluid. The mechanisms of unstable flow and the necessary conditions for the onset of instability have been studied experimentally and theoretically for nearly a century (Simmons and Sharp, 2000). Early work incorporated the use of a dimensionless Rayleigh number (Ra), which is the ratio of buoyancy-driven forces to dispersion and viscous forces, to predict the development of unstable flow (Wooding, 1962; List, 1965; Bachmat and Elrick, 1970; Bues and Aachib, 1991). However the use of a Ra carries with it several limiting assumptions: a homogeneous system with a uniform velocity distribution and a zone of dispersion that remains constant in space and time. In addition, one must determine an appropriate value for an

ambiguous parameter termed the "characteristic length" (List, 1965) or the "length of mixing" (Bues and Aachib, 1991).

More recently, studies incorporating heterogeneous media have demonstrated the limitations of a Ra in predicting the onset of instability (Schincariol et al., 1994, 1997; Schincariol 1998; Swartz and Schwartz, 1998; Simmons and Sharp, 2000; Simmons et al., 2001). In a heterogeneous system, the initiation and growth of instabilities are closely tied to the spatial correlation of high and low permeability materials, which are not accounted for in a Ra (Schincariol et al., 1997).

This study investigates the potential development of unstable brine transport at a potash mine site in Saskatchewan in which dense brine tailings are in direct contact with a heterogeneous till deposit. The objectives are to understand the spatial scales of heterogeneity that produce instability and to compare this with available geologic information at the site; and, to investigate the significance instability has when saturated-unsaturated flow is explicitly accounted for in the numerical model. Transient numerical simulations are conducted using heterogeneous permeability fields that vary in horizontal and vertical spatial structure, and in the magnitude of the heterogeneity. Both stable and unstable systems are simulated to elucidate the necessary spatial variability that is likely to produce unstable brine transport at the site. The results of this work are used in the development of two-dimensional (2D) and three-dimensional (3D) brine transport simulations that investigate implications of long-term brine storage at the mine site (Chapter 3).

2.2 Site Description

The site is located 18 km east of Saskatoon at the south end of Patience Lake (Figure 2.1), which is located in a local topographic low. The climate is semi-arid with a mean annual temperature of 2°C (Wittrock and Wheaton, 1993) and a basin-averaged groundwater recharge rate between 1 and 3 mm/yr (Hayashi et al., 1998). The brine tailings are mutually saturated with KCl and NaCl, and the total dissolved solids (TDS) concentration in Patience Lake (PL) has been reported at 340,000 mg/L (Clifton, 1993).

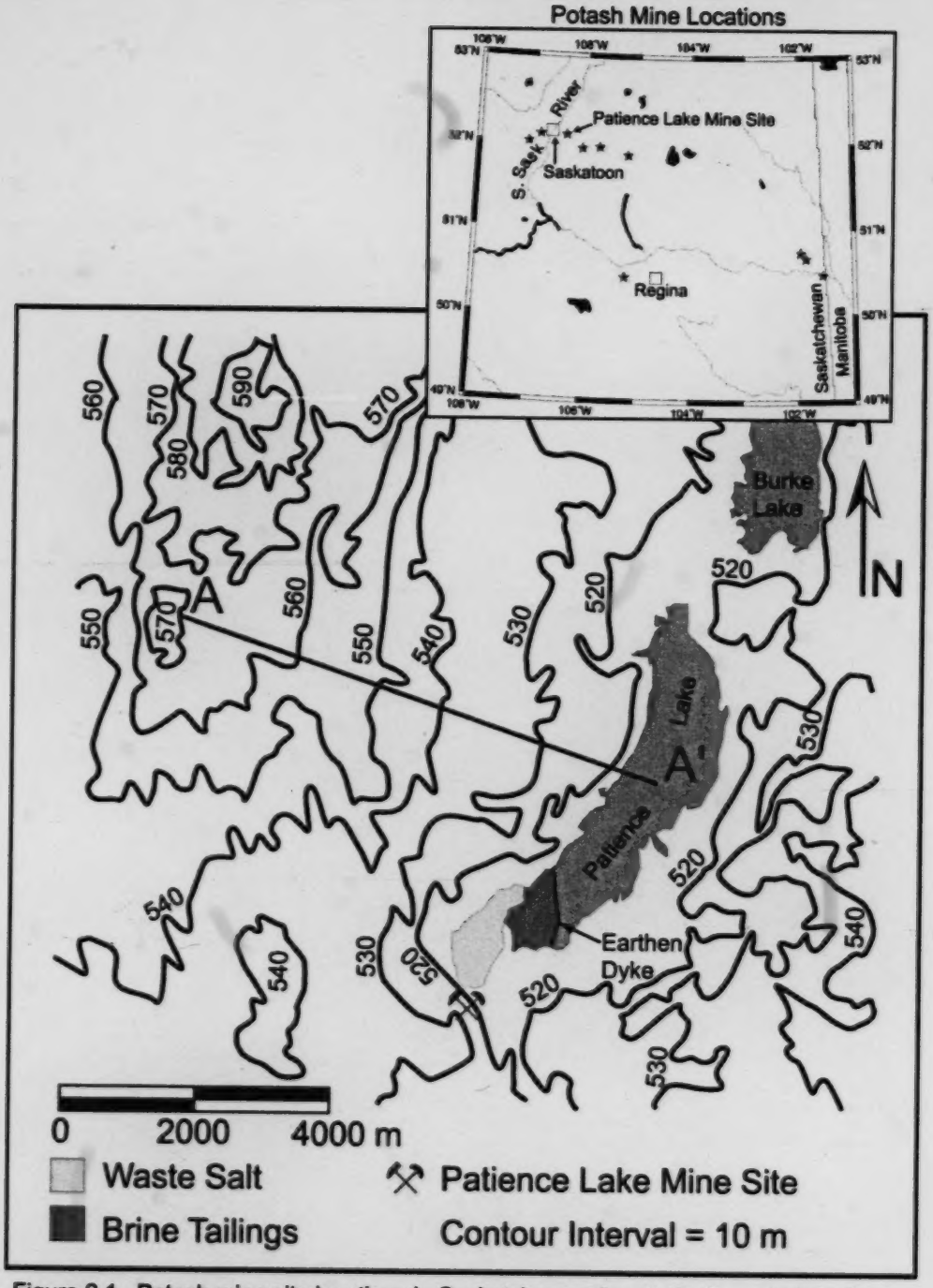

Figure 2.1. Potash mine site locations in Saskatchewan (inset), Patience Lake mine site location and numerical model cross section.

The geology directly underlying the mine site consists of Quaternary glaciolacusterine and till deposits (Battleford and Floral Formations). A regionally extensive aquifer (Forestry Farm Aquifer) is present approximately 25 m below the lake surface. Underlying the Forestry Farm Aquifer (FFA) is a thick, unoxidized, dense, grey till (Sutherland Group) and late Cretaceous age non-marine silt and clay bedrock (Chapter 1).

2.3 Modelling Methodology

Transient 2D, density-dependent solute transport simulations are conducted on an idealized cross section (A – A' on Figure 2.1) that represents the general topography and interpreted geology west of PL (Figure 2.2). Spatial scales of heterogeneity within the Battleford Formation till that produce unstable brine transport are investigated by changing the statistical parameters (horizontal and vertical correlation lengths and variance) of a stochastically generated permeability distribution.

Heterogeneity is represented using the natural log of permeability (ln{k}), which is assumed to be a random variable, Y_k, with a mean, $\overline{Y}_k$, and a variance, σ_Y^2. The correlation length, τ, is the distance at which the covariance of Y_k effectively becomes zero (i.e., the permeability at a point $\boldsymbol{x}$ is independent of permeability at some lag distance, $\boldsymbol{x} + \boldsymbol{h}$).

First, the horizontal correlation length and variance of the Battleford Formation permeability distribution are modified in a systematic manner to produce both stable and unstable brine transport, assuming fully-saturated groundwater flow. Additional simulations then consider the influence of the vertical correlation length and mean permeability on the stability of the system. Brine transport behavior, for both stable and unstable heterogeneous systems, is compared with the behavior of a homogeneous permeability distribution.

Finally, coupled saturated-unsaturated groundwater flow simulations are conducted for stable, unstable, heterogeneous and homogeneous systems and the brine transport results compared with the fully-saturated simulations, above.

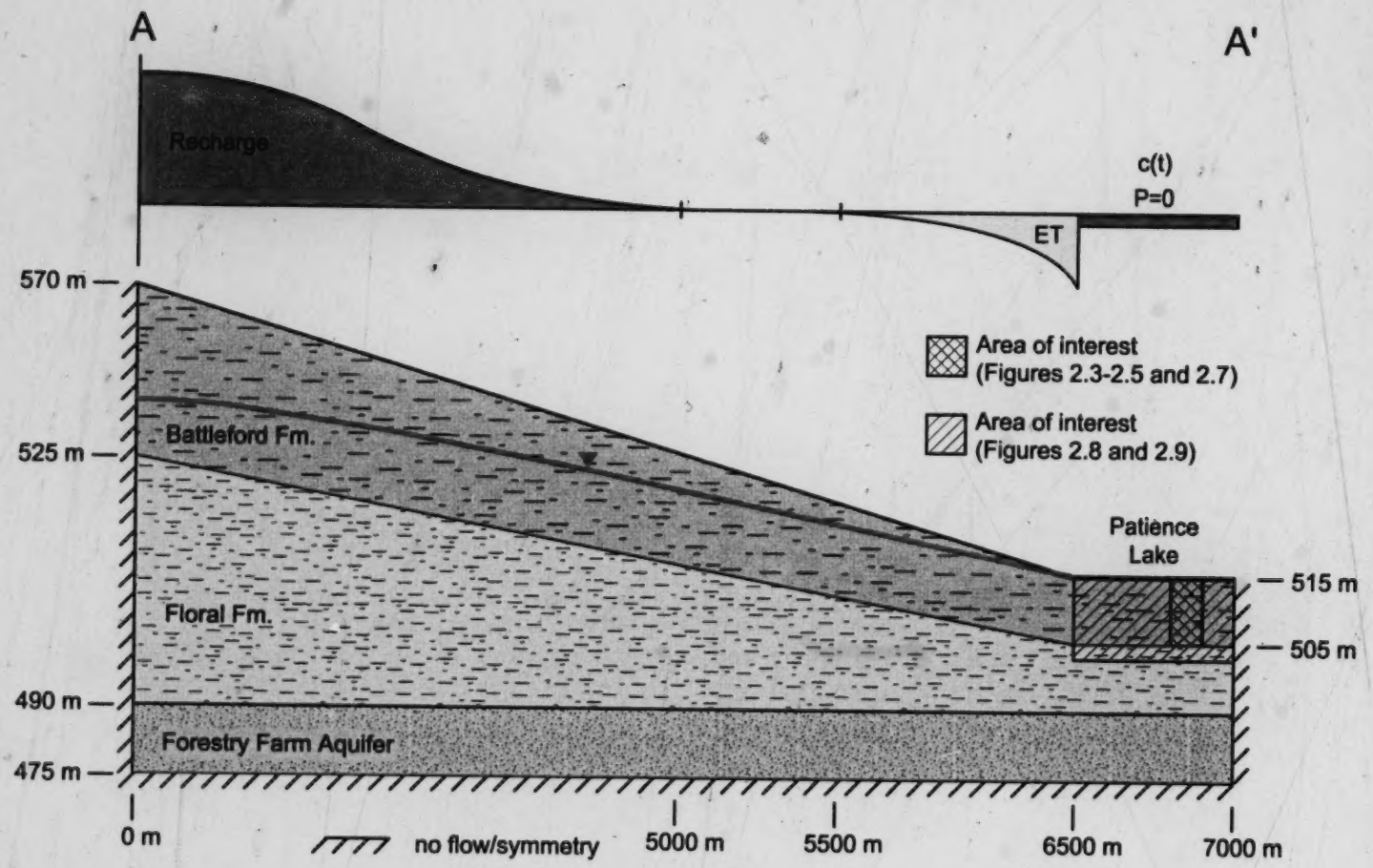

Figure 2.2. Cross section A - A'. Conceptual model and boundary conditions for numerical simulations (not to scale).

2.3.1 Conceptual Model

The mine site and PL are located in a topographic low with a mean surface elevation of 515 m above sea level (masl). In the north-south direction the land surface is nearly flat. Topographic divides east and west of the mine site create a local flow system that discharges into PL (Chapter 1). The base of the conceptual model is the Sutherland Group, a thick, clay till of early Pleistocene age, which is overlain by the FFA, a medium-grained sand aquifer. Two tills separate the FFA from the brine tailings: the Floral Formation is hard and has a higher clay content whereas the Battleford Formation above is soft and has a higher sand content (Christiansen, 1970). Average hydrogeologic parameters of the stratigraphic units are provided in Table 2.1.

The cross section chosen for the numerical simulations takes advantage of the symmetry of the problem. The domain is 7000 m long, 95 m deep at the west edge and 40 m deep at the east edge (Figure 2.2). The modelled system produces primarily vertical flow through the two tills into the FFA below and horizontal flow within the FFA, which then discharges into PL at the east.

Table 2.1. Hydrogeologic parameters used in numerical model

Formation	Material	k_h (m^2)	k_v (m^2)	n (-)
Battleford Fm.	Till	*$1x10^{-13}$	*$1x10^{-13}$	0.4
Floral Fm.	Till	$1x10^{-15}$	$1x10^{-14}$	0.4
Forestry Farm Aquifer	Sand	$4x10^{-12}$	$4x10^{-12}$	0.3

* mean permeability, see Table 2.3

2.3.2 The Numerical Model

SUTRA (Voss, 1984) has been used extensively to simulate 2D density-dependent solute transport problems. The model is based on a hybridization of finite-element and integrated finite-difference methods to solve the flow and transport equations. The SUTRA numerical formulation is described in Appendix B. The code has been previously verified (Voss and Souza, 1987). The solute analogue to the Elder (1967) thermal convection problem was solved to verify the version of the code used for the current simulations (Appendix C).

2.3.3 Boundary and Initial Conditions

The boundary conditions for the model domain are shown in Figure 2.2. The west and east sides of the model are groundwater divides and are considered no flow (symmetry) boundaries. The Sutherland Group, which lies below the section, has an estimated permeability of 10^{-18} to 10^{-17} m^2 (Chapter 1) and is of sufficient depth that its influence on the stability of the system, in the area(s) of interest (Figure 2.2), would be negligible. Thus, it was also considered a no flow boundary. Recharge is assumed to be normally distributed along the top of the domain (shown schematically in Figure 2.2). A positive (recharge) flux is applied at higher elevations. At lower elevations, where the water table is close to the land surface, a negative (discharge) flux is used to represent evapotranspiration (ET). A net flux of 2.51 mm/yr (recharge – evapotranspiration) represents approximately 0.7% of annual precipitation. The brine tailings are represented using a specified pressure and a time-dependent concentration boundary located along the top surface of the model from $6500 \leq x \leq 7000$ m. Pressure at an elevation of 515 m is set to 0 Pa, representing the brine surface. In SUTRA, fluid density varies linearly as a function of concentration. The brine is estimated to have a solute concentration of 0.3 kg/kg and a fluid density of 1200 kg/m^3, resulting in a coefficient of density change of 700 kg/m^3 (Table 2.2). The solute source function is ramped linearly from the background concentration (0.001 kg/kg) to 0.3 kg/kg over 1 month to maintain numerical stability.

Initial conditions for transient simulations consist of a uniform solute concentration of 0.001 kg/kg and a steady state pressure distribution generated from a non-density-dependent simulation.

2.3.4 Spatial and Temporal Discretization

The cross sectional domain is discretized into 17920 deformed rectangular elements and 18513 nodes. In the horizontal direction (Δx), elements are 15 m from $0 \leq x < 6300$ m and 5 m from $6300 \leq x \leq 7000$ m. In the vertical direction (Δz), elements within the Battleford Formation are 0.4 m beneath the brine source and increase to 1.8 m at $x = 0$ m. For the Floral Formation, Δz increases from 3 m beneath the brine source to

7 m at x = 0 m. For the FFA, Δz is 7.5 m. Time steps for transient simulations are geometrically ramped from Δt = 300 s to Δt = 86400 s using a multiplier of 1.02.

Table 2.2. Flow and transport parameters

Parameter	Value
Freshwater solute concentration (kg/kg)	0.001
Brine source solute concentration (kg/kg)	0.3
Freshwater density (kg/m^3)	1005.3
Coefficient of density change (kg/m^3)	700
Dynamic viscosity (kg/ms)	0.001
Fluid Compressibility (Pa^{-1})	4.5×10^{-10}
Longitudinal dispersivity (m)	2.5
Transverse dispersivity (m)	0.5
Molecular diffusion coefficient (m^2/s)	1×10^{-9}
Acceleration due to gravity (m/s^2)	9.81

2.3.5 Model Parameters

Flow and transport parameters are provided in Table 2.2. Unless otherwise specified, these model parameters remain constant for all simulations. The stochastic permeability distribution of the Battleford Formation is described in the following section. The permeability and porosity of the Floral Formation and FFA are given in Table 2.1.

2.3.6 Permeability Distributions of the Battleford Formation

The permeability (k) of the Battleford Formation is simulated stochastically to investigate the influence of geologic material heterogeneity in direct contact with the brine source. The spatial structure of this upper till will control the development of unstable fingers; therefore, the Floral Formation and FFA are modelled as homogeneous hydrostratigraphic units. Given the intensive CPU requirements in modelling density-dependent transport, a true stochastic analysis, involving multiple realizations for a single set of model parameters, would be time-prohibitive (a single, 1 yr simulation required 4 hours of CPU time on an IBM RS 6000 model 560 with a 266 MHz

processor). Instead, all simulations are carried out using the same random number seed, resulting in similar global permeability distributions. Varying the correlation length and variance result in statistically different permeability distributions that differ only locally (e.g., compare Figure 2.3a and 2.3b, described later).

Freeze (1975) suggested that the spatial distribution of permeability (k) is commonly log normal. Correlated random permeability fields were generated in log space ($Y_k = \ln\{k\}$) using the method developed by Robin et al. (1993). Resulting ln(k) values are then converted to real space ($k = e^{Y_k}$) for use in the SUTRA input files.

2.3.6.1 Horizontal Correlation Length and Variance

The first set of simulations (Group A) investigates the effect of horizontal correlation length (τ_x) and variance for permeability fields with a constant input mean $\overline{Y}_k$ of –29.933 ($k = 1x10^{-13}$ m^2) and vertical correlation length (τ_z) of 1.25 m. Table 2.3 provides a summary of Group A simulations conducted and the actual, back-calculated statistical parameters for each. The first number in the Simulation ID represents the nominal or input horizontal correlation length (τ_x). The second number refers to the input variance (σ_Y^2). The τ_x and σ_Y^2 are varied from 10 m to 40 m and 2.0 to 5.0, respectively. The horizontal discretization (Δx) of 5 m effectively limits the minimum scale of τ_x investigated to 10 m. Although the effective $\overline{Y}_k$ is not uniform between simulations, the overall difference is only 3% (in real space) and is considered insignificant.

The Battleford Formation mean permeability used in the Group A simulations is $1x10^{-13}$ m^2; however, Maathuis and van der Kamp (1994) estimate the hydraulic conductivity of shallow weathered tills in southern Saskatchewan between 10^{-8} and 10^{-7} m/s (corresponding to a permeability of 10^{-15} to 10^{-14} m^2). A higher mean permeability is selected for two reasons. First, a localized sand lens is interpreted at the site (Christiansen, 1999) that lies in direct contact with the PL sediments, which has a permeability of $7.5x10^{-12}$ m^2. In order to generate a permeability distribution encompassing both the reported range of values for a shallow till and the high permeability of the sand lens, a mean value of $1x10^{-13}$ m^2 is used. Second, using a

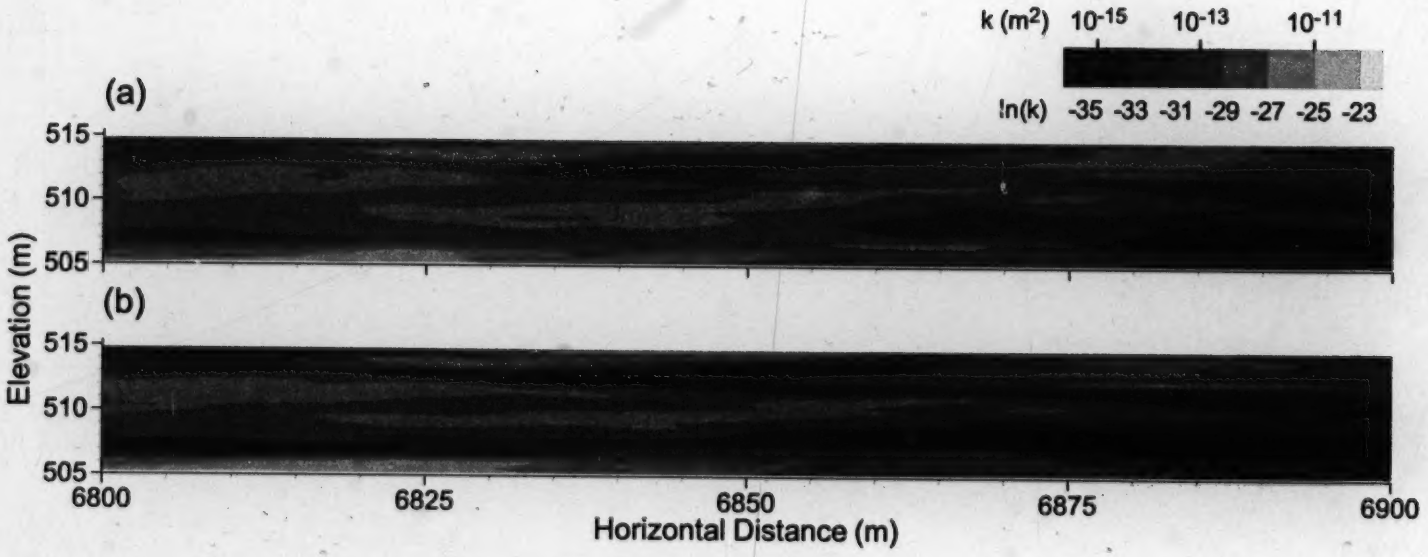

Figure 2.3. Simulated log permeability fields. (a) τ_x = 17.6 m, σ_Y^2 = 2.32 (A15-2.5). (b) τ_x = 41.8 m, σ_Y^2 = 4.28 (A40-5.0). τ_z = 1.4 m for both (a) and (b). (partial model domain, no vertical exaggeration)

higher mean permeability increases the likelihood of convective transport (Simmons and Sharp, 2000). This is considered a 'worst-case scenario' for convective brine transport from PL.

Table 2.3. Group A numerical simulation statistical parameters

Sim. ID*	$\overline{Y}_k$	k (10^{-14} m^2)	τ_x (m)	τ_z (m)	σ_Y^2
Nominal $\overline{Y}_k$ = -29.933 (k = 1x10^{-13} m^2)					
A10-2.0	-29.935	9.93	11.919	1.436	1.858
A10-2.5	-29.935	9.93	11.919	1.436	2.323
A10-3.0	-29.935	9.93	11.919	1.436	2.787
A10-3.5	-29.935	9.93	11.919	1.436	3.252
A15-2.5	-29.940	9.94	17.574	1.440	2.346
A15-3.0	-29.940	9.94	17.574	1.440	2.815
A15-3.5	-29.941	9.92	17.574	1.440	3.284
A15-4.0	-29.942	9.92	17.574	1.440	3.754
A20-3.0	-29.947	9.87	22.422	1.461	2.779
A20-3.5	-29.948	9.86	22.422	1.461	3.242
A20-3.7	-29.948	9.86	22.422	1.461	3.428
A20-4.0	-29.949	9.85	22.422	1.461	3.705
A20-4.5	-29.950	9.84	22.422	1.461	4.169
A25-3.0	-29.952	9.82	25.063	1.464	2.724
A25-3.5	-29.954	9.80	25.063	1.464	3.178
A25-3.75	-29.954	9.80	25.063	1.464	3.405
A25-4.0	-29.955	9.79	25.063	1.464	3.632
A25-4.5	-29.956	9.78	25.063	1.464	4.086
A30-3.5	-29.959	9.75	30.303	1.479	3.111
A30-4.0	-29.960	9.74	30.303	1.479	3.555
A30-4.5	-29.962	9.72	30.303	1.479	4.000
A30-5.0	-29.964	9.70	30.303	1.479	4.444
A35-4.0	-29.964	9.70	36.630	1.449	3.485
A35-4.5	-29.966	9.68	36.630	1.449	3.920
A35-5.0	-29.968	9.66	36.630	1.449	4.356
A40-4.5	-29.970	9.64	41.841	1.406	3.850
A40-5.0	-29.972	9.62	41.841	1.406	4.278

* See text for description of Sim. ID codes

2.3.6.2 Vertical Correlation Length and Mean Permeability

Simulations in Groups B and C, summarized on Table 2.4, consider both stable and unstable systems for the τ_x = 18 m permeability distribution in more detail. Group B simulations examine the effect of the vertical correlation length (τ_z); Group C simulations consider a factor of 10 reduction in mean permeability for three different σ_Y^2 values.

2.3.7 Unsaturated Flow

Group D simulations (Table 2.4) examine the effect of considering unsaturated flow. Once conditions for unstable brine transport are established, two simulations are re-run incorporating unsaturated flow to determine the effect on the transport solution. Water saturation (S_w) and relative permeability (k_r) are determined in the SUTRA model using the van Genuchten (1980) representation. Values specified for the residual saturation, S_r, and fitting parameters, α and n, are 0.25, $4x10^{-5}$ Pa^{-1} and 3.5 respectively and are chosen to represent a silty loam soil with an entry pressure of approximately 1 m (9860 Pa). No attempt is made to correlate the unsaturated soil properties with the simulated permeability field.

Table 2.4. Group B, C and D numerical simulation statistical parameters

Sim. ID	$\overline{Y}_k$	k (10^{-14} m^2)	τ_x (m)	τ_z (m)	σ_Y^2
Group B Simulations: Change τ_z					
B08-3.0	-29.933	10.00	17.794	0.842	2.773
B25-3.0	-29.951	9.83	18.416	3.458	2.807
B08-3.5	-29.933	10.00	17.794	0.842	3.235
B25-3.5	-29.952	9.82	18.416	3.458	3.275
Group C Simulations: $\overline{Y}_k$ = -32.236 (k = $1x10^{-14}$ m^2)					
C15-3.0	-32.244	0.992	17.574	1.440	2.815
C15-3.5	-32.244	0.992	17.574	1.440	3.284
C15-4.0	-32.245	0.991	17.574	1.440	3.754
Group D Simulations: Unsaturated Flow					
D15-3.0	-29.940	9.94	17.574	1.440	2.815
D15-3.5	-29.941	9.92	17.574	1.440	3.284

2.4 Model Results

The Group A simulations listed in Table 2.3 are used to establish whether unstable brine transport is likely to occur at this particular potash mine site. An unstable system is defined as one where (a) fingers of solute propagate into the subsurface and (b) solute fingers are accompanied by both upward and downward velocity vectors (convective flow).

Figures 2.4 and 2.5 show the simulated solute distribution after 0.3, 1 and 5 yr, for the area of interest indicated on Figure 2.2. The stable system (Figure 2.4) represents Sim ID. A15-2.5 (τ_x = 18 m, τ_z = 1.4 m, σ^2 = 2.3) and is the same permeability distribution as that shown in Figure 2.3a. The unstable system (Figure 2.5) represents Sim ID. A15-3.5. It has the same horizontal and vertical correlation length as the stable system but has a higher variance (σ^2 = 2.3; Table 2.3).

When the system is stable (Figure 2.4), brine migration beneath PL is uniform through both high and low permeability materials, indicating that solute transport is dominated by dispersion. The solute front (0.005 kg/kg) migrates to a depth of 1.5 m below the brine source after 1 yr and 3 m after 5 yr. When the system is unstable (Figure 2.5), increased brine migration is evident after 0.3 yr at x = 6840 m. After 1 yr, an unstable solute finger is well established and has propagated to a depth of 5.5 m. After 5 yr, the solute concentration at the base of the Battleford Formation (505 masl) has reached the source concentration of 0.3 kg/kg.

2.4.1 Horizontal Correlation Length and Variance

For a given τ_x (constant τ_z), Group A simulations are run with different variances (σ_Y^2) to produce both stable and unstable systems. Increasing the variance results in a broader range of simulated permeabilities. For example, a σ_Y^2 of 2.3 (A15-2.5) produces a permeability field where 95% of the values are between -26.9 and -33.0 (2.1×10^{-12} and 4.6×10^{-15} m^2), approximately one order of magnitude each side of $\overline{Y}_k$. In comparison, a σ_Y^2 of 4.3 (A40-5.0) results in a range of permeabilities between -25.8 and -34.1 (6.0×10^{-12} and 1.5×10^{-15} m^2), nearly two orders of magnitude each side of $\overline{Y}_k$. The differences are visually apparent in Figure 2.3 which shows the ln(k) distribution for A15-2.5 and A40-5.0 for a 100 m wide region of the model domain directly beneath the brine source. Given that a log normal distribution is skewed toward lower values, the low permeability regions (dark blue) in Figure 2.3a become even lower in Figure 2.3b when the variance increases. Because the same random number seed is used for each, high and low permeability lenses occur in the same approximate location. Figure 2.3b also illustrates that low permeability lenses become more continuous when τ_x increases.

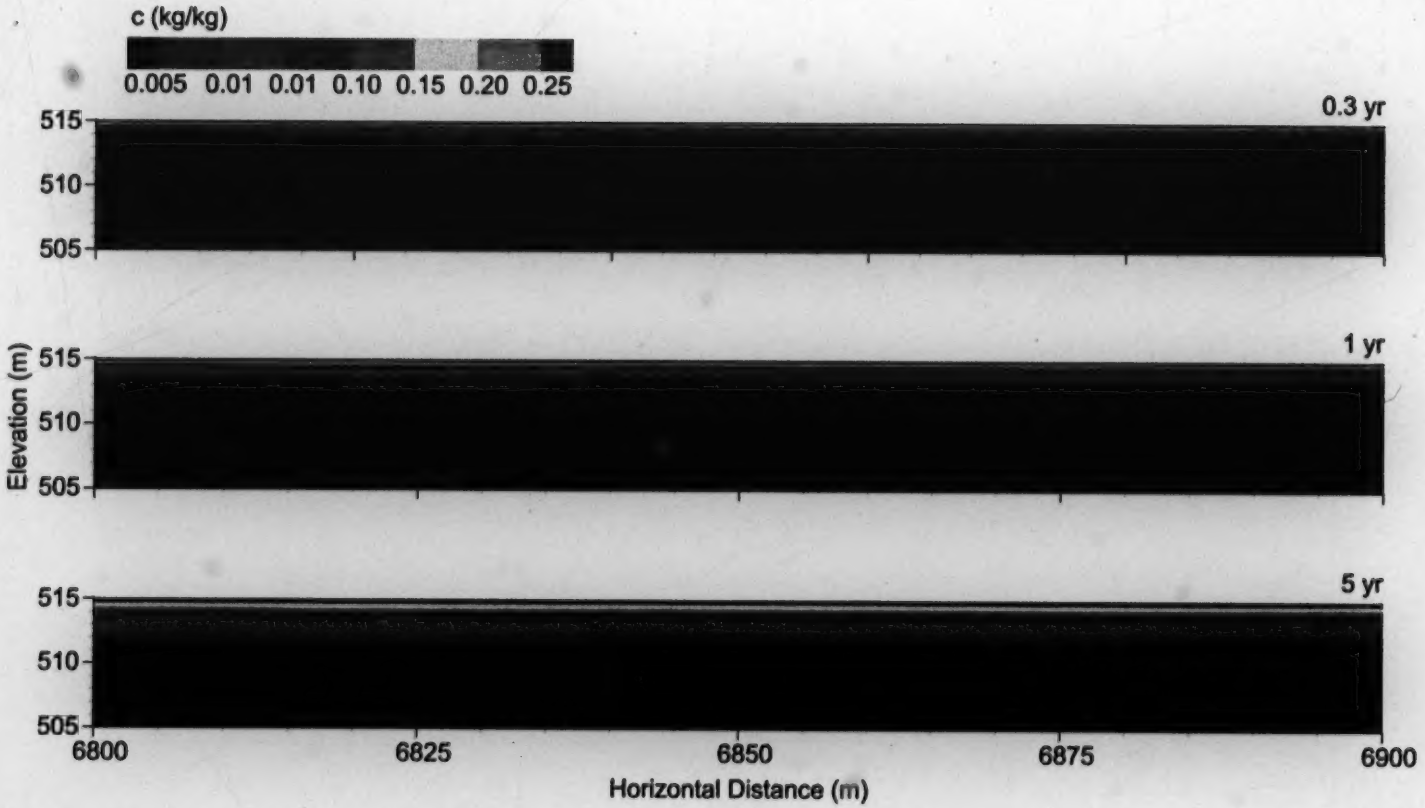

Figure 2.4. Simulated solute distribution for a stable system (A15-2.5) after 0.3, 1, and 5 yr.

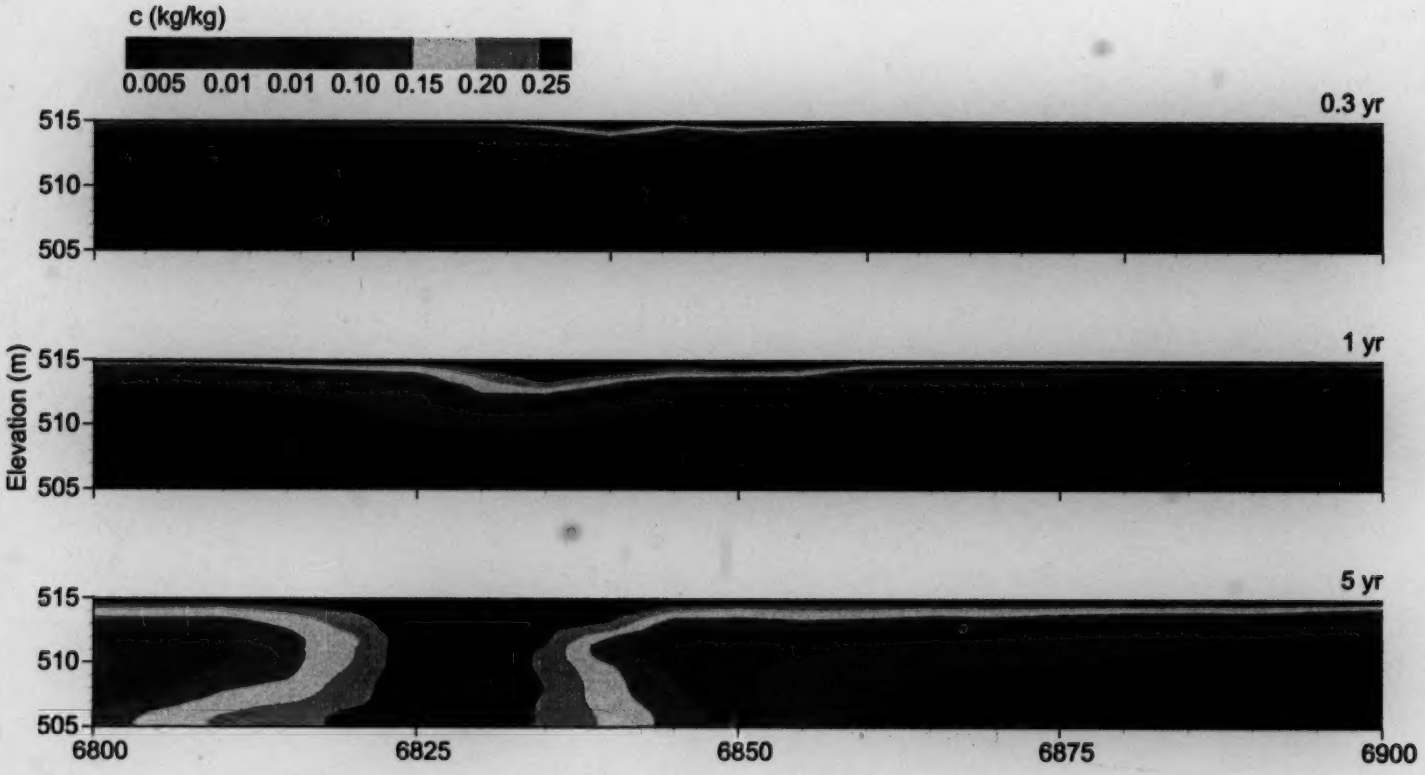

Figure 2.5. Simulated solute distribution for an unstable system (A15-3.5) after 0.3, 1, and 5 yr.

The results from Group A simulations are plotted on a graph of variance versus horizontal correlation length to produce a Stability Diagram (Figure 2.6). Stable simulations are indicated by a "●" and unstable simulations by a "✱". In the range of values tested, the stability relationship between ln(k) variance and horizontal correlation length is approximately linear. As τ_x increases, larger variances are required to produce unstable flow. At the maximum τ_x investigated (41.8 m), a total permeability range of approximately four orders of magnitude does not result in instability. Higher variances are not simulated because variability greater than four orders of magnitude on the scale of tens of metres is considered unlikely, even in a glacial geologic setting. As τ_x increases, both high and low permeability lenses become longer and more connected (Figure 2.3). The occurrence of low permeability lenses dominates a log normal distribution and therefore stability increases with τ_x.

Small perturbations are evident at early times for all stable simulations; however, they often decay over time and do not result in solute fingers or convective flow. After 1 yr, solute migrates only 1.5 m (estimated at c = 0.005 kg/kg) for stable simulations, indicating that transport is dominated by dispersion processes. For unstable simulations, the first fingers are evident after approximately 75 days and continue to propagate into the subsurface. The intensity of convective flow appears to increase with the variance. For instance, after 1 yr, Simulation A15-3.5 results in a single solute finger approximately 5.5 m deep whereas Simulation A15-4.0 produces two fingers reaching a maximum depth of 7.0 m (not shown).

Figure 2.6 illustrates the position of the stability-instability transition zone after 1 yr. To confirm that stable simulations do not eventually become unstable, shifting the position of the transition zone, 10 yr simulations are conducted for stable systems adjacent to the transition zone. All simulations stable after 1 yr remain stable at 10 yr.

2.4.2 Vertical Correlation Length

Group A simulations are run with a nearly constant vertical correlation length (τ_z) of approximately 1.45 m. However, the thickness of the high and low permeability lenses should affect the stability of the system. Four Group B simulations are considered in which the horizontal correlation length (τ_x) is held constant at approximately 18 m and τ_z

is adjusted up and down for both stable and unstable cases (Table 2.4; corresponding with A15-3.0 and A15-3.5 on Table 2.3). Recall that Simulation A15-3.5 is unstable after 1 yr. Decreasing τ_z to 0.84 m (B08-3.5) also results in an unstable system; however, increasing τ_z to 3.46 m (B25-3.5) produces a stable system. Hence, an unstable system becomes stable by increasing τ_z. A similar outcome results when beginning with a stable system (A15-3.0). Reducing τ_z to 0.84 m (B08-3.0) produces an unstable system, whereas increasing it to 3.46 m (B25-3.0) produces a stable system. A decrease in τ_z causes a stable system to become unstable.

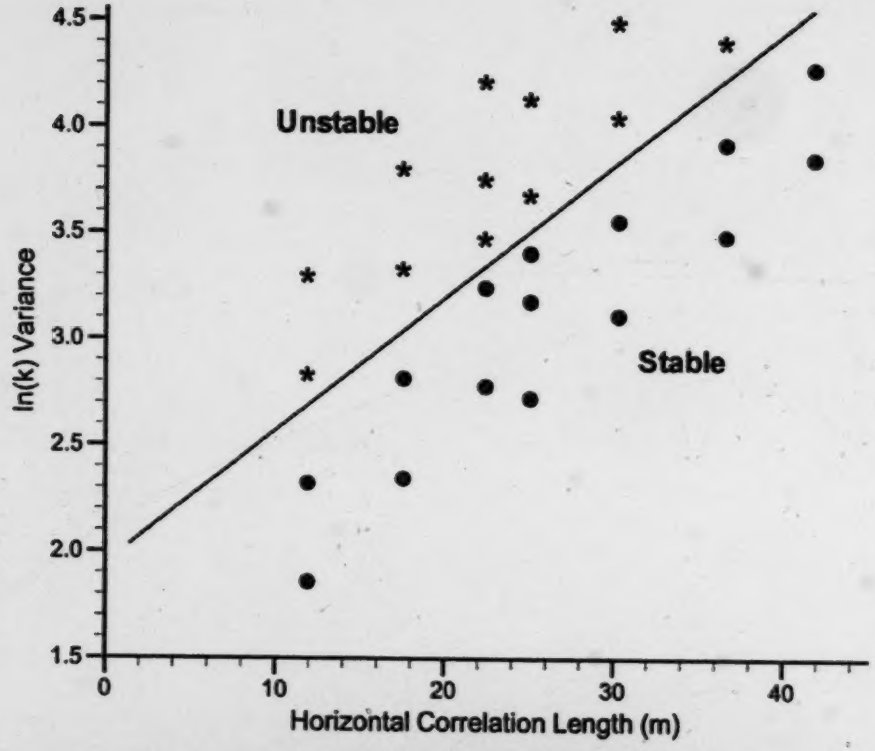

Figure 2.6. Variance versus horizontal correlation length for Group A simulations after 1 year. Stable simulations are indicated by a "●" and unstable simulations by a "*". The solid line indicates the transition from a stable to an unstable system.

Comparing the flow fields for an unstable, small τ_z case with a stable, large τ_z case provides some explanation as to why this occurs. The permeability distributions in Figure 2.7 are overlain with velocity vectors at t = 18 d (prior to the onset of instability).

When τ_z is small (Figure 2.7a), water is forced to follow a more tortuous path around thin, low permeability media. The orientation of the velocity vectors becomes highly variable as water approaches the brine surface. This divergent flow pattern must be a least partly responsible for the onset of instability. Compare this to velocity vectors in Figure 2.7b, which remains stable. The flow field is more uniform in the thicker high permeability lenses.

2.4.3 Reduced Mean Permeability

Previous studies on instability criteria have suggested that the stability of a system increases as the permeability decreases. However, such analyses did not incorporate an initial vertical groundwater flow component. Simmons and Sharp (2000) and Bachmat and Elrick (1970) considered systems that were initially hydrostatic. The system investigated by Schincariol et al. (1997) initially had a horizontal flow system. Bues and Aachib (1991) did investigate convective flow in a column with an initial upward flow; however, the effect of permeability was not investigated. In this study, the no flow boundary condition on the east side of the model domain forces all water flowing in the Forestry Farm Aquifer to discharge into PL, resulting in primarily vertical flow beneath the brine source.

Group C simulations hold τ_x and τ_z constant (17.6 m and 1.44 m respectively, Table 2.4) and reduce the mean k by an order of magnitude to 1×10^{-14} m^2 ($\overline{Y}_k = -32.24$). The σ_Y^2 is varied in order to cross the original stability-instability transition zone on Figure 2.6. The results show that stability does not necessarily increase but convective flow does diminish significantly. Solute concentration and velocity vectors are plotted on Figure 2.8 for corresponding Group A and C simulations after a period of 10 yrs. Simulation C15-3.0 should be stable (Figure 2.8b); however, a pseudo-stable system results. Small lobes of brine are produced in areas of high permeability, but these lobes are not density-derived. They are produced by increased dispersion due to preferential flow.

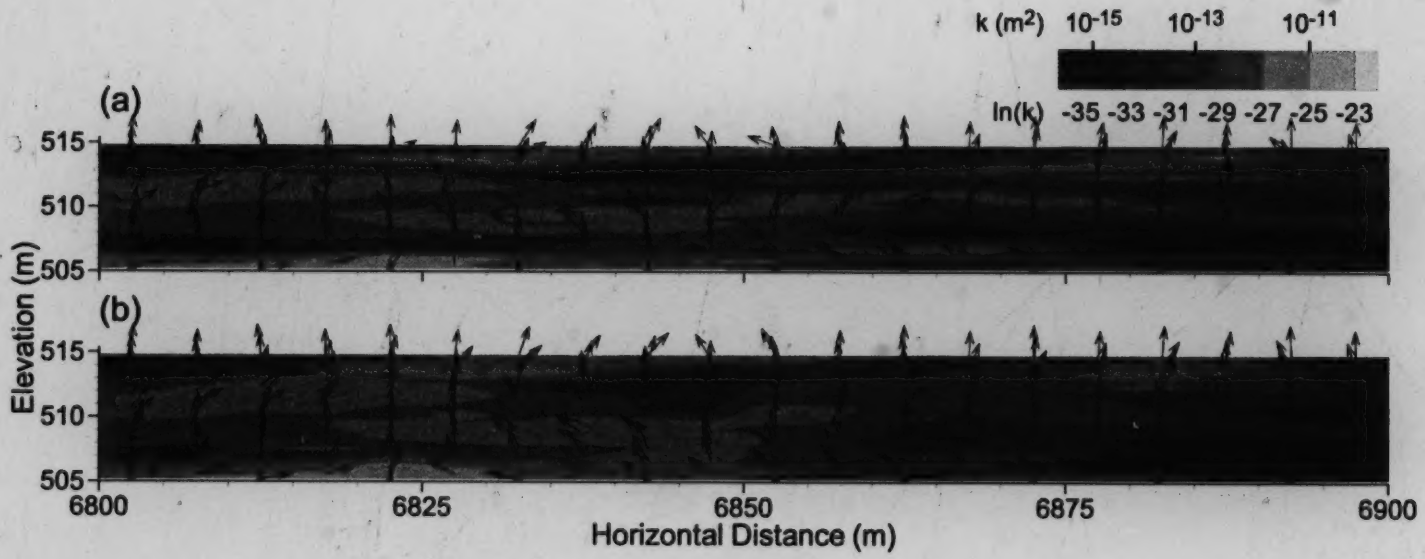

Figure 2.7. Simulated log permeability fields and velocity vectors at t = 18 days for different vertical correlation lengths. (a) τ_z = 0.84 m (B08-3.5). (b) τ_z = 3.5 m (B25-3.5). No vertical exaggeration.

A decrease in permeability results in a slight increase in the water table elevation in the recharge area. Thus, there is a larger vertical component of flow through the aquitard, resulting in higher flow through the FFA and higher vertical groundwater velocities discharging into PL. The higher flow is focused through higher permeability material and because dispersion ($D = \alpha_L v$) is a function of velocity magnitude, not direction, an increase in velocity results in the formation of dispersive lobes of brine. The dispersive nature of these lobes was confirmed using a non-density-dependent simulation with the same model and statistical parameters as in C15-3.0. The non-density-dependent simulation produced identical lobes as the density-dependent simulation.

For an unstable system, the finger of solute in the high permeability case (Figure 2.8c) extends to the bottom of the Battleford Formation and produces large vertical flow rates. In the low permeability case (Figure 2.8d), convective flow is significantly dampened and actually develops in a different location than in the high permeability case. During the simulation, the unstable finger encounters lower permeability material at z = 512 m, inhibiting its continued advance. After 10 yrs, the convective finger does not migrate beyond the dispersive zone in the stable portion of the plume (Figure 2.8d). Although convective flow does occur in the low permeability system, solute transport is dominated by dispersion.

2.4.4 Comparisons With a Homogeneous Permeability Field

The results of the heterogeneous simulations are compared with results from a homogeneous, isotropic Battleford Formation permeability distribution ($k = 1 \times 10^{-13}$ m^2). As expected, the homogeneous system is stable. Breakthrough curves of relative concentration versus time for two points beneath the brine source are used to compare homogeneous and both stable and unstable heterogeneous simulations (Figure 2.9). The first point (P1) is in the stable portion of the plume, near the west edge of the brine source, 0.4 m below the surface. The second point (P2) is within the unstable finger, shown in Figure 2.9, at a depth of 0.8 m.

At P1, the early time concentrations for both stochastic simulations (stable and unstable) are marginally higher than for the homogeneous case, indicating that P1 is located in a higher permeability lens (compared to the homogeneous case). However, as time

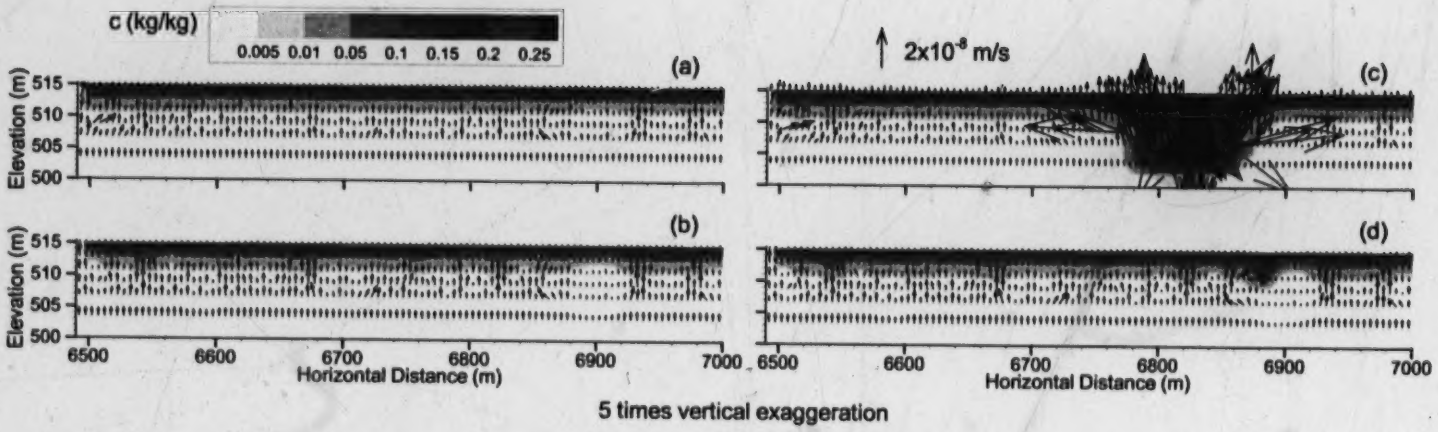

Figure 2.8. Concentration distribution and velocity vectors beneath the brine source after 10 years. (a) high k - stable (A15-3.0). (b) low k - pseudo-stable (C15-3.0). (c) high k - unstable (A15-3.5). (d) low k - unstable (C15-3.5).

progresses, these differences diminish, resulting in a $c/c_{max} = 0.79$ in all three cases after 10 yrs.

At P2, when the system is stable, there is essentially no difference between the heterogeneous and homogeneous simulations, where c/c_{max} only reaches 0.57 after 10 yrs. Conversely, when the system is unstable, the relative concentration reaches a value of 0.96 after only 1 yr, as the convective finger quickly migrates past the observation point (Figure 2.9).

For a stable system, there is no difference in brine transport between homogeneous and heterogeneous permeability distributions. When instabilities form, brine migration rates in the immediate vicinity of the instability are several times faster than for the homogeneous or stable systems. However, beyond the influence of the instability, brine migration rates match homogeneous results.

2.4.5 Unsaturated Flow

Incorporating unsaturated flow into a density-dependent model magnifies the complexity of the problem considerably. Unsaturated soil-water relationships (saturation versus pressure; relative permeability versus saturation) must be defined for each soil type and uncertainty in these input parameters results in additional uncertainty in the model results. In addition, the increased CPU time required for unsaturated flow calculations can become significant. Group D simulations are designed to determine, from a numerical standpoint, whether the transport solution is sensitive to unsaturated flow above the water table.

Two simulations incorporating unsaturated flow are conducted using the same statistical parameters as Simulations A15-3.0 and A15-3.5. The only difference is that, in order to achieve an initial steady state flow solution, transient unsaturated flow is simulated prior to introduction of the brine source. The resulting unsaturated steady state flow solution has a water table up to 20 cm higher than the saturated model, at the west edge of the model domain, where recharge was highest. Elsewhere within the domain, differences are less than 20 cm.

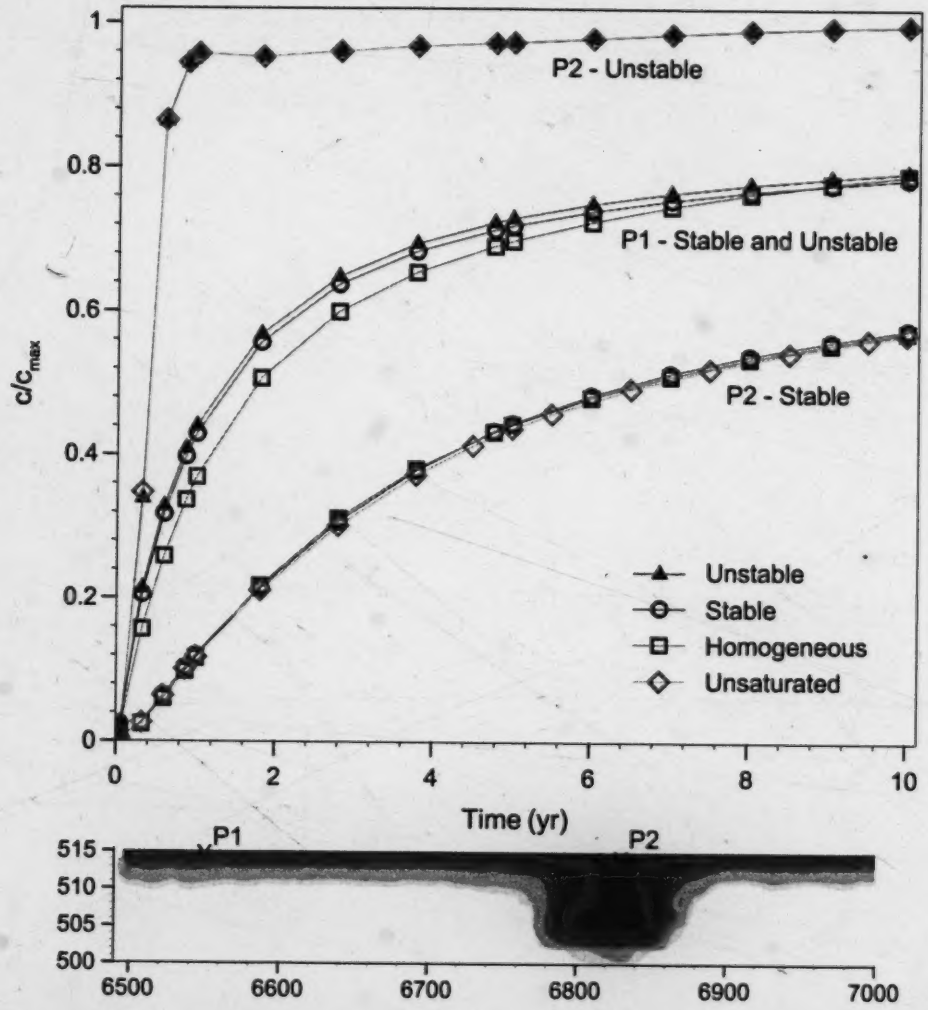

Figure 2.9. Breakthrough curves of relative concentration (c/c_{max}) for two points beneath the brine source. P1 (6550, 514.6) is within a stable portion of the plume. P2 (6835, 514.2) is within the unstable finger.

For both the stable (D15-3.0) and unstable (D15-3.5) simulations, there is no difference in the solute distribution after 10 yrs, compared with the saturated simulations (Figure 2.9, P2 only). The overall impact of simulating unsaturated flow is considered negligible.

2.5 Discussion and Conclusions

Previous studies have shown that for more complex systems, the use of a Rayleigh number to predict the onset of density-driven instabilities becomes unreliable. This study establishes the spatial correlation necessary to produce instabilities in a till with a mean permeability of $1x10^{-13}$ m^2, an overlying brine source of 0.3 kg/kg and upward groundwater flow. At a horizontal correlation length of 17.6 m, a ln(k) variance of 3.0 is necessary to create unstable flow. This corresponds to a range of permeabilities exceeding two orders of magnitude. When the horizontal correlation length is increased to 36.6 m, permeability values need to vary by 4 orders of magnitude to create instabilities. To accurately assess the spatial structure of the tills at this site, data would need to be collected at approximately the same scale as these numerical simulations. Unfortunately, such detailed information does not exist. Nevertheless, the available geologic data may still be of some use in determining whether groundwater flow is stable or unstable at this site.

Figure 2.10 is a cross section interpreted from four, relatively detailed, borehole logs of the Battleford Formation located south of the mine site. On a macro scale, fine-grained units (silt/clay, till) appear to be horizontally correlated over distances of at least several hundred metres, if not thousands of metres. Coarse-grained units appear more variable but horizontal correlation lengths are still on the order of hundreds of metres. The variability of the permeability between the fine- and coarse-grained units could reasonably be several orders of magnitude; however, based on the model results, given such long horizontal correlation distances, this variability is unlikely to produce density-driven instabilities. Within each of the units in Figure 2.10, the variability of the permeability would be significantly lower. It is unlikely the permeability within a single unit would vary by more than two orders of magnitude within 10 or 15 m. In addition, the current modelling demonstrates that an increased correlation length in the vertical direction promotes stability. Figure 2.10 illustrates that the vertical correlation length easily exceeds the 1.45 m used in the numerical simulations. Therefore, it is reasonable to conclude that groundwater flow at the mine site will be stable.

The stabilizing effect of a lower mean permeability is partially offset by increased dispersion. Small lobes of solute develop in the low permeability case that are absent in

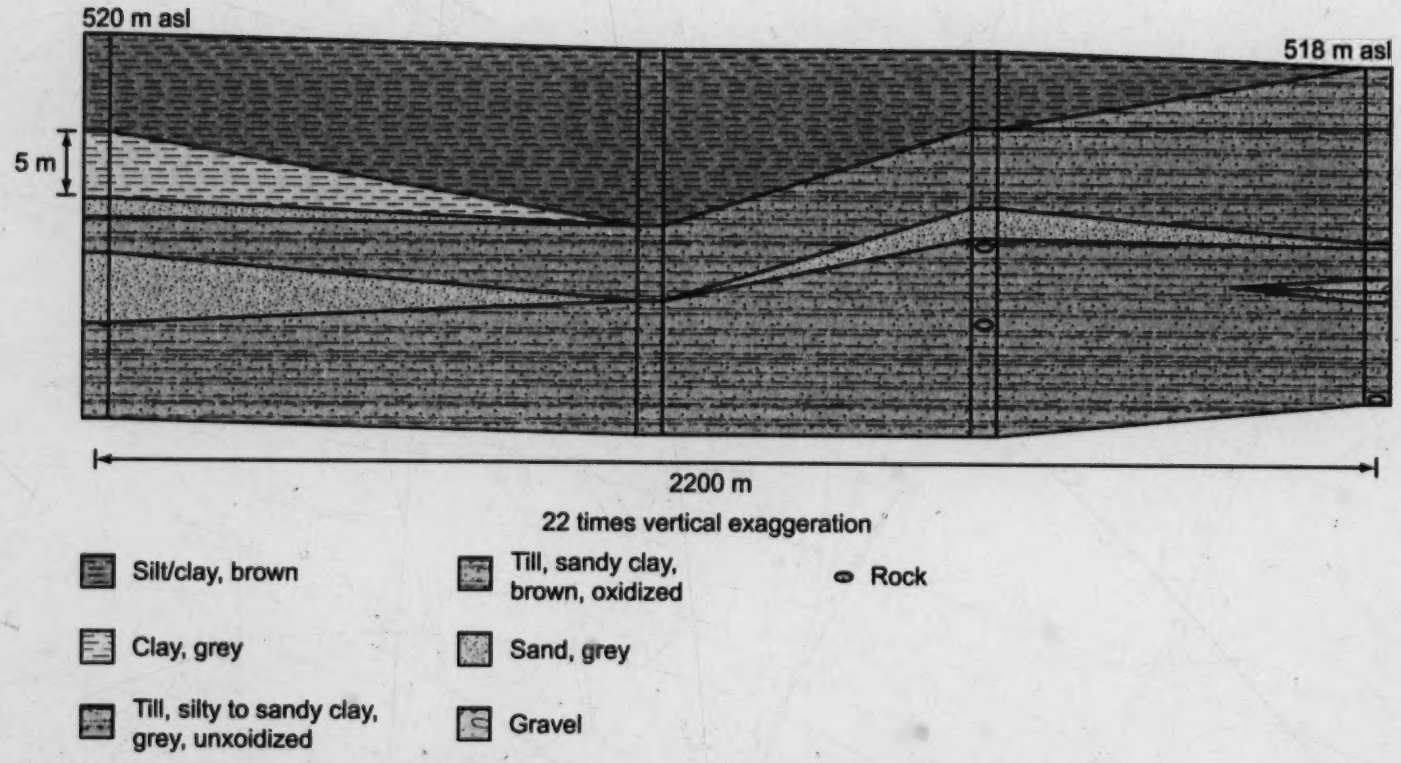

Figure 2.10. Cross section of Battleford Formation deposits south of the Patience Lake mine site.

the high permeability case. It is shown that fluid density differences do not produce these pseudo-stable lobes. When instabilities do occur, the lower mean permeability significantly dampens the solute migration rate and the instability does not extend beyond the dispersive front in the stable portion of the plume.

For stable flow, the solute distribution after 10 yrs in the heterogeneous system matches that of the homogeneous system and brine transport is dominated by dispersion. In addition, the incorporation of the unsaturated zone has a negligible impact on the transport solution. The results of this 2D modelling illustrate that, in the absence of large-scale high permeability features, the hydrodynamics beneath the brine retention pond behave as a saturated, homogeneous, and stable system.

More detailed brine transport analysis, conducted in Chapter 3, utilizes the results from the current study. Small-scale heterogeneities in direct contact with the brine source are modelled as homogeneous units. Unsaturated flow is neglected.

2.6 References

Bachmat, Y. and Elrick, D.E., 1970. Hydrodynamic instability of miscible fluids in a vertical porous column. Water Resources Research, 6(1): 156-171.

Bues, M.A. and Aachib, M., 1991. Influence of the heterogeneity of the solutions on the parameters of miscible displacement in saturated porous medium Part 1: stable displacement with density and viscosity contrasts. Experiments in Fluids, 11: 25-32.

Christiansen, E.A., 1970. Geology. In: E.A. Christiansen (Editor), Physical environment of Saskatoon, Canada. National Research Council of Canada, 68 p.

Christiansen, E.A., 1999. Geology of the PCS Patience Lake mine area, Unpublished report prepared for the Potash Corporation of Saskatchewan, June 21, 1999.

Elder, J.W., 1967. Transient convection in a porous medium. Journal of Fluid Mechanics, 27(3): 609-624.

Freeze, R.A., 1975. A stochastic-conceptual analysis of one-dimensional groundwater flow in nonuniform homogeneous media. Water Resources Research, 11(5): 725-741.

Frind, E.O., 1982. Simulation of long-term transient density-dependent transport in groundwater. Advances in Water Resources, 5: 73-88.

Huyakorn, P.S., Andersen, P.F., Mercer, J.W. and White, H.O., 1987. Saltwater intrusion in aquifers: development and testing of a three-dimensional finite element model. Water Resources Research, 23(2): 293-312.

Jones, G.D., Smart, P.L., Whitaker, F.F., Rostron, B.J., Machel, H.G., 2003. Numerical modeling of reflux dolomitization in the Grosmont platform complex (Upper Devonian), Western Canada sedimentary basin. AAPG Bulletin, 87(8): 1273-1298.

List, E.J., 1965. The stability and mixing of a density-stratified horizontal flow in a saturated porous medium. Report KH-R-11, California Institute of Technology, Pasadena.

Maathuis, H. and van der Kamp, G., 1994. Subsurface brine migration at potash waste disposal sites in Saskatchewan: final report. Saskatchewan Research Council, Pub. No. R-1220-10-E-94.

Robin M.J.L., Gutjahr, A.L., Sudicky, E.A. and Wilson, J.L., 1993. Cross-correlated random field generation with the direct Fourier transform method. Water Resources Research, 29(7): 2385-2397.

Schincariol, R.A., 1998. Dispersive mixing dynamics of dense miscible plumes: Natural perturbation initiation by local-scale heterogeneities. Journal of Contaminant Hydrology, 34: 247-271.

Schincariol, R.A. and Schwartz, F.W., 1990. An experimental investigation of variable density flow and mixing in homogeneous and heterogeneous media. Water Resources Research, 26(10): 2317-2329.

Schincariol, R.A., Schwartz, F.W. and Mendoza, C.A., 1994. On the generation of instabilities in variable density flow. Water Resources Research, 30(4): 913-927.

Schincariol, R.A., Schwartz, F.W. and Mendoza, C.A., 1997. Instabilities in variable density flows: Stability and sensitivity analyses for homogeneous and heterogeneous media. Water Resources Research, 33(1): 31-41.

Simmons, C.T. and Narayan, K.A., 1997. Mixed convection processes below a saline disposal basin. Journal of Hydrology, 194: 263-285.

Simmons, C.T. and Sharp, J.M., 2000. On variable-density groundwater flow in heterogeneous porous media. In: Groundwater: Past Achievements and Future Challenges, Sililo et al. (eds). Balkema, Rotterdam, 425-430.

Swartz, C.H. and Schwartz, F.W., 1998. An experimental study of mixing and instability development in variable-density systems. Journal of Contaminant Hydrology, 34: 169-189.

Tallin, J.E., Pufahl, D.E. and Barbour, S.L., 1990. Waste management schemes of potash mines in Saskatchewan. Canadian Journal of Civil Engineering, 17: 528-542.

van Genuchten, M.Th., 1980. A closed-form equation for predicting the hydraulic conductivity of unsaturated soils. Soil Science Society of America Journal, 44: 892-898.

Voss, C.I., 1984. SUTRA: A finite element simulation model for saturated-unsaturated, fluid-density-dependent groundwater flow with energy transport or chemically reactive single species solute transport. U. S. Geological Survey Water Resource Investigations, Report 84-4369, 409 p.

Voss, C.I. and Souza, W.R., 1987. Variable density flow and solute transport simulation of regional aquifers containing a narrow freshwater-saltwater transition zone. Water Resources Research, 23(10): 1851-1866.

Wooding, R.A., 1962. Free convection of fluid in a vertical tube filled with porous material. Journal of Fluid Mechanics, 13: 129-144.

Wooding, R.A., Tyler, S.W. and White, I., 1997. Convection in groundwater below an evaporating salt lake: 1. Onset of instability. Water Resources Research, 33(6): 1199-1217.

Chapter 3

Groundwater flow and brine transport modelling at a potash mine site in Saskatchewan

3.1 Introduction

Approximately one third of the world's potash reserves are located in Saskatchewan, Canada, which are mined for use in potassium fertilizer. However, for every tonne of potash produced, two tonne of solid NaCl and 1 to 2 m^3 of brine talings are produced (Tallin et al., 1990). These waste streams are commonly stored on the land surface or in unlined retention ponds and represent a potential threat to groundwater resources in the vicinity of potash mine sites. This study investigates the potential migration of brine tailings into the subsurface at the Potash Corporation of Saskatchewan (PCS) Patience Lake mine site, located 18 km east of Saskatoon, Saskatchewan (Figure 3.1).

Hydrologically closed lake basins, where evaporation exceeds precipitation for long periods of time, occur exclusively in arid and semi-arid climates. This long-term climatic imbalance results in perennial or "dry" lakes that are sustained by groundwater discharge and have no surface water outlet. Over time, groundwater discharge to such closed lakes can result in the accumulation of salts, creating a hydraulically unstable situation, where dense brine solutions overlie less dense native groundwater (Duffy and Al-Hassan, 1988). Convection of groundwater can occur if density gradients overcome hydraulic gradients, resulting in brine migration rates that exceed diffusion by several orders of magnitude (Simmons and Narayan, 1997). Patience Lake (PL) was a closed, saline lake prior to the onset of potash mining activities. Brine storage and disposal has accelerated the accumulation of dissolved salts in PL.

Several studies have investigated subsurface solute migration as a result of fluid density gradients in closed basin systems. Most recent investigations incorporated numerical modelling to determine whether convection of brine is likely to occur and to identify key characteristics that influence brine migration patterns and rates. Duffy and Al-Hassan (1988) used a 2D numerical model to simulate the Great Basin in western Utah. They

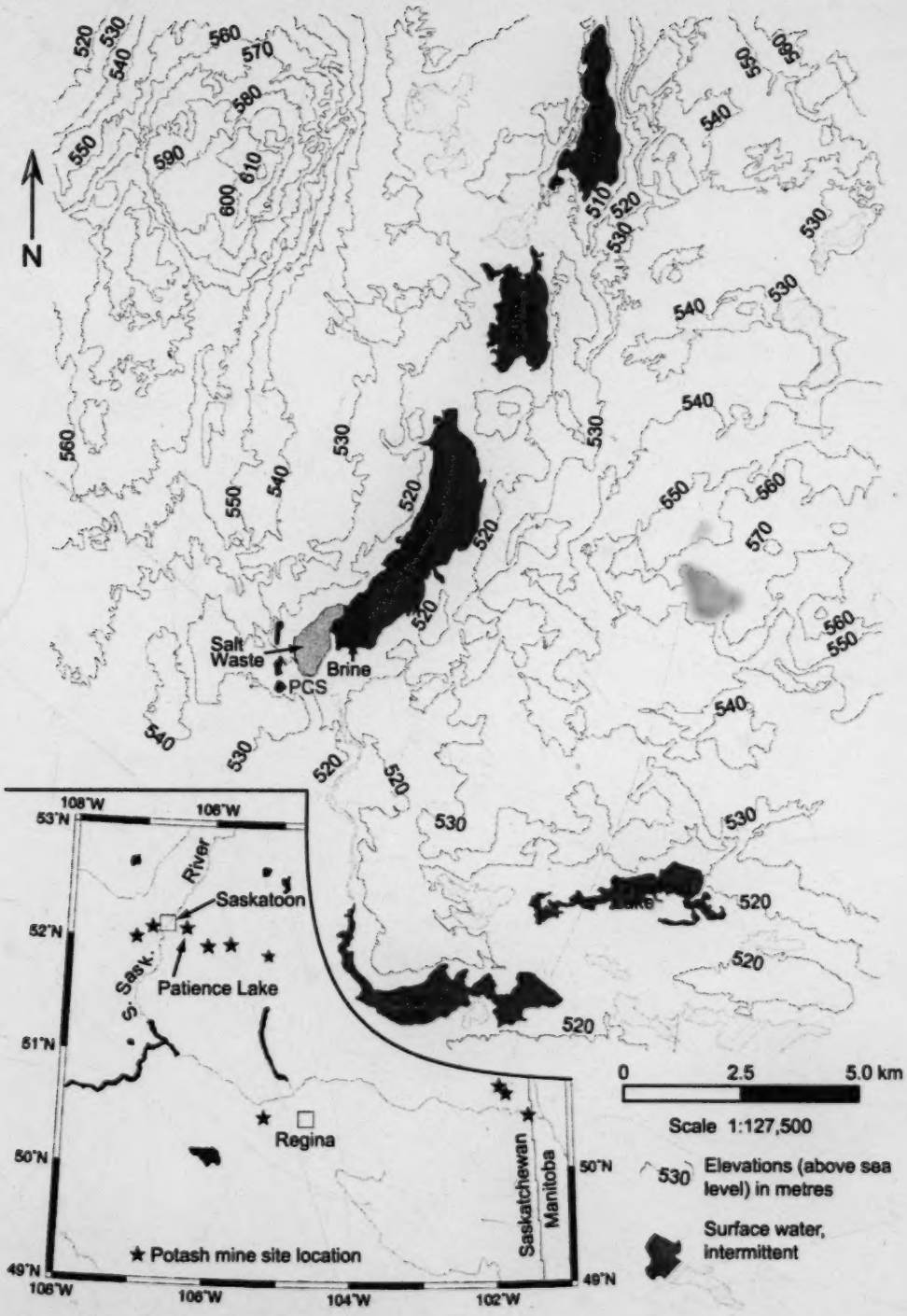

Figure 3.1. Site location and study area.

determined that large density contrasts and/or small hydraulic driving forces cause convection of dense brine fluids. Rogers and Dreiss (1995a) utilized a radially symmetric numerical model to simulate the steady-state solute distribution for Mono Lake basin in California. Instead of representing the asymmetry of the groundwater flow system using a 3D flow and transport model, a 2D sensitivity analysis was used. Their results indicate that higher recharge rates on one side of the basin force the saline-fresh groundwater interface beneath the saline lake; lower recharge rates on the other side of the basin push the interface beyond the lake, toward the basin edge. Rogers and Dreiss (1995b) simulated the effect of transient Mono Lake levels on the solute distribution. Higher lake levels increased the density gradient and forced solute into the subsurface, shifting the fresh-saline groundwater interface toward the basin edge; lower lake levels favoured hydraulic forces resulting in a shift of the fresh-saline groundwater interface toward the lake margin and increased the solute concentration in the lake.

Narayan and Armstrong (1995), Simmons and Narayan (1998) and Simmons et al. (2002) investigated brine migration from saline water disposal basins in southeast Australia. 2D numerical simulations were used to estimate solute fluxes from the Lake Ranfurly disposal basin to the River Murray for various groundwater interception (pumping) scenarios (Narayan and Armstrong, 1995). Their results show that the salt load to the River Murray was sensitive to the pumping rate and was over 10% greater when density-dependent flow was accounted for. Simmons and Narayan (1998) determined that salt transport near Lake Tutchewop was controlled by diffusion and dispersion, and was sensitive to elevated lake and salinity levels. Simmons et al. (2002) studied brine migration at the Lake Mourquong disposal basin, Australia. The hydrogeologic setting at Lake Mourquong is similar to that of PL because it is a natural groundwater discharge area (subsequently altered by saline water disposal) and a localized, high permeability, hydraulic connection exists between the brine disposal facility and a regional aquifer (see Section 3.2.1). Modelling results determined that convective transport was likely in areas of high permeability, resulting in brine migration to the base of the regional aquifer in less than their 23 year simulation period. The salt load to the aquifer was most sensitive to disposal basin salinity, hydraulic conductivity and disposal basin hydraulic head. Simmons et al. (2002) noted that the large dispersivities they used, which were needed to maintain numerical stability for their coarse horizontally discretized mesh, overestimated mechanical solute mixing in areas

where dispersion dominated over convection and advection, and resulted in a less distinct saline-fresh groundwater interface than was likely in reality.

Uwiera (1998) simulated 3D, density-dependent, groundwater flow and solute transport for the Potash Corporation of Saskatchewan Cory potash mine site (10 km southwest of Saskatoon). The depositional environment and hydrogeology at the Cory mine site are similar to that of the PL mine site, except that the Cory mine site is not located in a groundwater discharge area. Her results indicated that engineered brine containment systems at the site are ineffective. After a 50 year period, simulated brine concentrations exceeded 100 times background levels in the underlying Floral Aquifer.

Except for Uwiera (1998), numerical investigations of transport from saline water/brine disposal facilities have considered coupled groundwater flow and solute transport in 2D only. Both Rogers and Dreiss (1995a), and Narayan and Armstrong (1995) acknowledged the 3D nature of the groundwater flow systems they studied and the limitations imposed by 2D investigations. Narayan and Armstrong (1995) suggested that the limited data available did not warrant the additional computational effort.

In this study, a pre-release, but tested, version of the SUTRA2D3D code (Voss and Provost, 2003) is used to simulate steady-state 3D groundwater flow at the study site (PL). Transient, density-dependent brine transport simulations are performed for a 2D cross section that honours the 3D nature of the groundwater flow system. The objectives are to determine whether hydraulic or density forces are likely to control brine transport beneath the WMA and PL, and to assess the long-term effect of brine storage on local groundwater resources. Sensitivity analyses are used to investigate important hydrogeologic uncertainties controlling brine transport at the PL site. The SUTRA2D3D numerical formulation, and independent model verification, are presented in Appendices B and C, respectively.

3.2 Site Description

The PL mine site is 18 km east of Saskatoon at the south end of Patience Lake (Figure 3.1). The lake is situated within a series of natural saline lakes that lie in a north-south trending topographic low. Saskatoon is in a semi-arid climate that experiences a net

water deficit, with average annual rainfall of 361 mm/year and potential evaporation of 988 mm/year. The mean annual air temperature is 2 °C (Wittrock and Wheaton, 1993).

The study area is 400 km^2, which includes the mine site, Porter and Burke Lakes to the north, and Cheviot and Crawford Lakes to the south (Figure 3.1). Shallow groundwater, originating from the topographic highs to the east and west, flows toward the central topographic low, and discharges into the series of lakes. The mine site and PL are generally underlain by low permeability glaciolacusterine and till deposits; however, a regional aquifer exists approximately 25 to 40 m below ground surface (bgs). There is evidence that a local sand unit may hydraulically connect PL to the regional aquifer (Golder, 1996; Christiansen, 1999).

Mining operations began in 1958 and PL was used to contain mining fluids. An earthen dyke was constructed across the south end of PL in 1976 to segregate mine wastes. Mine flooding ended conventional mining operations in 1987. The mine is now operated using solution mining techniques, which utilizes only the brine retention pond (Figure 3.1). Brine tailings are mutually saturated with KCl and NaCl, which has an estimated fluid density of 1235 kg/m^3 (discussed in Chapter 1). The total dissolved solids (TDS) concentration in PL has been reported at 340,000 mg/L (Clifton, 1993).

3.2.1 Hydrostratigraphy

The geology in the study area consists of Quaternary glacial and non-glacial deposits, underlain by Cretaceous marine silt and clay, and non-marine silt and sand bedrock. Stratigraphy for the study area is characterized in Chapter 1 and for the Saskatoon region in Christiansen (1970; 1992). A short description of the hydrostratigraphic units within the study area follows. Cross section B – B' (Map 7) illustrates the interpreted hydrostratigraphy across the study area at the north end of PL (Figure 3.2).

Over most of the study area, the top of the Battleford Formation till contacts the land surface. Accumulations are thickest east and west of PL, coinciding with topographic highs. At lower lying elevations, stratified sand, silt and clay deposits overlie the Battleford Formation. These stratified deposits and the Battleford Formation sediments form the uppermost hydrostratigraphic unit (Figure 3.2). The underlying Floral Formation

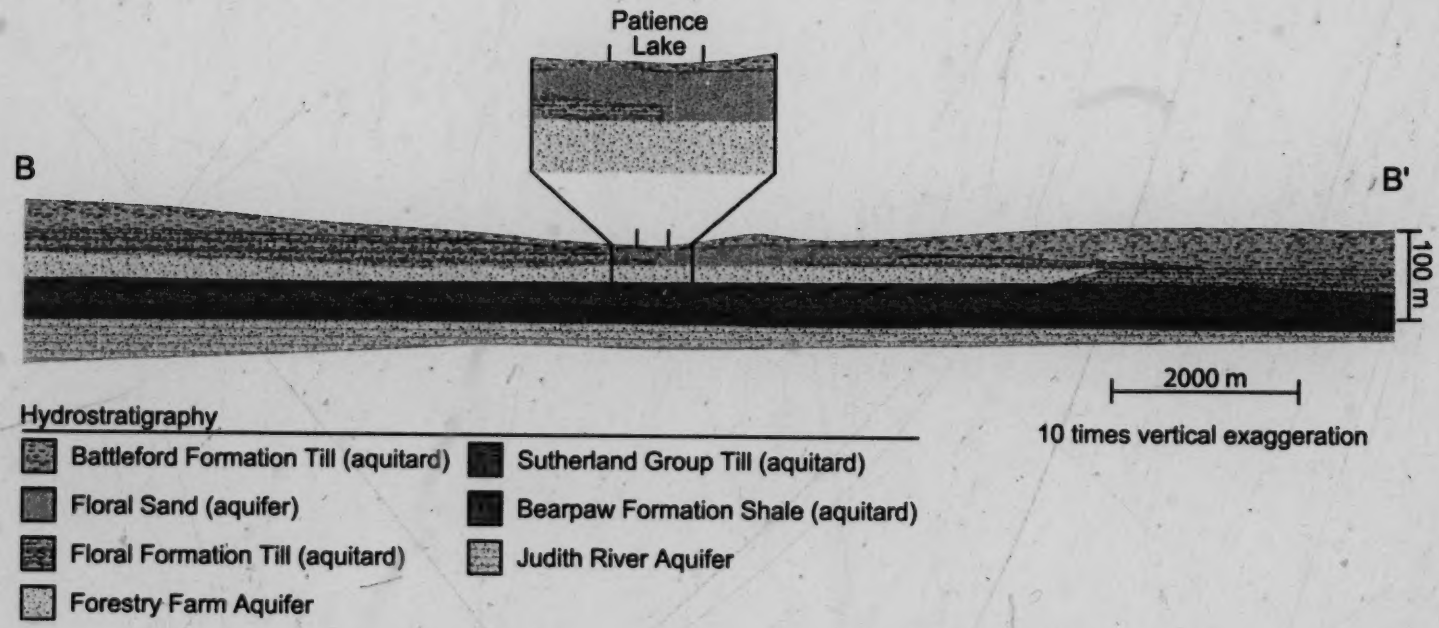

Figure 3.2. Hydrostratigraphy for an east-west cross section at the northern edge of Patience Lake.

till is more dense than the Battleford Formation and is commonly oxidized. The regionally extensive Forestry Farm Aquifer (FFA) underlies the Floral Formation. The aquifer ranges in thickness from 2 to 25 m (Map 4) and is commonly interbedded with thin silt and clay lenses. The FFA is laterally continuous over most of the study area but pinches out to the east.

The Floral Sand is a local sand unit, 3 to 20 m thick, at the top of the Floral Formation till. It lies directly beneath the northern two thirds of PL and extends northeast to Burke Lake (Map 5). At the south end of the Floral Sand, a hydraulic connection with PL may exist (Christiansen, 1999) and there is borehole evidence at the northern tip of PL that the Floral Sand connects with the FFA (Golder, 1996; Christiansen, 1999) (Figure 3.2).

The Sutherland Group till underlies the FFA. It is considered an aquitard because it is unoxidized, dense and has a higher clay content than the overlying Battleford and Floral Formations. Underlying the Sutherland Group aquitard is the Cretaceous silt and clay aquitard of the Bearpaw Formation. The Judith River Formation, a deep, bedrock aquifer, is the bottom hydrostratigraphic unit of the study area. It is underlain by 240 m of marine silt and clay of the Lea Park Formation.

3.2.2 Hydrogeology

Shallow groundwater flow within the study area is generally expected to flow toward PL (Tóth, 1962; Tóth, 1963). Groundwater divides are inferred at the east and west edges of the study area, corresponding with the topographic highs (Figure 3.1). Depression-focused groundwater recharge occurs at the topographic highs and is estimated between 1 and 3 mm/yr (Hayashi et al., 1998). Recharging groundwater flows down through low permeability sediments of the Battleford and Floral Formation tills toward the underlying FFA. In the study area, lateral groundwater flow within the FFA converges on the topographic low, discharging into Patience, Burke and Porter Lakes.

Observed hydraulic heads in the FFA (Map 6) indicate that groundwater flows toward the east along the west side of the study area and toward northwest on the southeast side of the study area. Groundwater flow converges beneath PL, resulting in a northeast direction of flow along the topographic low.

The observed vertical component of groundwater flow between the FFA and PL is upward, indicating groundwater discharge into PL. Since there is no surface water outlet from PL, the only output is evaporation. The vertical hydraulic gradient between the FFA and Judith River Aquifer indicates there is a downward flux of groundwater through the Sutherland and Bearpaw aquitards.

The geochemistry of the FFA is dominated by dissolved sulphate and bicarbonate with average concentrations of 1,200 and 500 mg/L, respectively. Dissolved chloride concentrations range from 20 to 250 mg/L. Dissolved cation concentrations are represented equally by calcium, magnesium and sodium with averages ranging from 140 to 280 mg/L. The total dissolved solids (TDS) concentration generally ranges between 2,000 and 3,000 mg/L. The geochemical composition of the overlying Battleford and Floral Formation till deposits is consistent with the FFA. The TDS is generally less than that of the FFA, ranging from 250 to 2,500 mg/L. The Judith River aquifer is dominated by sodium and chloride and has a TDS ranging between 3,000 and 7,000 mg/L (Clifton, 1993).

Average chloride concentrations obtained from piezometers near the mine site and PL are summarized on Map 6. Piezometers completed within the Battleford Formation till with elevated chloride concentrations are located immediately west of the salt pile (A9, A10 and A45) or south of the mine site (A11 and A39). The single piezometer completed within the Floral Sand (94-8) is located along the west shore of PL. It has a chloride concentration exceeding 160,000 mg/L. Piezometers 94-2 and 96-5 (Map 6), completed within the FFA, have chloride concentrations of approximately 1,500 mg/L (~10 times background values). Background chloride concentrations are observed at three other nearby piezometers completed within the FFA.

3.3 Modelling Methodology

Analysis of brine transport at the mine site is investigated using both 2D and 3D model domains. First, steady-state groundwater flow is calibrated to existing hydraulic head data using a 3D numerical model. Second, brine transport is analyzed along a 2D vertical section (C – C') oriented along the length of the WMA and PL (Map 7). The 3D

nature of groundwater flow is incorporated into the 2D model domain by assigning boundary conditions such that the initial, steady-state hydraulic head distribution in the 2D model matches that of the calibrated 3D flow model. Finally, a sensitivity analysis is performed using the 2D model to investigate important uncertainties in brine transport model results. The rationale for the modelling approach follows.

Groundwater flow within the study area certainly has important 3D characteristics. For instance, within the FFA, the converging east and northwest flow paths result in a component of flow toward the north-northeast, along the topographic low (Map 6). However, flow directly beneath PL is primarily vertical due to groundwater discharge. Therefore, brine migration is closely tied to the hydraulic head distribution in the FFA, the flux of groundwater into PL and the apparent hydraulic connection between PL, and the FFA (Golder, 1996, Christiansen, 1999), via the Floral Sand.

Given that PL is a discharge feature in a hydrologically closed basin, groundwater flow at the margins and beneath the lake is primarily vertical (Duffy and Al-Hassan, 1988). Therefore, horizontal brine migration at the margin of the WMA and PL will be dominated by dispersion, and the vertical pathway, through the Battleford till and Floral Sand deposits, represents the primary pathway for brine migration. Thus, the chosen model domain (Map 7) is appropriate for brine transport analysis.

Use of a 2D model section significantly reduces the computational effort of a coupled density-dependent model, allowing for a more in-depth analysis of brine transport along the section. However, the challenge then becomes representing the 3D nature of groundwater flow in a 2D model. Boundary conditions for the 2D model are defined, based on the 3D flow characteristics of the calibrated groundwater flow model. This is similar to a nested model approach where large-scale features are modelled in a coarse, regional-scale model and boundary conditions for smaller, more refined geographic areas are defined from the regional-scale simulations (Anderson and Woessner, 1992). In this way, important groundwater flow characteristics beneath the brine source are adequately represented and the problem is simplified to economize transport modeling.

3.4 Three-Dimensional Groundwater Flow Calibration

3.4.1 Conceptual Model

Groundwater flow within the study area is represented numerically using a 230 km^2 model domain (Map 7). It is centered on PL, encompasses Burke, Porter, Cheviot and Crawford Lakes, and extends to the topographic highs to the east and west. Hydrostratigraphic units (Figure 3.2) from the land surface to the base of the Judith River Aquifer are represented. Groundwater recharge at higher elevations flows vertically and laterally, converging on the topographic low (Figure 3.3). Regional groundwater flow in the FFA, from beyond the southeast side of the model domain (Golder 1996), combines with the recharge-derived groundwater, and also converges along the topographic low. There is a lateral component of flow northward, toward Porter Lake and a small vertical component downward, through aquitard materials, to the Judith River Aquifer.

The modelled thickness of the Floral Sand increases between the north end of PL and Burke Lake (Map 5), connecting to the FFA (Figure 3.2). Near the south-central portion of PL, the Floral Sand sub crops and is in direct contact with PL. This results in a direct hydraulic connection between PL, Floral Sand and FFA.

3.4.2 Model Domain and Discretization

The 3D model domain extends approximately 16 km in the x- (east-west) and 17 km in the y- (north-south) directions (Map 7). Land surface topography is imported from an electronic 1:50,000 scale map of Cheviot, Saskatchewan (Energy, Mines and Resources, 1987). Elevations range from 610 m above sea level (masl) at the topographic high, 11 km west of Porter Lake, to 510 masl at Porter Lake. Elevations of hydrostratigraphic units are inferred from geologic borehole logs and piezometers logs in Christiansen (1999) (Map 6). The total thickness of the model domain ranges from 107 to 212 m. The hydrostratigraphic and hydrogeologic data are input into Argus Open Numerical Environments (Argus, 1997), which is used to generate the finite-element mesh and create SUTRA input files.

The model domain is discretized into 83, 131 and 20 irregular quadrilateral elements in the x, y and z directions, respectively, resulting in a mesh with a total of 202,540 elements and 217,460 nodes. In the horizontal direction, elements range from 20 to 100 m in the vicinity of PL and the WMA, and increase to a maximum of 750 m at the edges of the model domain (Figure 3.3). Each hydrostratigraphic unit is discretized vertically into three elements, except for the Battleford Formation and Judith River Aquifer, which are discretized into two elements each.

3.4.3 Boundary Conditions

Most vertical edges of the model domain are specified as no flow boundary conditions, representing inferred groundwater divides or vertical flow through low permeability aquitards. Specific exceptions, where different boundary conditions are specified at the model edges, are discussed below. The base of the model is also specified as a no flow boundary. It represents the top of the Lea Park Formation, which is considered impermeable and at sufficient depth to have a negligible effect on near surface brine transport.

The top surface of the model domain is represented with both specified pressures and fluxes (Figure 3.3). Lake surfaces are assigned a pressure of 0 Pa at elevations of 518.5 m (Crawford Lake), 517.5 m (Cheviot Lake), 514 m (Patience Lake), 513 m (Burke Lake) and 510 m (Porter Lake). Groundwater recharge is represented as a spatially variable specified flux applied to the surface of the model domain. The final recharge distribution is determined as part of the model calibration process and is described in more detail in Section 3.4.4.1.

A specified flux boundary is applied to the FFA along the southeast edge of the model domain to represent the regional component of groundwater flow within the FFA that contributes water from beyond the extent of the model domain (Figure 3.3). A flux of 6×10^{-8} m/s is applied to a cross-sectional area of 96,900 m^2 (i.e., 5,700 m long by 17 m average FFA thickness). Given an estimated hydraulic conductivity of 3×10^{-4} m/s (see Section 3.4.4.2), this boundary condition produces a horizontal hydraulic gradient of 0.0002 m/m, which is reasonable for central Saskatchewan.

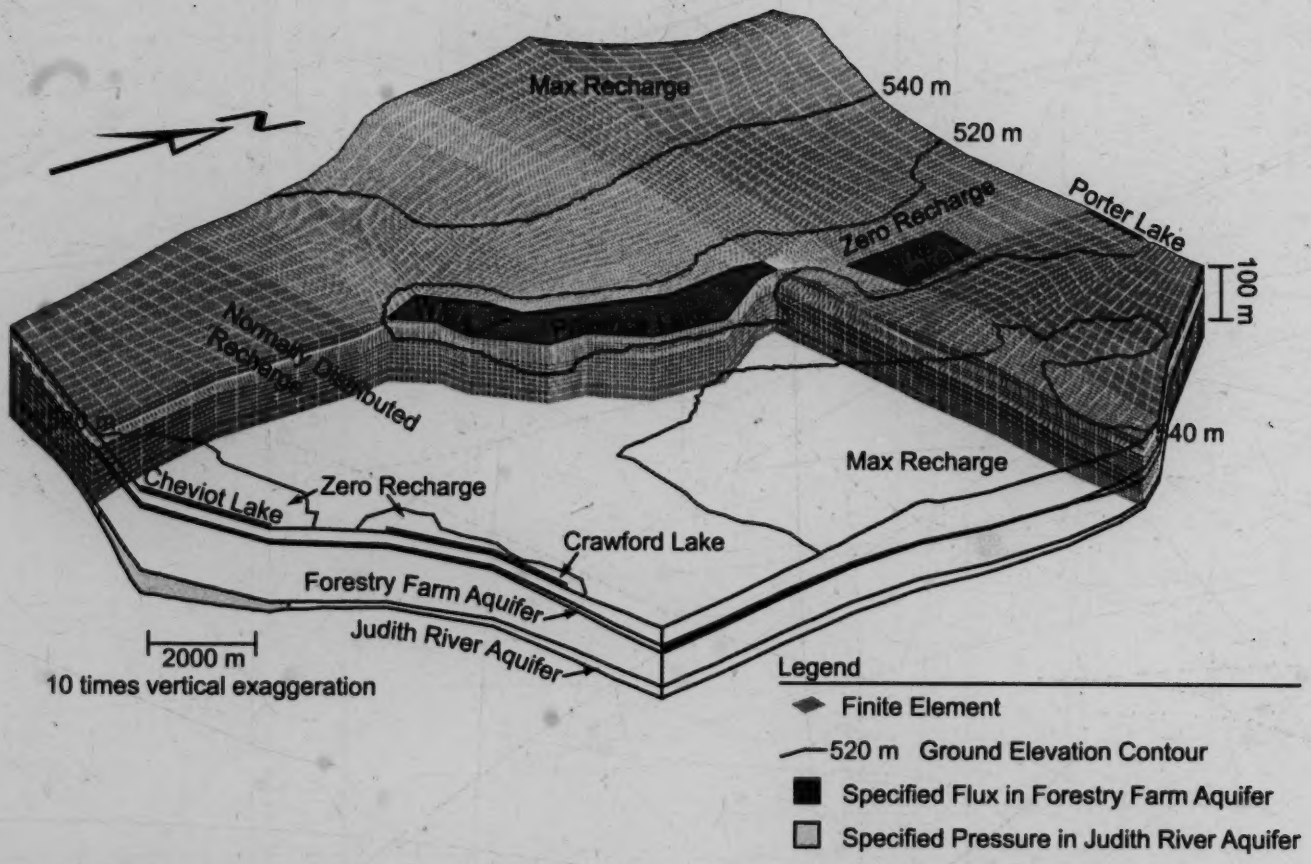

Figure 3.3. Cut-away representation of spatial discretization and boundary conditions for the 3D numerical model.

The Judith River Aquifer is a regional bedrock aquifer that extends beyond the limits of the model domain. Regional groundwater flow directions are generally west-northwest (Meneley, 1970). To honour the conceptual model, specified pressures, corresponding to interpreted hydraulic heads of 510.5 and 511.4 masl, are applied to the south and west topographic lows of the Judith River Aquifer (Map 2; top of the Lea Park Formation corresponds to the base of the Judith River Aquifer) to allow deep groundwater to exit the numerical model. This approach allows groundwater in the Judith River Aquifer to exit the model domain under gradients that are consistent with the conceptual model.

3.4.4 Three-Dimensional Flow Calibration

Steady-state groundwater flow is calibrated using a process of trial and error, where simulated hydraulic heads are matched, as closely as possible, to observed hydraulic heads. First, hydrogeologic properties and boundary conditions are systematically modified to assess their influence on the simulated flow system. Then important aquifer characteristics and system responses are used to refine model parameters and boundary conditions to match simulated and observed hydraulic heads.

Calibration success is ascertained using both qualitative and quantitative measures because most observation data is limited to the immediate area surrounding the WMA and PL. Data near the perimeter of the model domain is sparse; therefore, a qualitative assessment of general flow patterns in the various hydrostratigraphic units is used. A quantitative assessment is applied to hydraulic head measurements available in the Battleford Formation till, Floral Sand, FFA and Judith River Aquifer. Quantitative methods used included the residual error for each calibration point (observed minus simulated hydraulic head) and three measures of average error suggested by Anderson and Woessner (1992) as traditional evaluation methods for model calibration. The average error estimates include the Mean Error (ME), Mean Absolute Error (MAE) and Root Mean Squared (RMS) error and are defined as follows:

$$ME = \frac{1}{N}\sum_{i=1}^{n}(h_o - h_s)$$

$$MAE = \frac{1}{N}\sum_{i=1}^{n}|(h_o - h_s)|$$

$$RMS = \sqrt{\frac{1}{N}\sum_{i=1}^{n}(h_o - h_s)^2}$$

where N is the number of calibration points, h_o is the observed hydraulic head and h_s is the simulated hydraulic head (Anderson and Woessner, 1992).

3.4.4.1 Calibrated Recharge Distribution

To provide a smooth transition between recharge and discharge areas of the local flow system, the recharge distribution applied to the top surface of the model is varied as a function of elevation. Maximum values of 9.0 and 4.0 mm/year (corresponding to 2.5 and 1.1% of the mean annual precipitation) are applied to elevations greater than 540 masl west and east of PL, respectively. Recharge decreases following a normal distribution, for elevations between 540 and 520 masl (Figure 3.3). Zero recharge is applied to elevations less than 520 masl, resulting in a no flow boundary condition. The total recharge applied to the model, averaged over the model area of 230 km^2, is 3.3 mm/year, corresponding to 0.9% of mean annual precipitation. Hayashi et al. (1998) estimated groundwater recharge on the Saskatchewan prairies between 1 and 3 mm/yr (0.3 to 0.8 % of annual precipitation). The recharge value of 3.3 mm/yr, used in the calibrated model, is slightly higher than the estimated range of Hayashi et al. (1998) but represents a reasonable groundwater recharge estimate for the study site.

3.4.4.2 Calibrated Model Parameters

The calibration process focuses on permeability distributions. Permeability values are modified, based on published and non-published sources (refer to Section 1.5). Porosity values, which only affect transport velocities, are obtained from published sources and not modified further. Final permeability and porosity (n) values for the calibrated model are summarized in Table 3.1. All values are within the literature ranges (refer to Table 1.1) except for the permeability of the Bearpaw Formation aquitard, which is approximately 2 orders of magnitude higher than the estimated range provided by Shaw

and Hendry, 1998. The Bearpaw Formation permeability used in the calibrated model represents an average, regional-scale value, whereas Shaw and Hendry (1998) based their estimates on small-scale laboratory and slug test results.

Table 3.1. Calibrated model parameters.

Hydrostratigraphic Unit	k_h (m^2)		k_v (m^2)	n (-)
	Low*	High*		
Battleford Formation				
Till	$5x10^{-15}$	$4x10^{-14}$	$1x10^{-14}$	0.4
Sand/Gravel	$5x10^{-12}$		$5x10^{-12}$	0.3
Floral Sand	$4x10^{-12}$	$7.5x10^{-12}$	$4x10^{-14}$	0.3
Floral Formation Till	$8x10^{-16}$		$8x10^{-16}$	0.27
FFA				0.3
Anisotropic	$3x10^{-12}$	$9x10^{-12}$	$9.9x10^{-14}$	
Isotropic	$3x10^{-11}$		$3x10^{-11}$	
Sutherland Group	$1x10^{-17}$		$1x10^{-17}$	0.33
Bearpaw Formation	$5x10^{-17}$		$5x10^{-17}$	0.4
Judith River Aquifer	$4x10^{-12}$		$4x10^{-12}$	0.25

* Minimum and maximum horizontal permeability values in calibrated model.

The calibrated horizontal permeability (k_h) of the Battleford Formation till ranges from $5.0x10^{-15}$ to $4.0x10^{-14}$ m^2. Surficial sand and gravel deposits, west of the WMA, are assigned a permeability of $5.0x10^{-12}$ m^2.

The lateral extent of the Floral Sand is interpreted along the topographic low, beneath Patience and Burke Lakes (Map 5) and has a horizontal permeability ranging between $4.0x10^{-12}$ and $7.5x10^{-12}$ m^2. The vertical permeability (k_v) is $4.0x10^{-14}$ m^2, representing thin, interbedded till deposits within the Floral Sand, resulting in a permeability anisotropy ratio (k_h/k_v) between 100 and 190.

Where present, the Floral Formation till is represented with a homogeneous, isotropic permeability of $8.0x10^{-16}$ m^2. The Floral Formation till is not present south of the WMA or north of Burke Lake, where thick accumulations of Battleford Formation till exist. Between the north end of PL and north end of Burke Lake, the Floral Sand attains a maximum thickness of 24 m and connects with the underlying FFA.

The permeability of the FFA is anisotropic where interbedded till deposits are present (Table 3.1). The permeability anisotropy ratio for the west and central portions of the

model domain ranges from 90 to 110. At the southeast corner of the domain, interbedded till is not present and an isotropic permeability of $3.0x10^{-11}$ m^2 is used. Calibrated horizontal permeability of the FFA ranges by an order of magnitude, from $3.0x10^{-12}$ to $3.0x10^{-11}$ m^2, based on sand and gravel descriptions in geologic logs.

Hydrostratigraphic units underlying the FFA are simulated using homogeneous, isotropic permeability distributions (Table 3.1).

The Floral Sand connects to the land surface at the west shore of PL, consistent with the interpretation in Christiansen (1999). As a result, a direct connection exists between PL and the FFA with a horizontal permeability between $4.0x10^{-12}$ and $7.5x10^{-12}$ m^2. Beneath the remainder of PL, thin Battleford till deposits (2 to 5 m thick) lie between the lake bottom and the Floral Sand.

3.4.4.3 Steady State Model Calibration Results

Figure 3.4 is a plot of simulated versus observed hydraulic heads for piezometers in the Battleford Formation till, Floral Sand, FFA and Judith River Aquifer. The distribution of simulated hydraulic head is similar to the observed. Most residuals (observed minus simulated hydraulic head) are within 1 m, or 5% of the total hydraulic head difference in the model, and within an acceptable range for model calibration. The errors are both positive and negative, illustrating that there is no significant bias toward higher or lower simulated hydraulic heads.

The highest variability in the calibrated hydraulic heads occurs in the Battleford Formation till. Five of the eleven piezometers have residuals greater than 1 m, reaching a maximum error of 4.4 m. When the observed hydraulic head ranges are considered in the calibration, only two of the eleven Battleford Formation piezometers lie outside the 1 m calibration range (Figure 3.4). The variability in the simulated versus observed hydraulic heads in the Battleford Formation is likely associated with the heterogeneous nature of the till. The Battleford Formation permeability is represented as a homogeneous unit whereas observed flow within the till will be strongly influenced by small-scale permeability variations that are not accounted for in the numerical model.

Errors within the Battleford Formation are both positive and negative, suggesting that the model adequately represents average, large-scale, flow characteristics.

The average errors associated with the model calibration are summarized in Table 3.2. With the exception of the Judith River Aquifer calibration locations, the ME is greater than zero, indicating that simulated hydraulic heads generally exceed those observed. A lower ME, compared with MAE and RMS, illustrates that the positive and negative errors tend to cancel each other out. The MAE and RMS are highest for the Battleford Formation calibration points which is consistent with the higher variability noted in the simulated versus observed residuals (Figure 3.4).

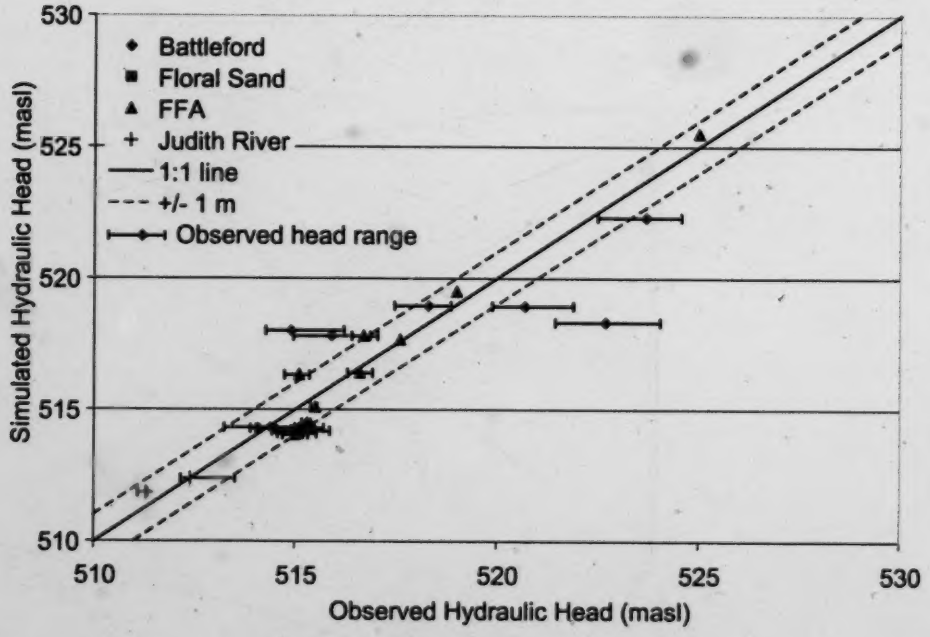

Figure 3.4. Simulated versus observed hydraulic heads for calibrated 3D flow model.

Table 3.2. Average errors calculated from calibration data.

	N	ME (m)	MAE (m)	RMS (m)
Battleford Formation	11	0.37	1.44	1.90
Floral Sand	1	1.00	---	---
FFA	11	0.07	0.68	0.77
Judith River Aquifer	2	-0.28	0.28	0.39
Total	25	0.21	1.00	1.38

3.4.4.3.1 Steady-State Groundwater Flow

Adequately representing groundwater flow within the FFA is considered the most important factor in the model calibration because the hydraulic head distribution in the vicinity of the mine site will have the largest influence on groundwater discharge into PL and, therefore, on brine transport. Simulated steady-state hydraulic head patterns (Figure 3.5) represent the observed patterns quite well (compare Figure 3.5 to Map 6). Flow is toward the east along the west side of PL and toward the northwest along the east side. Along the topographic low, flow is toward the north-northeast. The simulated and observed lateral hydraulic gradients west of PL are 0.0027 and 0.0017 m/m, respectively. East of PL, the simulated and observed lateral hydraulic gradients are 0.0011 and 0.0008 m/m, respectively (Figure 3.5 and Map 6).

Simulated 3D groundwater velocity is illustrated in Figure 3.6 using three east-west oriented cross sections and a single north-south section oriented along the topographic low. The blue and green colours represent groundwater flow in the aquitards (Battleford, Sutherland and Bearpaw hydrostratigraphic units) where vertical flow tends to dominate over horizontal flow. Red and yellow colours represent groundwater flow in the aquifers (Floral Sand, FFA and Judith River hydrostratigraphic units) where horizontal flow dominates.

Groundwater in the recharge areas to the east and west of PL flows vertically through the Battleford and Floral Formation tills toward the underlying FFA. Simulated velocities range from $1x10^{-10}$ to $1x10^{-9}$ m/s (0.003 to 0.03 m/yr). Beneath the FFA, downward vertical flow through the Sutherland and Bearpaw aquitards ranges between $6x10^{-12}$ and $1x10^{-10}$ m/s (0.0002 to 0.003 m/yr).

Within the FFA, flow converges on the topographic low and ranges from $1x10^{-7}$ to $5x10^{-7}$ m/s (3 to 15 m/yr). Maximum groundwater velocities $7x10^{-7}$ m/s (22 m/yr) occur at

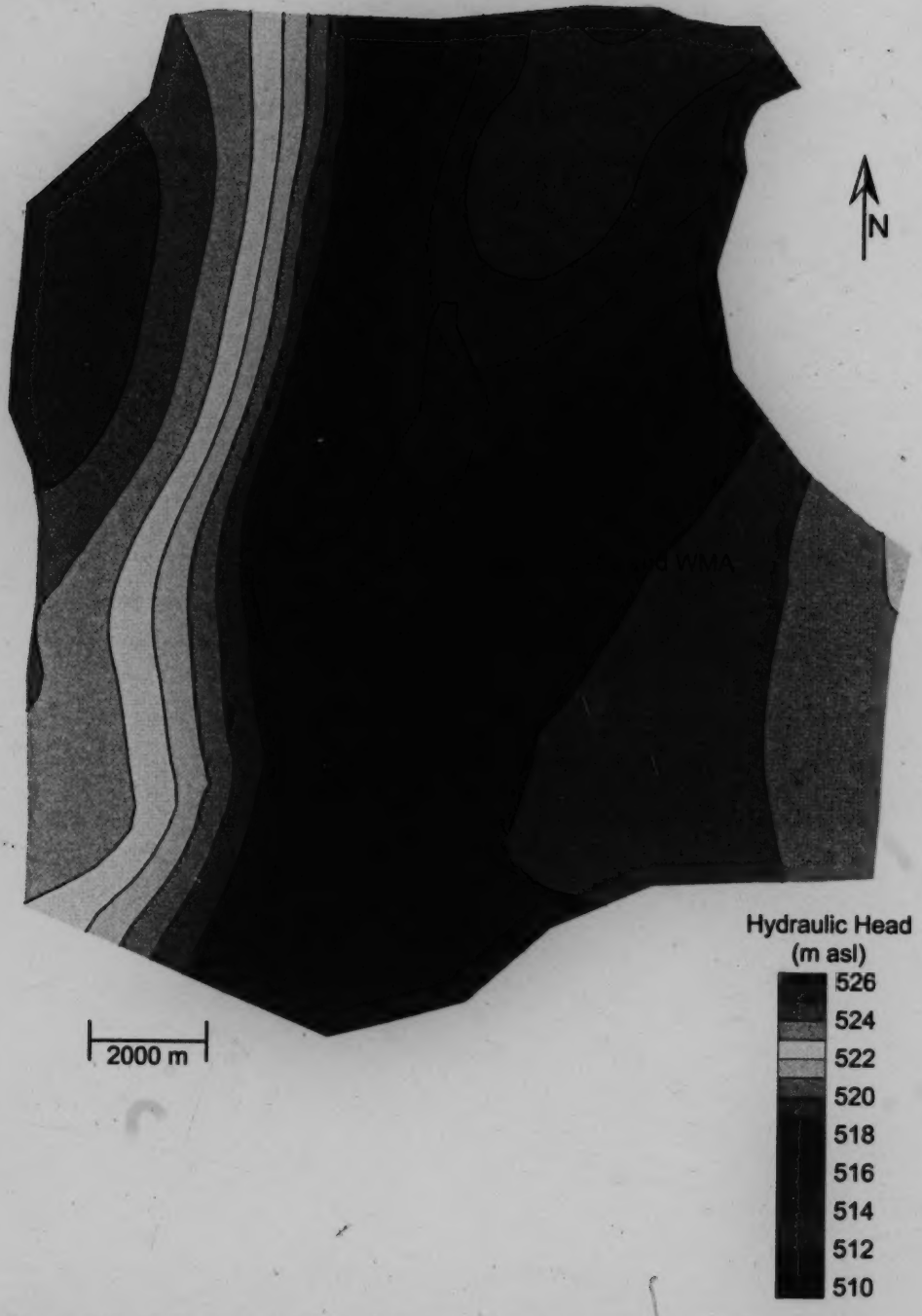

Figure 3.5. Calibrated steady state hydraulic head distribution in the Forestry Farm Aquifer.

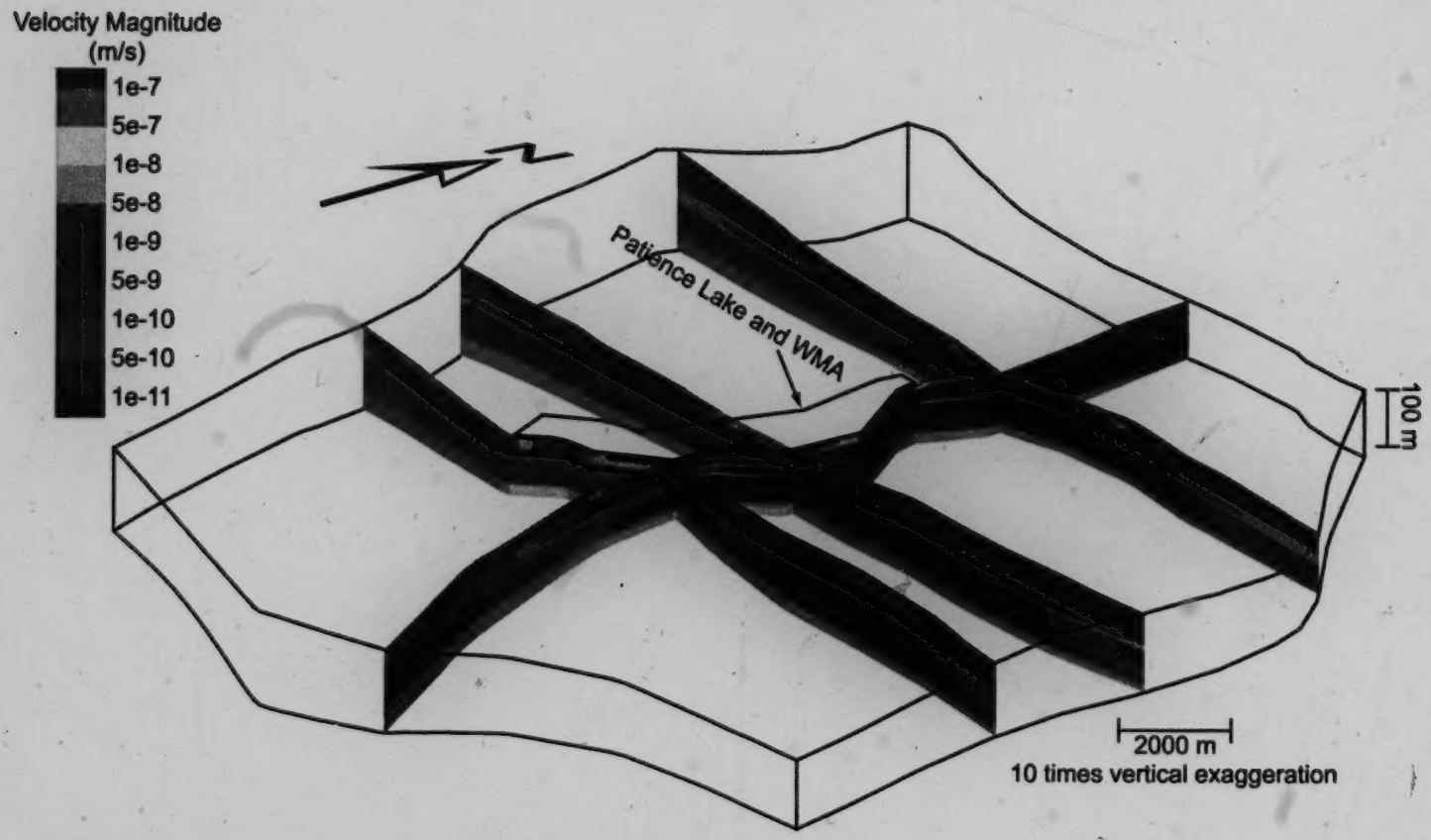

Figure 3.6. Groundwater velocity magnitude for the 3D calibrated flow model.

the north end of PL, where the Floral Sand and FFA connect. Northward flowing groundwater within the FFA flows up through the Floral Sand/FFA connection, discharging into PL. Beneath PL, vertical velocities in the Battleford Formation till, between the lake sediments and the Floral Sand, range from $5x10^{-9}$ to $1x10^{-8}$ m/s (0.1 to 0.3 m/yr).

3.5 Two-Dimensional Brine Transport Analysis

SUTRA2D3D (Voss and Provost, 2003) is used to investigate transient brine transport along the 2D cross section, C – C' (Map 7). Groundwater flow characteristics elucidated in the 3D flow calibration, and the available information available pertinent to brine transport (e.g., brine properties, PL levels and measured solute concentrations) are used to develop a numerical model that approximates the present solute distribution at the PCS PL mine site. The transient brine distribution is simulated from the onset of continuous conventional mining operations (1965) to present (2002). The potential future brine distribution is simulated for a 25 year period to 2037. Sensitivity analyses investigate potential differences in the present and future simulated brine distribution.

3.5.1 Conceptual Model

The 2D numerical model is a vertical slice oriented along the topographic low, extending from south of the WMA to Porter Lake (Map 7). The cross section is 12,850 m long, between 110 and 129 m deep, and 4 m wide. This section facilitates analysis of vertical brine transport as well as potential brine migration within the Floral Sand and FFA. Hydrogeologic data (permeabilities, porosities, elevations of hydrostratigraphic units) for the 2D model section are interpolated directly from the calibrated 3D model domain.

The initial steady-state hydraulic head distribution along the 2D section must represent the conditions established in the 3D groundwater flow calibration. Using the 3D fluid balance data, fluid fluxes are applied along the length of the FFA to reproduce the flow behavior observed in the 3D model. Conceptually, these fluid fluxes represent groundwater flow within the FFA that is converging beneath PL from the east and west (the 3D component of groundwater flow, perpendicular to the 2D model section). In this way, a realistic initial, steady-state flow solution is used for the brine transport

simulations, external fluid fluxes applied to the model remain known (yet constant) and fluid pressures calculated by the model are able to change as a function of density (the essence of a density-dependent model).

3.5.2 Boundary Conditions

Boundary conditions for the 2D model domain are illustrated in Figure 3.7. Specified pressures (P) are used to represent the WMA, PL and Burke Lake along the top surface of the model domain. The pressure of Burke Lake is held constant throughout the simulation, representing a lake elevation of 513 masl. During the first 9 yrs of the simulation, the pressure of the WMA and PL are maintained at P = 0 Pa, representing an elevation of 514 masl. Pressures are then varied in a stepwise manner (refer to Section 3.5.5.2) to approximate the change in historical lake elevation (Figure 1.3). The WMA and PL levels increase from 514 masl in 1974 to a maximum of 515.4 masl in 1986 and then decrease again to 514 masl by 1999. From 1999 to the end of the simulation period (2037), WMA and PL levels are held constant at 514 masl.

The base of the model domain is considered a no flow boundary. The north and south ends of the model domain are represented using both specified pressure and no flow boundaries. Specified pressures are applied to the ends of the model domain at the top surface, FFA and Judith River Aquifer that match the results of the 3D groundwater flow calibration (Table 3.3). No flow boundaries are applied to the aquitards at each end of the model domain.

Table 3.3. Hydraulic heads (h) (masl) from the 3D flow calibration used to determine specified pressure (P) boundary conditions in the 2D numerical model.

	South End of Domain	North End of Domain
Top Surface	519.2	510.0
Forestry Farm Aquifer	519.1	512.3
Judith River Aquifer	512.0	512.7

$P = (h-z)\rho_o g$

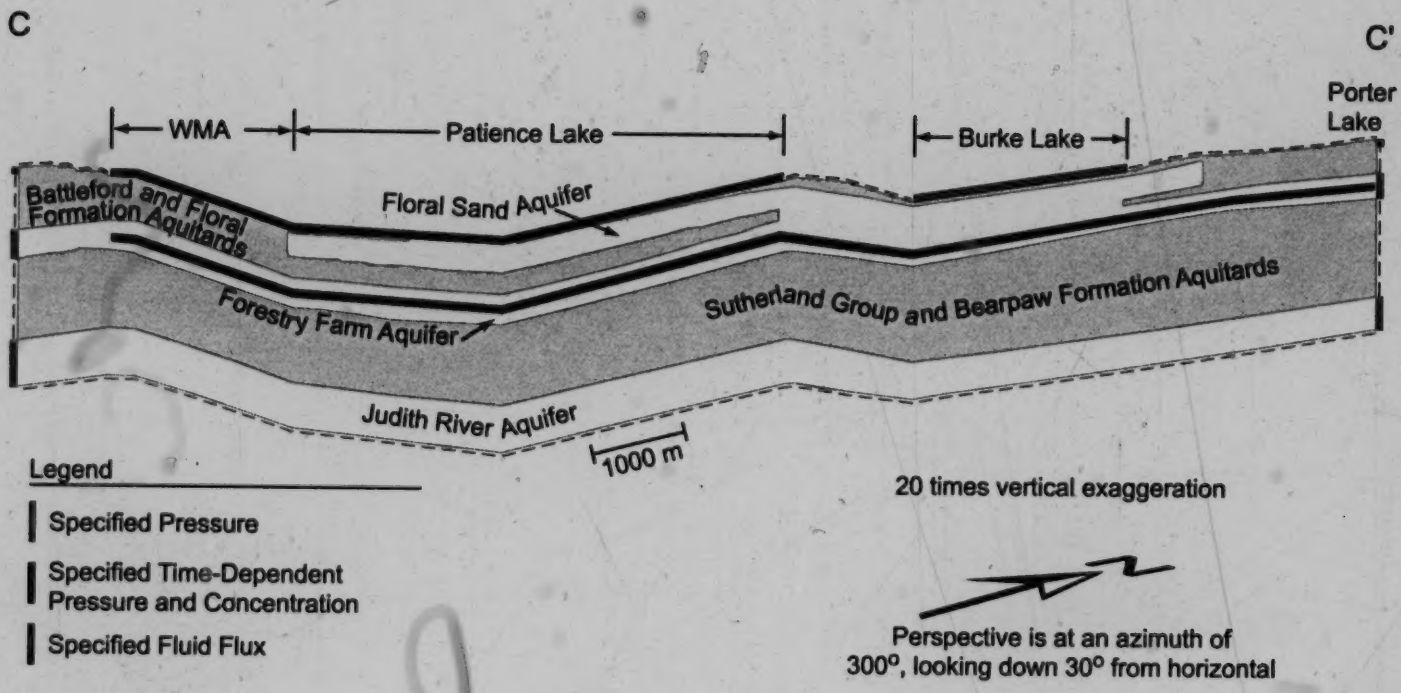

Figure 3.7. Boundary conditions for the 2D numerical model.

The 3D component of groundwater flow converging on the 2D model section from the east and west is represented as a fluid flux boundary applied to nodes along the length of the FFA (Figure 3.7). The fluid flux ranges from 0.008 to 0.06 $m^3/yr/m^2$, totaling 1700 m^3/yr. The resulting steady-state hydraulic head distribution in the FFA along the topographic low for both the ***Base*** case, (2D) cross section and the calibrated (3D) model is illustrated in Figure 3.8. There is a very close match between the 2D and 3D simulated hydraulic heads, suggesting that the groundwater flow in the 2D model reasonably represents the behavior determined in the calibrated 3D model. The hydraulic head decreases from south to north, indicating a northern component of groundwater flow within the FFA, which is consistent with observations (Map 6). The horizontal hydraulic gradient is highest (0.001 m/m) at the south end of the model section, beneath the WMA. The horizontal gradient decreases to 0.0005 m/m beneath PL and is fairly constant along its length. The lowest simulated hydraulic gradient (0.0001 m/m) occurs beneath Burke Lake. Between Burke and Porter Lakes, a small topographic feature produces a localized mound in the potentiometric surface, resulting in a groundwater flow southward, toward Burke Lake and northward toward Porter Lake.

The solute concentration in the WMA and PL likely increased over a period of years as mining wastes accumulated at the site. This gradual increase was approximated in the numerical model to better represent the solute source function and to reduce potential numerical errors associated with an abrupt solute concentration increase. The solute source ($c_{source}(t)$), representing the WMA and PL, is implemented using the complementary error function (erfc):

$$c_{source}(t) = c_0 + \frac{1}{2}[2 - \mathrm{erfc}(\beta)](c_{max} - c_0)$$

where c_0 is the background concentration, c_{max} is the maximum source concentration and t_{max} is the time when maximum solute concentration is attained. $\beta = 6^*t/t_{max}-3$, producing values of erfc between 2 and 0 at $t = 0$ and $t = t_{max}$, respectively. The overall effect is a smooth solute source function that increases gradually (Figure 3.9). Initially, both the WMA and PL solute concentrations are increased from $c_0 = 0.001$ kg/kg to $c_{max} = 0.200$ kg/kg over a 5 year period. The PL concentration is then held constant and the WMA source concentration is further increased to 0.294 kg/kg over an additional

4 year period. Fluid density ($\rho(c)$) varies as a function of concentration ($\rho(c)=\rho_0+802(c-c_0)$) (Figure 1.4), resulting in maximum source densities of 1,230 and 1,160 kg/m^3 for the WMA and PL, respectively.

An initial pressure distribution for transient brine simulations is generated by solving a steady state problem with a brine source concentration equal to c_0 (0.001 kg/kg).

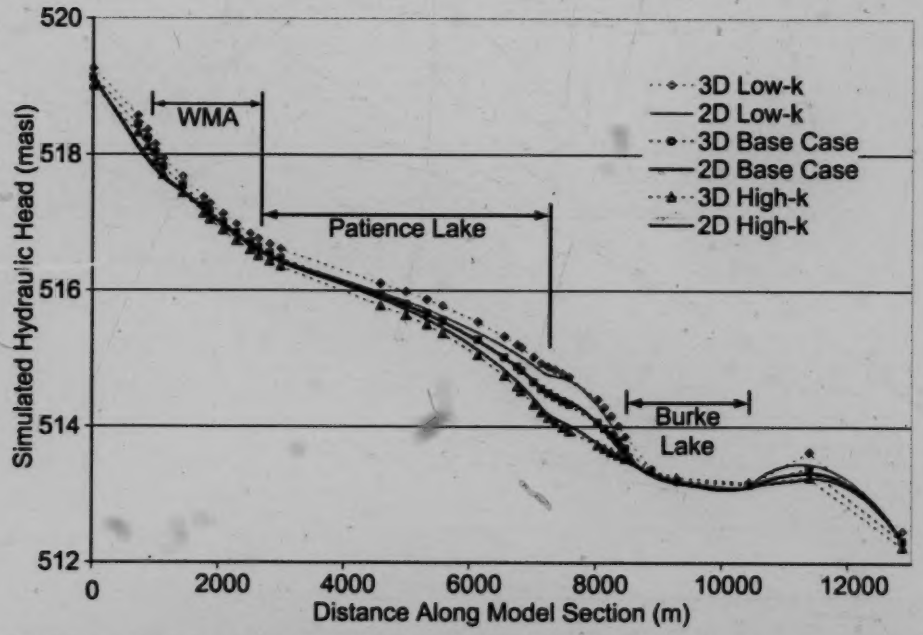

Figure 3.8. Simulated hydraulic head in the Forestry Farm Aquifer for both the 2D and 3D numerical models. The Base Case represents the hydraulic head distribution for the calibrated model. Low-k and High-k represent sensitivity analysis results (Section 3.6).

3.5.3 Spatial and Temporal Discretization

The cross sectional domain is discretized into 99,528 elements and 154,530 nodes. At the brine source margins (at the south end of the WMA and the north end of PL), horizontal discretization is refined to a minimum of 0.6 m. At the centre of the brine source and beyond the brine source margins, horizontal discretization is relaxed to a maximum of 10 m. Directly beneath the brine source, the vertical discretization of the isotropic Battleford till ranges from 0.4 to 1.0 m, resulting in aspect ratios (lateral

discretization (Δx)/vertical discretization (Δz)) ranging between 0.6 and 25. The vertical discretization of the Floral Sand and FFA is approximately 2 m. Deeper within the domain, vertical discretization ranges from 3.5 m (Floral Formation till) to 15 m (Judith River Aquifer).

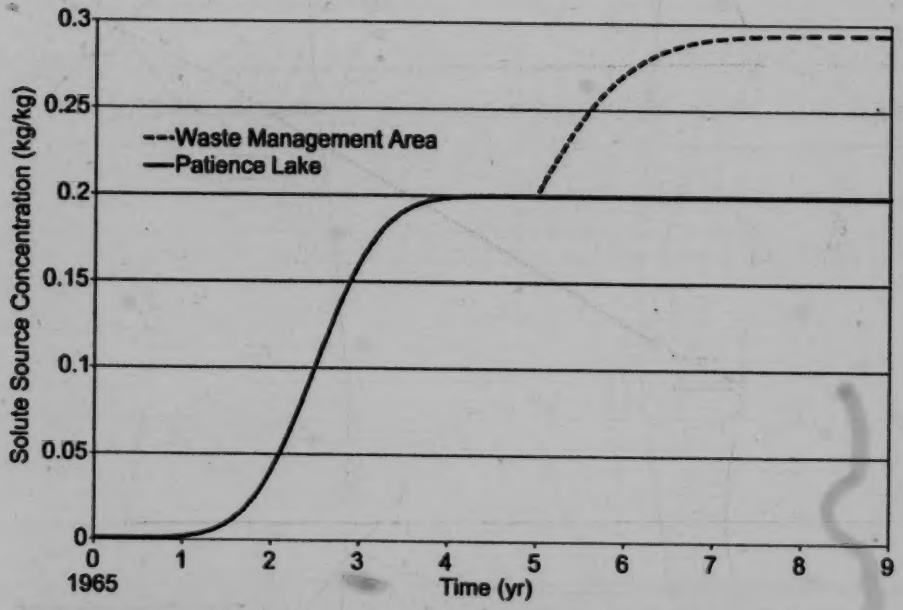

Figure 3.9. Transient solute source function applied to Patience Lake and the Waste Management Area.

Time steps (Δt) remain small as the source concentration is increased. As the rate of change in the source concentration decreases and fresh-saline groundwater interface spreads out via dispersion and diffusion, time steps are gradually increased. The minimum and maximum time step sizes are 0.125 and 5 days, respectively. For linear problems, Anderson and Woessner (1992) recommend selecting times steps so that the Courant Number ($C = v\Delta t/\Delta z$) remains less than 1. Given a maximum steady state groundwater velocity of 1.5×10^{-8} m/s directly beneath the brine source and a 1 m vertical discretization, the Courant Number ranges from 0.0002 to 0.006. Such small time steps are necessary to maintain numerical stability when solving this highly coupled groundwater flow and solute transport problem.

3.5.4 Model Parameters

The fluid and matrix properties and transport parameters used in the transient simulations are listed in Table 3.4. These model parameters are spatially and temporally constant, and unless otherwise specified later, remain constant for all simulations.

Table 3.4. Flow and transport parameters

Parameter	Value	Units
Background solute concentration	0.001	kg/kg
Background fluid density	999.7	kg/m^3
Coefficient of density change [1]	801.6	kg/m^3
Dynamic viscosity [2]	0.001	kg/ms
Fluid Compressibility [2,3]	$4.5x10^{-10}$	Pa^{-1}
Matrix Compressibility [3]	$5.0x10^{-8}$	Pa^{-1}
Longitudinal dispersivity	2.0	m
Transverse dispersivity	0.2	m
Effective molecular diffusion coefficient [4]	$5.5x10^{-10}$	m^2/s
Acceleration due to gravity	9.81	m/s^2

[1] McCain (1991)

[2] Fetter (1994)

[3] Freeze and Cherry (1979)

[4] Maathuis and van der Kamp (1994)

3.5.5 Transient Model Results

3.5.5.1 Analysis Locations and Methods

The transient brine distribution is simulated from 1965 to 2037 and is illustrated along the 2D vertical cross section after 9, 23, 37 and 60 years (Figure 3.10). The results are also analyzed using breakthrough curves and vertical concentration profiles at four locations of interest: (1) beneath the Waste Management Area (***WMA***), (2) at the northern edge of the "Floral Sand connection" with PL (***Connection***), (3) 150 m downgradient (north) of the Floral Sand connection location (***MidPL***) and (4) at the north

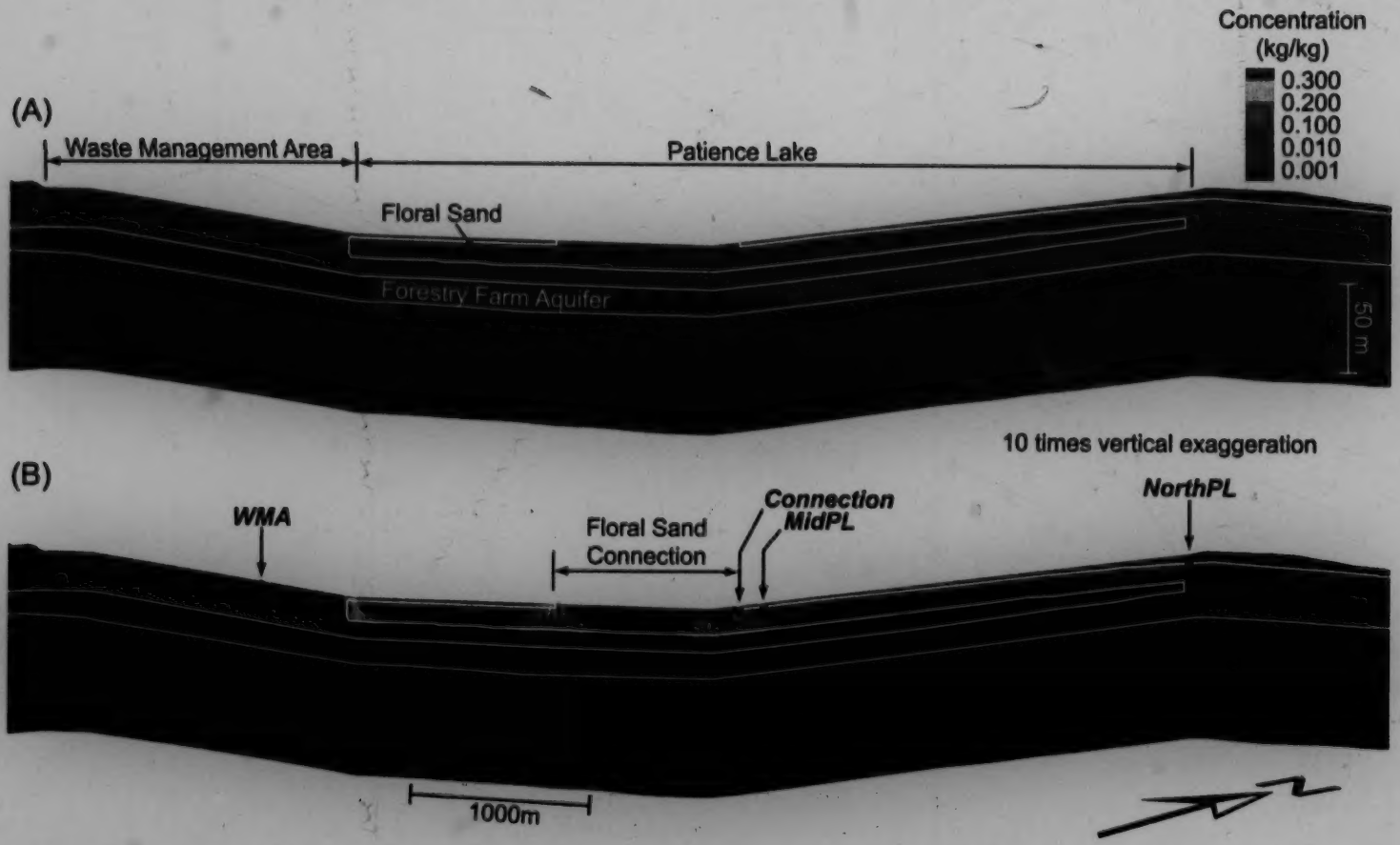

Figure 3.10. Simulated 2D transient brine distribution beneath the Waste Management Area and Patience Lake.
(A) 9 years; (B) 23 years

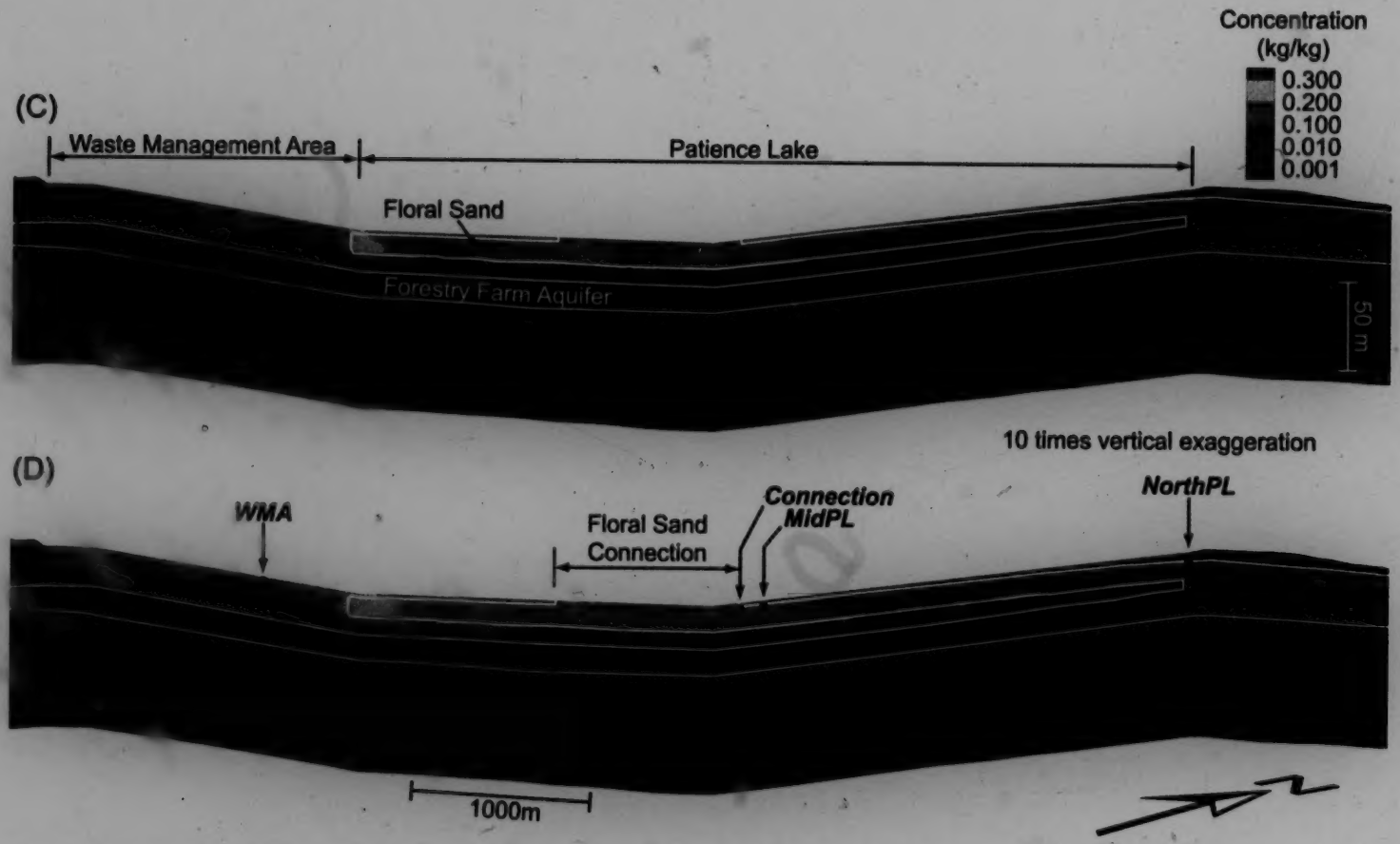

Figure 3.10. Simulated 2D transient brine distribution beneath the Waste Management Area and Patience Lake. (C) 37 years; (D) 60 years

end of Patience Lake (***NorthPL***) (Figure 3.10). The ***WMA*** location is of interest because maximum brine source concentrations (0.294 kg/kg) are applied at this location; however, thick accumulations of Battleford and Floral till units separate the brine source and FFA. Maximum brine migration rates occur at the Floral Sand connection (***Connection***), where density-driven convection is expected through the high permeability material. The ***MidPL*** location monitors lateral brine transport within the Floral Sand, toward the north end of PL and the FFA. The ***NorthPL*** location characterizes brine migration through the thin Battleford till to the underlying Floral Sand, which is in direct contact with the FFA.

When referring to the position of the leading edge of the transient brine plume, its location is defined at the simulated 0.01 kg/kg (about 10 times the background concentration) TDS solute concentration contour.

3.5.5.2 Transient Brine Transport

After a 9 year simulation period, brine source concentrations of the WMA and PL are at the maximum values of 0.294 and 0.200 kg/kg, respectively. The solute distribution beneath the source zone is evenly distributed and convection of fluid has not developed (Figure 3.10 A). At this point, brine migration occurs only by diffusion and dispersion. To approximate historical lake level changes, the elevation of the WMA and PL are raised in a stepwise manner from 514 masl in 1974 (9 yr) to a maximum of 515.4 masl in 1986 (21 yr), which is then maintained to 1988 (Figure 3.11). The solute distribution after 23 yrs (1988) is illustrated in Figure 3.10 B. Density-driven convection cells have developed at the Floral Sand connection and WMA/PL interface. Where convection occurs, brine has migrated to the base of the Floral Sand. The plume then encounters the top of the Floral till aquitard and is forced to spread laterally, within the Floral Sand. Elsewhere beneath the brine source, concentrations at the base of the Floral Sand remain at background levels.

From year 23 (1988) to 34 (1999), the level of the WMA and PL is decreased to 514 masl (Figure 3.11) and maintained at that level to the end of the simulation in 2037. After 37 years (present day), brine has completely invaded the Floral Sand beneath the connection with PL (Figure 3.10 C) and continues to migrate laterally. The leading edge

of the plume has migrated 450 m downgradient of the Floral Sand connection, toward the north end of PL. By year 37 (2002), brine has dispersed through the Battleford till, and where it is underlain by the Floral Sand, additional convective fingers begin to develop (Figure 3.10 C). After 60 years (Figure 3.10 D) these fingers have propagated to the base of the Floral Sand. The solute plume originating from the Floral Sand connection has migrated a total of 730 m after 60 years. The average lateral brine migration rate in the Floral Sand is 12 m/year and could potentially migrate to the north end of PL as early as 2070.

Figure 3.11 shows concentration breakthrough curves for the base of the Battleford hydrostratigraphic unit at the four analysis locations. At ***WMA*** it represents the interface between the Battleford and Floral tills; at ***Connection***, no Battleford till is present so it located within the Floral Sand; the ***MidPL*** and ***NorthPL*** locations represent the interface between the Battleford till and top of the Floral Sand.

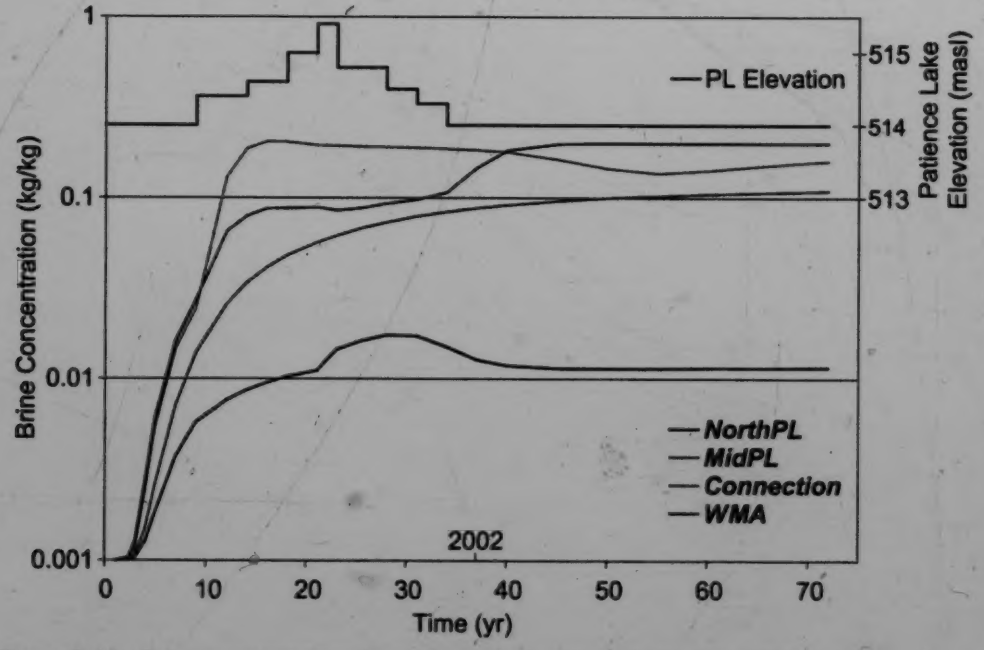

Figure 3.11. Brine concentration breakthrough curves and simulated Patience Lake elevations.

At ***WMA***, the Battleford till is only 2 m thick, but is underlain by Floral till. Solute concentration increases gradually over time and reaches a maximum of 0.11 kg/kg (c/c_{source} = 0.37) after the 72 year simulation period (Figure 3.11). The low permeability of the Floral till ($8.0x10^{-16}$ m^2) results in dispersion-dominated brine transport.

Connection is 1.5 m beneath the brine source and the concentration initially increases in a manner similar to ***WMA*** (Figure 3.11). However, after 9 yr, a convecting finger begins to propagate, and concentrations increase rapidly to the source concentration of 0.20 kg/kg after 16 yr. Concentrations then fluctuate mildly as transient convection cells develop and propagate.

MidPL is also located 1.5 m beneath the brine source and the breakthrough curve matches ***Connection*** up to 9 years (Figure 3.11). The concentration at ***MidPL*** is influenced by the convection cell at the Floral Sand connection and increases sharply after 9 years and then remains constant for a period of time as solute disperses into the Floral Sand. From 30 to 45 yr, the concentration increases, to the source concentration, as the convecting plume from the Floral Sand connection migrates.

At the north end of PL the monitoring location (***NorthPL***) is located 5 m beneath the brine source. Brine concentration increases gradually and reaches a steady state concentration (0.011 kg/kg) after approximately 21 yr (Figure 3.11). The anomalous, yet transient, increase in concentration is due to the increase, then decrease in PL water levels. From 21 to 23 yr, when the PL elevation is at a maximum (515.4 masl), density-driven convection develops at the north end of PL, resulting in groundwater recharge and higher brine migration rates. The period of convective flow is short and when lake levels decrease, groundwater discharge conditions re-develop. For the preceding period from year 18 to 21, when the PL elevation is 515 masl or less, convection is not observed.

3.5.5.3 Evaluation

Only a limited data set is available to calibrate the brine transport model. A single monitoring location exists within the Floral Sand, located along the west shore of PL (94-8 on Map 6), near the Floral Sand connection in the 2D model. Since 1994, the

chloride concentration has averaged 168,000 mg/L, likely representing transport from PL. The simulated solute concentration of 0.200 kg/kg (232,000 mg/L) at the base of the Floral Sand shows similar behavior.

There is also some evidence that brine has impacted the FFA at the north end of PL. Two monitoring locations within the FFA (94-2 and 96-5) have chloride concentrations of 1,500 mg/L (10 times the background concentration); however, three other nearby piezometers (94-1, 94-3 and A102) have background chloride concentrations (Map 6). The present simulated brine concentration in the FFA at the north end of PL remains at background levels. Thus, overall, the numerical model appears to adequately represent groundwater flow and the observed transient solute distribution beneath the PCS PL potash mine site.

3.5.5.4 Discussion

Initially, as the brine source is increased to maximum values, solute transport is dominated by dispersion and is stable across the entire model domain. After 9 yr, WMA and PL levels rise and density-driven instabilities develop at the interface between the WMA and PL and at the high permeability connection between PL and the Floral Sand. When maximum lake levels are simulated (from 21 to 23 yr) a convection cell develops at the north end of PL. This cell dissipates when lake levels decrease. Along the interface between the Battleford till and Floral Sand (between ***Connection*** and ***NorthPL***), transport remains stable until approximately 37 years when density gradients at the interface become sufficient to overcome upward-discharging groundwater flow. Where the Floral Sand is not present beneath the WMA, convection cells do not develop, and dispersion controls brine migration rates.

After both source concentrations of the WMA and PL reach maximum values (after 9 yr), the specified concentration changes abruptly from 0.294 to 0.200 kg/kg at the interface between the WMA and PL. The nature of the specified concentration boundary condition does not allow the sharp concentration gradient to dissipate over time and may artificially sustain a large density contrast that does not occur in reality. It is uncertain whether convection of brine at this interface is a numerical artifact or a physical

phenomenon. Regardless, the instability at this interface does not appear to impact the stability at other areas of the model.

The short-lived instability at the north end of PL propagates when the level of PL increases to 515.4 masl. Convection is not observed at lower lake elevations either before or after the peak. This indicates that brine transport behavior at the north end of PL is very sensitive to changes in lake elevation. The critical lake level (above which, density-driven convection develops) at this location is greater than 515 masl and less than 515.4 masl.

The instability at the connection between PL and the Floral Sand is due, at least in part, to high density brine in direct hydraulic contact with high permeability materials. However, the instability begins to propagate as the level of PL increases from 514 to 514.4 masl. As illustrated above, stability appears to be sensitive to lake elevation. The lower critical lake level at the Floral Sand connection may be due to the higher permeability sand.

Where Battleford till overlies the Floral Sand, density-driven instability develops only once the solute front migrates through the till. There are geological variations in the Battleford till thickness beneath PL, which result in slightly irregular elements and small variations in groundwater velocity. Vertical groundwater velocities are slightly lower where the till is thin (less than 2 m) and instability tends to develop preferentially at these locations. At the north end of PL, the Battleford thickness increases to 5 m and convection does not develop, except the short-term convection when PL levels are at a maximum.

The brine plume at ***NorthPL*** reaches steady state after 21 years. The hydraulic forces of groundwater discharging into PL are balanced by the density-driving forces that cause the downward migration of brine. As a result, the brine-groundwater interface reaches steady state (Figure 3.11) and local hydrodynamic containment of the brine plume is observed. A similar steady-state condition develops beneath the WMA after 60 years, where the Floral Sand is not present. The steady-state concentrations at ***WMA*** and ***NorthPL*** (Figure 3.11) are a function of the monitoring location depth with respect to the brine source and the brine source concentration. ***NorthPL*** is deeper in the subsurface

(5 m, compared to 2 m at ***WMA***) and the brine source concentration is lower (0.200 kg/kg, compared to 0.294 kg/kg at ***WMA***). As a result, the steady-state concentration at ***NorthPL*** is only 0.011 kg/kg compared to 0.11 kg/kg at ***WMA*** (relative concentrations (c/c_{source}) are 0.06 and 0.37, respectively).

Where brine migration intercepts the Floral till (at the Battleford/Floral till interface beneath the WMA, and at the base of the Floral Sand elsewhere), solute transport is dominated by dispersion, slowing vertical migration to the underlying FFA. For instance, the solute front at ***Connection*** migrates 4 m into the Floral till after 72 yr and is 9 m from reaching the top of the FFA (Figure 3.12). At ***WMA***, the solute front is 19 m above the FFA at the end of the 72 yr simulation.

Prior to the onset of convection, groundwater discharge conditions exist beneath PL and the WMA. The downward convection of dense brine results in local areas of groundwater recharge.

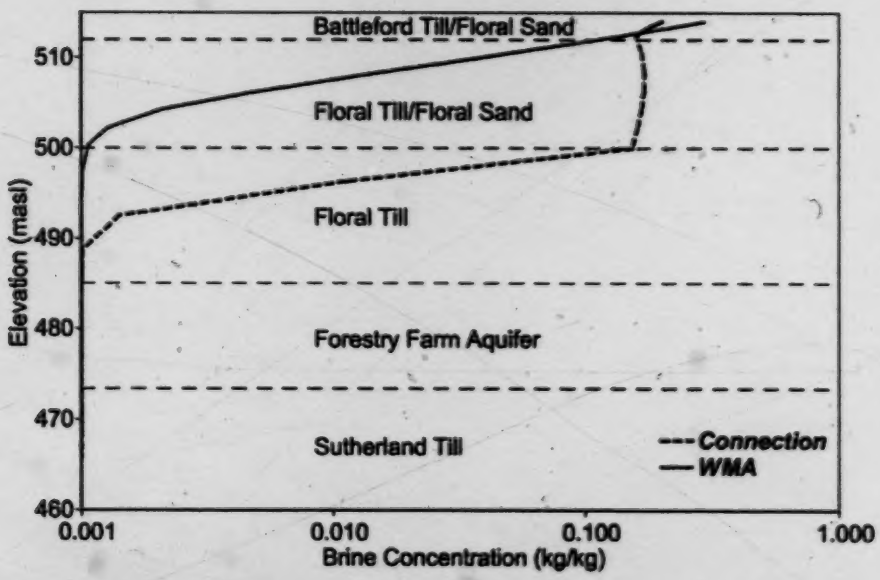

Figure 3.12. Vertical brine concentration profiles after 72 yr (2037) for ***Connection*** and ***WMA*** analysis locations.

3.6 Sensitivity Analysis

A sensitivity analysis is conducted by systematically modifying hydrogeologic properties or processes, boundary conditions or model parameters to determine what effect the change has on model output. The goal is to assess the uncertainty in model results, elucidate the important factors that control the system under investigation and understand how the system might respond under specific, perhaps unknown, stresses. In the present study, the most significant uncertainty is in the geologic environment, due to the sparse, point-source nature of the data and the heterogeneous nature of glacial deposits. This, in turn, creates uncertainty in the interpretation of hydrogeologic properties, primarily intrinsic permeability distributions. The most important system response is, of course, brine migration from the WMA and PL.

The sensitivity analysis results are compared to the ***Base*** case 2D brine transport model results in Section 3.5. The sensitivity analysis is comprised of five changes to the ***Base*** case numerical model:

1. Increased Floral Sand permeability (***High-k***);
2. Decreased Floral Sand permeability (***Low-k***);
3. Increased longitudinal and transverse dispersivities (***High Dispersivity***);
4. Constant historical WMA and PL elevation of 514 masl to present (***Constant Lake***); and
5. Increased future WMA and PL elevation.

Breakthrough curves for the four analysis locations (***WMA***, ***Connection***, ***MidPL*** and ***NorthPL***) are used to compare the results of the sensitivity analysis with the ***Base*** case results.

3.6.1 Floral Sand Permeability

Brine transport in the ***Base*** case model occurs primarily in the Floral Sand. Due to sparse data, there is uncertainty in the hydraulic connection between PL, the Floral Sand and the FFA. However, these connections may have a significant influence on brine migration rates and long-term brine impacts on groundwater resources. To simulate

both an increased and decreased hydraulic connection via the Floral Sand, the horizontal permeability of the entire Floral Sand hydrostratigraphic unit is modified. The ***Base*** case permeability of the Floral Sand is 7.5×10^{-12} m^2. To study its influence, two separate scenarios are considered, where a five times increase and decrease to the horizontal Floral Sand permeability is applied. In the high permeability case (***High-k***) the permeability is 3.8×10^{-11} m^2 and in the low permeability case (***Low-k***) the permeability is 1.5×10^{-12} m^2.

A change in the Floral Sand permeability will have an impact on the fluid flux into PL and the hydraulic head distribution beneath the WMA and PL. To ensure that changes applied to the 2D transport model still adequately represent steady state groundwater flow conditions, the changes in permeability are also applied to the 3D groundwater flow model. The differences in hydraulic head distribution between the 2D and 3D sensitivity models are compared with the ***Base*** case transport model and the 3D calibrated flow model (Figure 3.8). In the ***High-k*** case, the hydraulic head decreases along the section (compared to the ***Base*** case) in both the 2D and 3D models; in the ***Low-k*** case, the hydraulic head increases in both models. Along most of the section, the hydraulic head change is relatively small and the overall hydraulic gradient remains unchanged. The largest change in hydraulic head occurs at the north end of PL (Figure 3.8). In the 3D model, a five times increase or decrease in Floral Sand permeability causes a 40 cm decrease or increase in FFA hydraulic head at the north end of PL. In the 2D model the decrease and increase in hydraulic head is 30 cm. In general, the hydraulic response of the 2D model matches that of the 3D model.

Figure 3.13 illustrates breakthrough curves comparing the ***High-k*** and ***Low-k*** cases with the ***Base*** case. The Floral Sand does not extend beneath ***WMA***, so neither an increase nor a decrease in Floral Sand permeability has any effect on brine transport at that location (Figure 3.13 A).

At ***Connection*** (Figure 3.13 B), a decrease in Floral Sand permeability delays the onset of convection and an increase accelerates the onset of convection. Regardless, over the range of permeabilities investigated, the long-term result at ***Connection*** is the same: convection results in the rapid migration of brine and in the best-case scenario (***Low-k***), the solute concentration at the base of the Floral Sand reaches the source value of

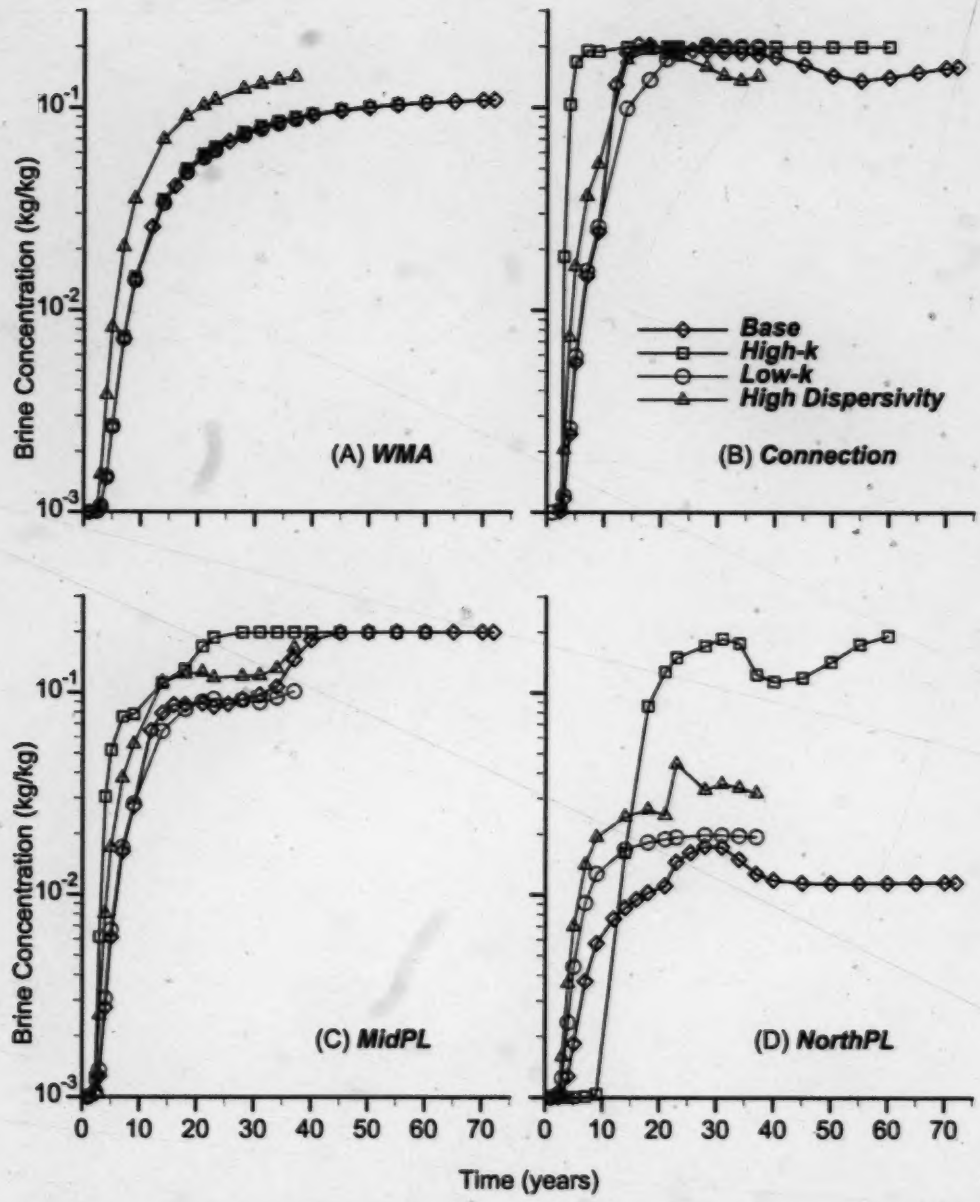

Figure 3.13. Brine concentration breakthrough curves at ***WMA***, ***Connection***, ***MidPL*** and ***NorthPL*** locations for Floral Sand permeability and dispersivity sensitivity analysis.

0.200 kg/kg after only 23 years (1988). Likewise, at ***MidPL***, a change in the Floral Sand permeability only affects the response time of the system. Convecting brine migrates northward within the Floral Sand toward ***MidPL***. In the ***High-k*** case, source concentrations reach ***MidPL*** in 28 years (Figure 3.13 C), compared to 45 years in the ***Base*** case. The response of the ***Low-k*** case is even slower, reaching a concentration of 0.10 kg/kg after 37 yr (maximum time simulated).

At ***NorthPL***, an increase in Floral Sand permeability results in a lower vertical groundwater velocity discharging into PL and, initially, dispersion of brine is slower than the ***Base*** case (Figure 3.13 D). The lower dispersion increases the instability of the system and convection develops earlier, and at a lower lake level. The critical lake level in the ***High-k*** case decreases 1 m to 514.5 masl, compared to the ***Base*** case. For the ***Low-k*** case however, convection does not develop at the north end of PL and a steady state concentration of 0.019 kg/kg is attained (Figure 3.13 D). This concentration is slightly higher than the steady state concentration of the ***Base*** case, due to a higher vertical groundwater velocity than the ***Base*** case and greater dispersion.

The average lateral brine migration rate in the Floral Sand for the ***High-k***, ***Base*** and ***Low-k*** cases is 33, 12 and 7 m/year, respectively (results not shown).

The most significant difference between the ***Base*** case and the Floral Sand permeability sensitivity models occurs at the north end of PL for the ***High-k*** case. Convection propagates earlier and is sustained to the end of the simulation. As a result, brine impacts the Floral Sand and FFA after only 23 years (Figure 3.14 A). By year 60 (2025), the brine front migrates 1000 m downgradient of PL, toward Burke Lake (Figure 3.14 B), and the solute concentration at Burke Lake begins to increase above the background value of 0.001 kg/kg (1000 mg/L).

3.6.2 Increased Dispersivity

Increased dispersion tends to increase the stability of a fluid density-stratified system (Simmons and Narayan, 1997). In the absence of convection, (beneath the WMA and at the north end of PL), brine transport is controlled by dispersion in the ***Base*** case. The longitudinal dispersivity and transverse dispersivity are increased from 2.0 and 0.2 m to

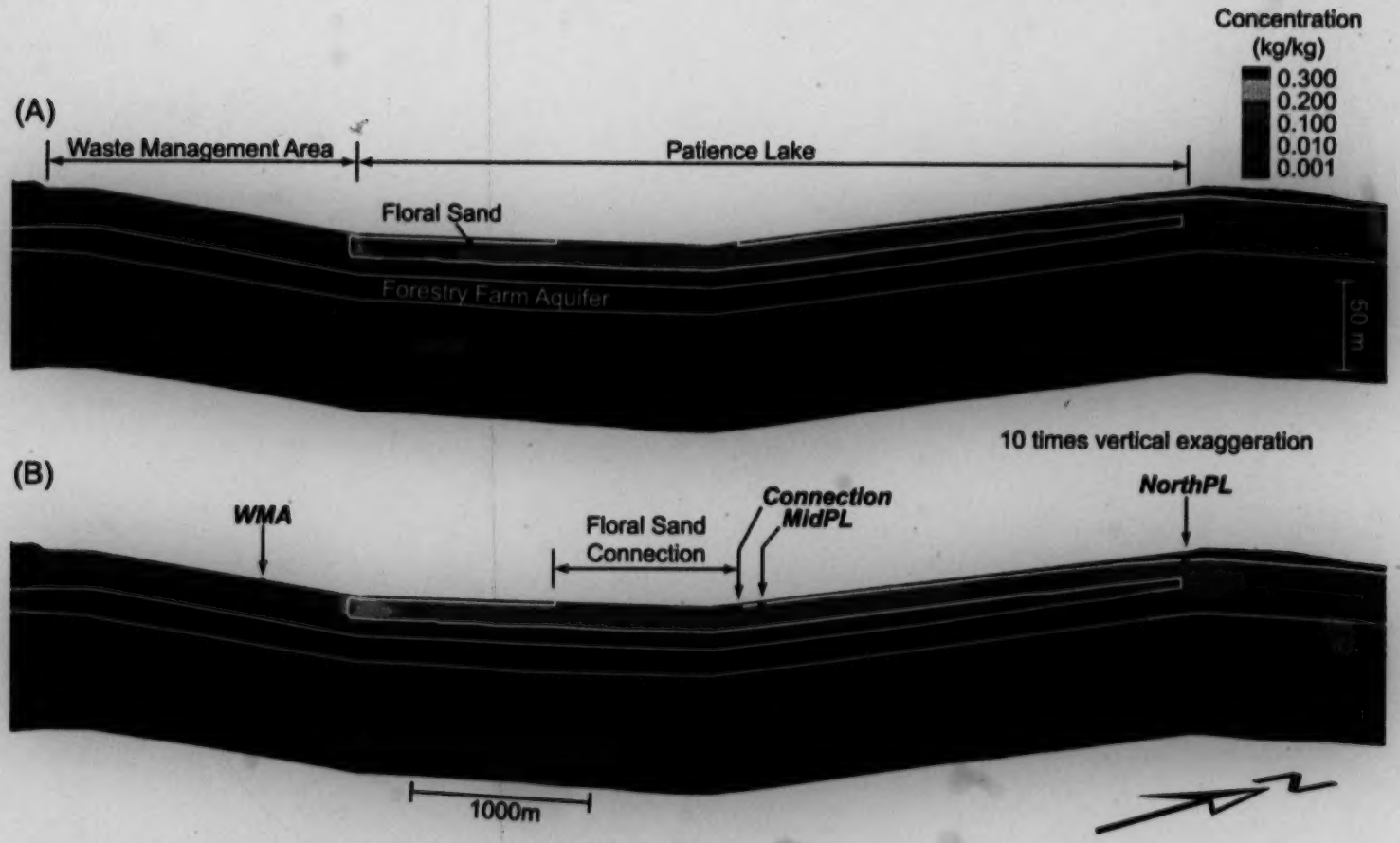

Figure 3.14. Simulated 2D transient brine distribution beneath the Waste Management Area and Patience Lake for the high Floral Sand permeability sensitivity simulation. (A) 23 years; (B) 60 years

4.0 and 0.4 m, respectively to assess the affect on stable brine transport and determine if instabilities are dampened.

At ***Connection*** and ***MidPL***, brine transport is controlled by convection/advection and an increase in dispersivity has little effect on the transient solute distribution (Figure 3.13 B and C). Increased dispersivity does influence the solution in areas where dispersion dominates over advection. The steady-state concentration at ***WMA*** and ***NorthPL*** is higher than in the ***Base*** case (Figure 3.13 A and D), indicating that the steady-state solute front migrates further into the subsurface. For example, after 37 years, the solute front at ***WMA*** migrated 8.5 m into the subsurface in the high dispersivity case and only 5.0 m in the ***Base*** case (data not shown).

Doubling the dispersivity of the system marginally increases stability. The short-lived convection cell that develops at the north end of PL when lake elevations are raised to 515.4 masl, occurs in both the ***Base*** case and high dispersivity case. This results in a transient increase in the breakthrough concentration at ***NorthPL*** (Figure 3.13 D). Along the Battleford till/Floral Sand interface, between ***MidPL*** and ***NorthPL***, dispersion initially controls brine transport but convection develops in the ***Base*** case after 37 years (Figure 3.10 C); whereas brine migration remains stable after 37 years in the high dispersivity case (data not shown). While this suggests a more stable system, the high dispersivity simulation ends after 37 years; therefore, it is uncertain whether instability eventually develops in this area of the model domain.

3.6.3 Historical Patience Lake Elevations

In the ***Base*** case simulation (Section 3.5.5), there is evidence that brine convection at the north end of PL is sensitive to historical lake levels. Convection at the Floral Sand connection may also be influenced by the simulated rise in lake level. To investigate the influence of historical lake levels on model results, the WMA and PL are maintained at a constant elevation of 514 masl throughout the simulation .

Breakthrough curves comparing ***Base*** case results with the ***Constant Lake*** level results for ***Connection*** and ***NorthPL*** are plotted in Figure 3.15. In the ***Base*** case, convection at ***Connection*** is evident by 12 yr, as soon as lake levels increase to 514.4 m (refer to

Figure 3.11). When lake levels are maintained at 514 masl, convection does not begin to propagate until after 25 yr, when the solute concentration increases rapidly from 0.055 to 0.19 kg/kg (Figure 3.15). At ***NorthPL***, convection is observed in the ***Base*** case when the lake level increases to 515.4 masl and then dissipates when the lake level recedes again. For the ***Constant Lake*** case, convection does not develop and the steady state concentration of 0.011 kg/kg remains constant throughout the simulation (Figure 3.15).

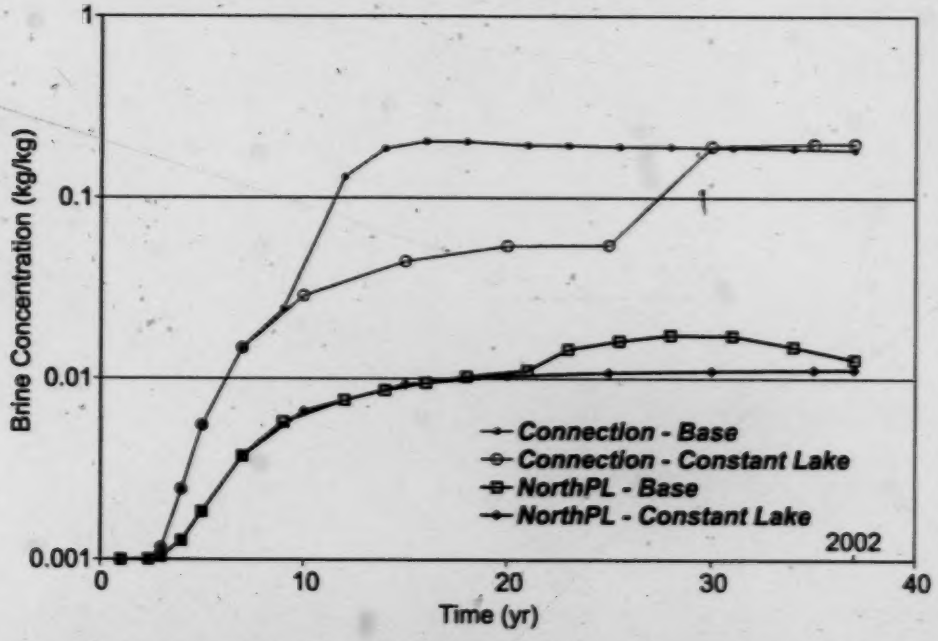

Figure 3.15. Brine concentration breakthrough curves at ***Connection*** and ***NorthPL*** illustrating the effect of simulating historical lake elevations changes.

3.6.4 Long-Term Patience Lake Elevation

The long-term management of mining wastes is likely to include management of PL. Therefore, it is important to consider the potential impact of future PL elevations on brine migration. Two predictive simulations, from 37 to 60 yr (2002 to 2025) are considered: the first increases the WMA and PL elevations by 50 cm to a maximum of 514.5 masl; the second considers an additional 50 cm increase to 515 masl (Figure 3.16). Recall that management of excess brine due to mine flooding in 1987 caused PL to reach a

maximum elevation of 515.6 masl (Figure 1.3). This increase was short-lived and not sustainable over the long-term in the semi-arid environment of central Saskatchewan. Therefore, long-term lake elevations above 515 masl are not considered in the sensitivity analysis.

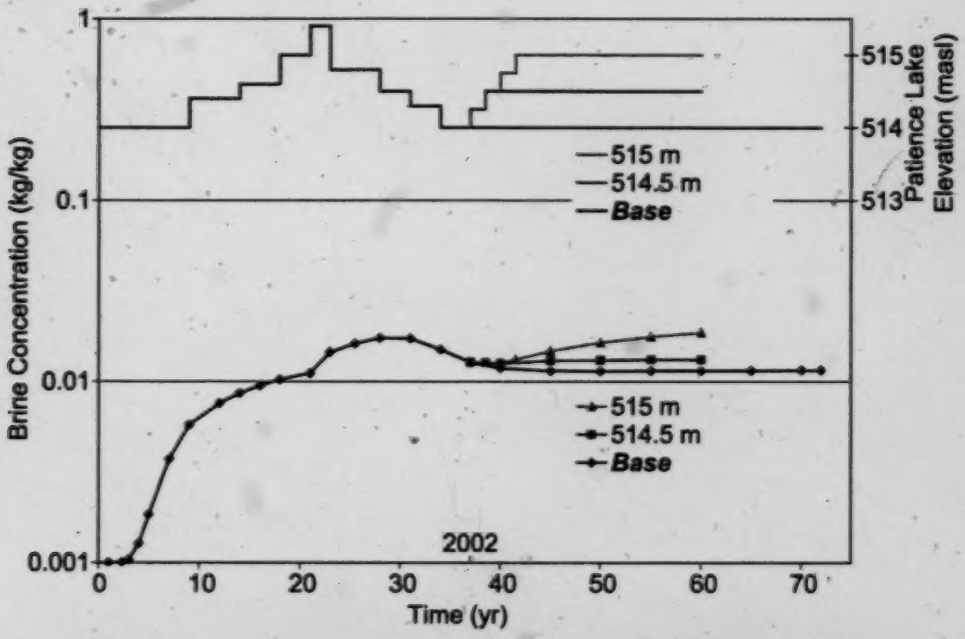

Figure 3.16. Brine concentration breakthrough curves at ***NorthPL*** and simulated Patience Lake elevation illustrating the effect of long-term lake level changes.

Overall, raising the elevation of PL has a minor effect on the future transient brine distribution. By 2002, when the sensitivity simulation begins, brine has migrated 450 m downgradient of ***Connection*** and convection is beginning to develop at the Battleford till/Floral Sand interface (Figure 3.10 C). The solute concentration at ***Connection*** and ***MidPL*** has already reached the source concentration of 0.200 kg/kg and a subsequent increase in lake level has no influence on the long-term solute concentration. Brine transport at ***WMA*** is unaffected by the transient increase in lake elevation (Figure 3.13 A) and is similarly unaffected by the long-term increase in lake elevation. At ***NorthPL***, a balance between hydraulic and density forces results in a steady state brine-groundwater interface. An increase in the long-term lake elevation shifts the position of the brine-groundwater interface and the simulated steady state solute concentration at

NorthPL increases (Figure 3.16). The steady state ***Base*** case concentration is 0.011 kg/kg and it increases to 0.013 and 0.019 kg/kg for the 514.5 and 515 m lake level simulations, respectively. Convection at the north end of PL is not observed for the higher long-term lake elevations and the FFA is not impacted at the end of either sensitivity simulation.

3.6.5 Discussion

The sensitivity analysis investigated the potential effect of uncertainties in Floral Sand permeability, dispersivity, transient lake level and long-term lake level, compared to the ***Base*** case results.

Brine migration is most sensitive to Floral Sand permeability. In the ***Base*** case, brine does not impact the FFA within the 72 year simulation period. At the north end of PL, a 5 times increase in the Floral Sand permeability decreases the hydraulic head within the Floral Sand by 30 cm. As a result, the reduced discharge into PL favours density forces, destabilizing the system. Brine migration via density-driven convection impacts the Floral Sand and FFA after only 23 years and Burke Lake after 60 years.

The influence of a 2 times increase in longitudinal and transverse dispersivity on brine migration rates is insignificant. In stable areas of the model, brine transport is dominated by dispersion and dispersivity has a strong influence. However, transport in these areas of the model do not appear to represent a threat to groundwater in the FFA. Density-driven transport at the Floral Sand connection and at the north end of PL (in the ***High-k*** case) does represent a long-term threat to groundwater quality in the FFA. At these locations, convection/advection dominates and increased dispersion has a negligible effect on brine migration rates.

The sensitivity analysis indicates that the increase in historical WMA/PL level may influence the onset of unstable brine transport. In the ***Base*** case, historical water levels are approximated in a step-wise manner. Compared to a constant lake level of 514 masl, unstable transport propagates more quickly at the Floral Sand connection. At the north end of PL, convection develops with a lake elevation of 515.4 masl for the ***Base***

case and 514.4 masl for the ***High-k*** case. This illustrates that the critical lake level is dependent upon the hydrogeology beneath the lake.

The investigation of long-term lake levels considered a maximum elevation of 515 masl. The only observable effect occurs at the north end of PL where the steady state solute concentration in the Battleford till increases, but density-driven convection does not develop. This demonstrates that, given the simulated hydrogeologic conditions, the maximum anticipated long-term lake elevation will not create instabilities at the north end of the lake.

3.7 Conclusions

This study utilizes a pre-release version of the SUTRA2D3D code (Voss and Provost, 2003) to investigate brine transport from the PCS PL potash mine site, east of Saskatoon. Groundwater flow is first characterized for the study area using a steady state 3D model. Important groundwater flow characteristics from the 3D model are incorporated into a 2D cross section model to simulate transient brine transport. A sensitivity analysis investigates the influence of important hydrogeological parameters and boundary conditions on brine transport.

PL lies in a north-south trending topographic low. Groundwater recharge east and west of PL creates a local flow system that discharges into Patience, Burke and Porter Lakes. There is also a northern component of groundwater flow (along the topographic low) in the FFA. There is geologic evidence that a locally continuous sand unit (Floral Sand) beneath the northern two thirds of PL may be hydraulically connected to both the underlying FFA and to PL.

Calibrated steady-state hydraulic heads are generally within 1 m of the observed values, and the simulated hydraulic head distribution in the FFA matches the observed. The calibrated horizontal permeability of the Floral Sand ranges from 4.0×10^{-12} to 7.5×10^{-12} m^2, and is 9.0×10^{-12} m^2 for the FFA (beneath the topographic low).

2D density-dependent transport modelling identifies several key features of the system: Where the high permeability Floral Sand is in direct contact with the brine source,

density-driven instability develops. Initially, stable, dispersion-dominated transport occurs within the Battleford till, but instabilities eventually propagate as the solute front reaches the underlying Floral Sand. Model results suggest that thicker Battleford till deposits, separating PL and the Floral Sand, promote stability. Where the Floral Sand is absent, stability persists and dispersion is the primary transport mechanism. In the ***Base*** case scenario, hydraulic and density forces balance at the north end of PL, resulting in a steady state solute front that does not impact the FFA.

In the ***Base*** case simulation, stable areas of the plume are hydrodynamically contained. Therefore, the greatest threat to groundwater resources is convection and advection originating from the Floral Sand connection. The average lateral brine migration rate in the Floral Sand was 12 m/year. Assuming similar conditions persist, brine migration through the Floral Sand could potentially reach the north end of PL by 2070.

Brine migration is sensitive to Floral Sand permeability and PL elevation. In the ***Base*** case simulation, instability (at the north end of PL) develops only at the highest simulated lake level and brine migration stabilizes before reaching the FFA. Given a five times increase in Floral Sand permeability, instability propagates at a lower lake level and brine migrates quickly to the FFA. When lake levels are maintained at 514 masl, convection (at the north end of PL) does not develop at all with ***Base*** case permeability and it is retarded 16 yr in the ***High-k*** case.

Observed chloride concentrations in the FFA are approximately 10 times background levels at the north end of PL, potentially indicating brine migration. In the ***Base*** case, the simulated solute concentration remains at background levels whereas concentrations exceed 1000 times background levels after only 23 yr in the ***High-k*** case. Given that the model is highly sensitive to both Floral Sand permeability and PL elevation, it is uncertain which factor may contribute to the differences in modelled and observed concentrations at the north end of PL.

Beneath the WMA, thick till deposits between the brine source and FFA function as a barrier to vertical brine migration. Dispersion dominates over convection and advection. Hydraulic forces (upward flux of discharging groundwater) offset and balance density

forces, resulting in a steady state solute front and hydrodynamic containment of brine. Increased dispersivity simply shifts the vertical position of the steady state solute front.

The hydrogelogical conceptual model of the study area identifies the importance of the three-dimensional nature of groundwater flow in the immediate vicinity of the dense mine tailings. The combined 3D and 2D modelling approach facilitates the incorporation of a 3D component of flow into a 2D model. The use of a 2D transport model allows fine spatial discretization and reasonable representation of both convective and dispersive processes. Modelling results indicate unstable convection develops where high permeability deposits are in contact with PL for all scenarios considered. Instability at the north end of PL is sensitive to aquifer permeability, lake level and till thickness.

3.8 References

Anderson, M.P. and Woessner, W.W., 1992. Applied groundwater modeling: simulation of flow and advective transport. Academic Press, Inc., 381 pp.

Argus Interware Inc., 1997. Argus Open Numerical Environments, ver 4.1. Argus Holdings, Ltd.

Christiansen, E.A., 1970. Geology. In: E.A. Christiansen (Editor), Physical environment of Saskatoon, Canada. National Research Council of Canada, 68 p.

Christiansen, E.A., 1992. Pleistocene stratigraphy of the Saskatoon area, Saskatchewan, Canada: an update. Canadian Journal of Earth Sciences, 29: 1767-1778.

Christiansen, E.A., 1999. Geology of the PCS Patience Lake mine area, Unpublished report prepared for the Potash Corporation of Saskatchewan, June 21, 1999.

Clifton Associates Ltd., 1993. Study of environmental impact potential of Patience Lake basin and Potash Company of America mine site Saskatoon, Saskatchewan. S551, Unpublished report prepared for the Potash Company of America.

Duffy, C.J. and Al-Hassan, S., 1988. Groundwater circulation in a closed desert basin: Topographic scaling and climatic forcing. Water Resources Research, 24(10): 1675-1688.

Energy, Mines and Resources, 1987. Map of Cheviot, Saskatchewan. Energy, Mines and Resources, Canada, 73 B/1, Edition 3, Scale 1:50,000.

Fetter, C.W., 1994. Applied hydrogeology, third edition. Prentice-Hall, Inc., 691 p.

Freeze, R.A. and Cherry, J.A., 1979. Groundwater. Prentice-Hall, Inc., 604 p.

Hayashi, M., van der Kamp, G. and Rudolph, D.L., 1998. Water and solute transfer between a prairie wetland and adjacent uplands, 1. Water balance. Journal of Hydrology, 207: 42-55.

Maathuis, H. and van der Kamp, G., 1994. Final Report: Subsurface brine migration at potash waste disposal sites in Saskatchewan. R-1220-10-E-94, Saskatchewan Research Council.

McCain Jr., W.D., 1991. Reservoir-fluid property correlations - state of the art. SPE Reservoir Engineering, 6: 266-272.

Meneley, W.A., 1970. Groundwater Resources. In: E.A. Christiansen (Editor), Physical environment of Saskatoon, Canada. National Research Council of Canada, 68 p.

Narayan, K.A. and Armstrong, D., 1995. Simulation of groundwater interception at Lake Ranfurly, Victoria, incroporating variable density flow and solute tranport. Journal of Hydrology, 165: 161-184.

Rogers, D.B. and Dreiss, S.J., 1995a. Saline groundwater in Mono Basin, California 1. Distribution. Water Resources Research, 31(12): 3131-3150.

Rogers, D.B. and Dreiss, S.J., 1995b. Saline groundwater in Mono Basin, California 2. Long-term control of lake salinity by groundwater. Water Resources Research, 31(12): 3151-3169.

Simmons, C.T. and Narayan, K.A., 1997. Mixed convection processes below a saline disposal basin. Journal of Hydrology, 194: 263-285.

Simmons, C.T. and Narayan, K.A., 1998. Modelling density-dependent flow and solute transport at the Lake Tutchewop saline disposal complex, Victoria. Journal of Hydrology, 206: 219-236.

Simmons, C.T., Narayan, K.A., Woods, J.A. and Herczeg, A.L., 2002. Groundwater flow and solute transport at the Mourquong saline-water disposal basin, Murray Basin, southeastern Australia. Hydrogeology Journal, 10: 278-295.

Tallin, J.E., Pufahl, D.E. and Barbour, S.L., 1990. Waste management schemes of potash mines in Saskatchewan. Canadian Journal of Civil Engineering, 17: 528-542.

Tóth, J., 1962. A theory of groundwater motion in small drainage basins in central Alberta, Canada. Journal of Geophysical Research, 67(11): 4375-4387.

Tóth, J., 1963. A theoretical analysis of groundwater flow in small drainage basins. Journal of Geophysical Research, 68(16): 4795-4812.

Uwiera, M., 1998. Numerical simulation of brine migration in the vicinity of a potash mine. M. Sc. Thesis, University of Saskatchewan, Saskatoon, 208 pp.

Voss, C.I., 1984. SUTRA: a finite-element simulation model for saturated-unsaturated fluid-density-dependent ground-water flow with energy transport or chemically-reactive single-species solute transport. 84-4369, U. S. Geological Survey Water-Resources Investigations.

Voss, C.I. and Provost, A.M., 2003. SUTRA: a model for saturated-unsaturated, variable-density ground-water flow with solute or energy transport. 02-4231, U. S. Geological Survey Water-Resources Investigations.

Wittrock, V. and Wheaton, E.E., 1993. Saskatoon SRC Climatological Reference Station Annual Summary, 1992. E-2900-5-B-93, Saskatchewan Resarch Council.

Chapter 4

Conclusions

The objective of this thesis was to assess the potential long-term effects of brine storage on local groundwater resources at the PCS Patience Lake potash mine site. Density-dependent solute transport modelling was conducted utilizing available hydrogeologic data and the SUTRA code (Voss, 1984; Voss and Provost, 2003).

A two-dimensional (2D) model domain, with simple geometry, was used to investigate and justify two primary hydrogeological assumptions: that both (1) the influence of small-scale till heterogeneity and (2) saturated-unsaturated flow do not have a significant effect on brine transport. With these assumptions established, site-specific, yet regional, groundwater flow and brine transport modelling was conducted to characterize the hydrogeology and brine transport behavior at the mine site.

4.1 Hydrogeological Assumptions

Log normal permeability distributions of the Battleford Formation till were generated with a mean permeability of $1x10^{-13}$ m^2, horizontal correlation lengths ranging between 12 and 42 m and vertical correlation lengths between 0.8 and 3.5 m. Shorter correlation lengths (either horizontal or vertical) favoured unstable, density-driven solute transport and longer correlation lengths promoted stable, dispersion-dominated transport. Reducing the mean permeability also promoted stable brine transport.

When the stability results were compared with available geologic data, it appeared unlikely that heterogeneity-controlled instability will develop in the Battleford Formation till. Simulation results suggested that the permeability would need to vary by more than 4 orders of magnitude, for horizontal correlation length scales on the order of tens of metres, to produce instability. Low permeability clay till units at the mine site appeared to be horizontally correlated over hundreds of metres.

Simulations were conducted to compare brine transport behavior of heterogeneous and homogeneous Battleford Formation till distributions. When the system remained stable, brine migration was dominated by dispersion and there was no difference between heterogeneous and homogeneous simulations. Combined with the evidence that brine migration in the Battleford Formation till will likely be stable, it was concluded that simulation of small-scale heterogeneity was unnecessary and the Battleford Formation could be treated as a homogeneous hydrostratigraphic unit.

The influence of saturated-unsaturated flow on brine transport was investigated by comparing saturated-unsaturated versus fully saturated simulations under homogeneous, heterogeneous, stable and unstable conditions. Saturated-unsaturated flow had a negligible effect on brine transport.

4.2 Hydrogeology and Brine Transport at the Patience Lake Mine Site

In the development of the conceptual model for the Patience Lake (PL) mine site, the importance of three-dimensional (3D) groundwater flow was identified. To minimize computational requirements and incorporate 3D groundwater flow, a nested model approach was utilized. 3D steady state groundwater flow was first calibrated to available data. The results of the 3D groundwater flow calibration were then incorporated into a 2D model domain by assigning representative boundary conditions. Transient 2D density-dependent brine transport simulations and sensitivity analysis were conducted using the 2D model domain.

There is geological evidence to suggest that the Floral Sand is hydraulically connected to the FFA at the north end of PL. In addition, the Floral Sand may sub-crop near the west shore of PL, creating a direct, high permeability connection between the brine source and FFA. Preliminary modelling concluded that small-scale heterogeneities in the till could be neglected; however, these lager-scale heterogeneities were explicitly accounted for in the 3D and 2D model domains as separate hydrostratigraphic units.

4.2.1 Groundwater Flow Calibration

The calibrated 3D groundwater flow model agreed with the conceptual model and available field data. Groundwater recharge from topographically high areas flowed to the Forestry Farm Aquifer (FFA) and then converged at the north-south trending topographic low, discharging into Patience, Burke and Porter Lakes. The simulated steady state hydraulic head distribution in the FFA agreed with available field data.

A rigorous sensitivity analysis was not performed on the 3D groundwater flow model. As part of the 2D brine transport sensitivity analysis however, the permeability of the Floral Sand, in both the 2D and 3D models, was modified to determine if steady-state groundwater flow responded in a similar manner. A 10-fold change in Floral Sand permeability resulted in a maximum change of 80 cm in the steady state hydraulic head beneath the north end of Patience Lake. The response of the 2D and 3D models was in close agreement. An increase in Floral Sand permeability decreased hydraulic heads within the FFA, reducing the magnitude of the negative vertical hydraulic gradient and the groundwater discharge into PL.

4.2.2 Brine Transport

In the ***Base*** case simulation, brine at the north end of PL was hydrodynamically contained. Convection and/or advection within the Floral Sand represented the primary pathway for brine migration to the FFA. Based on simulated migration rates, brine migration within the Floral Sand could potentially reach the FFA as early as 2070.

Brine transport behavior at the north end of PL was sensitive to transient lake levels and Floral Sand permeability. For the ***Base*** case Floral Sand permeability, the critical lake level was 515.4 masl; convection developed but dissipated when the lake elevation decreased below the critical level. At the higher Floral Sand permeability, the critical lake level decreased to 514.4 masl, convection persisted to the end of the simulation and brine migrated into the Floral Sand and FFA. As a result of this convection, solute concentrations at Burke Lake began to increase after only a 60 yr (2025) simulation period .

Density-driven convection at the Floral Sand connection was also sensitive to transient PL level changes. When lake levels were maintained at a constant elevation of 514 masl, the onset of convection was slowed by 16 years, compared to the ***Base*** case simulation which approximated historical lake level changes.

Beneath the WMA, thick, low permeability till deposits separated the brine source and FFA. For all scenarios considered, brine transport was stable and controlled by dispersion. The downward migration of brine was balanced by upward hydraulic forces and a steady state brine front was established, resulting in hydrodynamic containment of brine.

The effects of long-term lake level changes were considered for the ***Base*** case Floral Sand permeability. A maximum lake elevation of 515 masl did not influence brine migration behavior since the system was stable at the north end of PL. The effect of long-term lake level changes was not considered for increased Floral Sand permeability.

4.3 Future Work

Additional research directions should focus on the primary hydrogeological uncertainties identified in the current study, which are outlined below.

4.3.1 Field Data

Delineation of the Floral Sand is incomplete. Additional geologic data along the west and east shores of PL would help identify the lateral and vertical extent of the Floral Sand and reduce uncertainty in the connectivity with the FFA. Additional hydraulic head and geochemistry data from the Floral Sand would help refine the conceptual model and quantify the extent of brine migration beneath PL. This data could be used to better-calibrate the brine transport model.

Detailed vertical concentration profiles within the Battleford and Floral Formation tills, immediately adjacent to or beneath PL and the WMA, would provide information on brine migration rates and hydrodynamic dispersion parameters. Monitored over time, vertical

concentration profiles would help confirm or refute whether a steady state (hydrodynamically contained) brine plume exists within the till deposits.

Most existing piezometers are located in close proximity to the PL mine site and PL. Additional piezometers, completed at greater lateral distances from PL, would increase knowledge of the groundwater flow system within the study area and increase the reliability of future numerical model calibrations.

4.3.2 Numerical Modelling

The additional numerical modelling suggested below would reduce uncertainty in the current numerical modelling results.

1. Re-calibrate the 3D groundwater flow and 2D brine transport models as additional data is obtained;
2. Perform a sensitivity analysis on the 3D steady state groundwater flow model. Hydrogeological parameters that have a large influence on the groundwater flow solution could then be altered in the brine transport model to evaluate the potential effect on brine transport;
3. Consider transient historical lake elevations in more detail. The observed lake level changes were approximated by applying discrete, instantaneous increases/decreases to a constant specified pressure boundary condition. Transient specified pressure boundary conditions could be implemented to better reflect observed lake levels;
4. Simulate the effect of long-term lake level increases for the high Floral Sand permeability scenario. This would help characterize how convective brine transport at the north end of PL might be affected by higher lake levels; and,
5. Investigate the sensitivity of the brine transport model to WMA and PL brine source concentrations.

4.4 References

Voss, C.I., 1984. SUTRA: a finite-element simulation model for saturated-unsaturated fluid-density-dependent ground-water flow with energy transport or chemically-

reactive single-species solute transport. 84-4369, U. S. Geological Survey Water-Resources Investigations.

Voss, C.I. and Provost, A.M., 2003. SUTRA: a model for saturated-unsaturated, variable-density ground-water flow with solute or energy transport. 02-4231, U. S. Geological Survey Water-Resources Investigations.

Appendix A

Study Area Maps

Map 1: Study Area and Land Surface Topography for the PCS Patience Lake Mine Site

Map 2: Lea Park Formation Topography

Map 3: Bearpaw Formation Topography

Map 4: Isopach of Forestry Farm Aquifer

Map 5: Isopach of Floral Sand

Map 6: Piezometer Locations, Geochemistry and Observed Hydraulic Head Distribution in the Forestry Farm Aquifer

Map 7: 2D Numerical Model Cross Section Locations and 3D Numerical Model Domain Outline

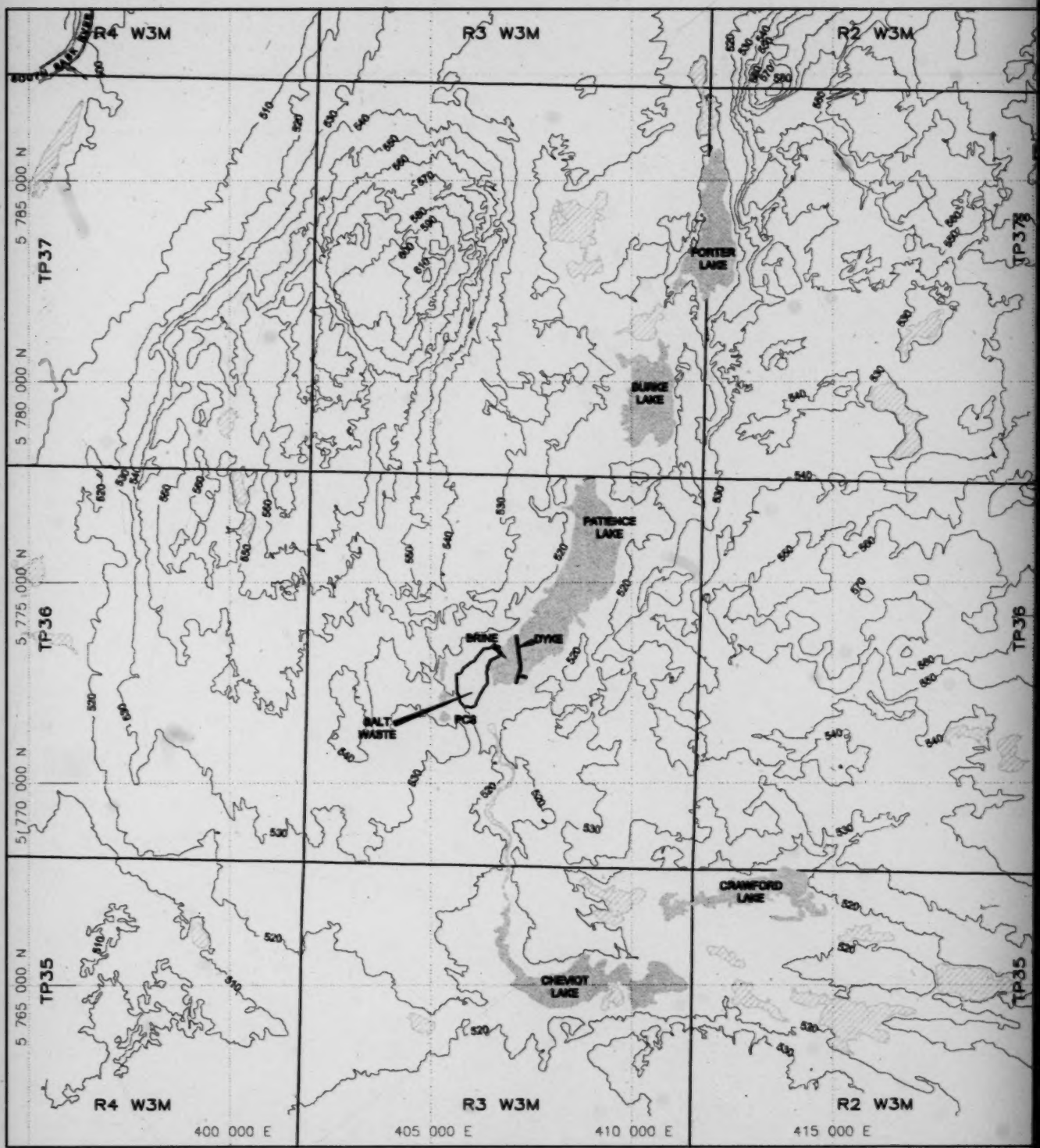
R4 W3M
R3 W3M
R2 W3M
TP37
TP36
TP35
5 785 000 N
5 780 000 N
5 775 000 N
5 770 000 N
5 765 000 N
PORTER LAKE
BURKE LAKE
PATIENCE LAKE
BRINE
DYKE
SALT WASTE
PCB
CRAWFORD LAKE
CHEVIOT LAKE
400 000 E
405 000 E
410 000 E
415 000 E

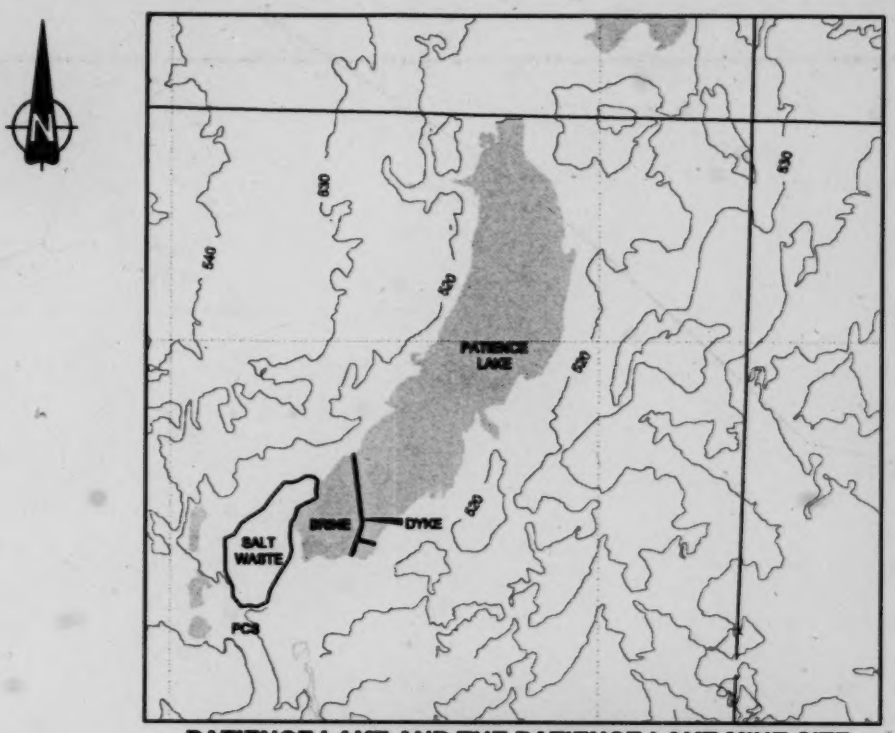

PATIENCE LAKE AND THE PATIENCE LAKE MINE SITE
SCALE 1 : 75 000

LEGEND

SURFACE WATER, INTERMITTENT

530 GROUND SURFACE ELEVATION CONTOUR (masl)
(10 m CONTOUR INTERVAL)

0 1 2 3 4 5 km
SCALE 1 : 125,000

COORDINATES ARE UTM NAD27 ZONE 13.

MAP 1

STUDY AREA AND LAND SURFACE TOPOGRAPHY FOR THE PCS PATIENCE LAKE MINE SITE

DEPARTMENT OF EARTH AND ATMOSPHERIC SCIENCES
UNIVERSITY OF ALBERTA

DAN BORN | **2003**

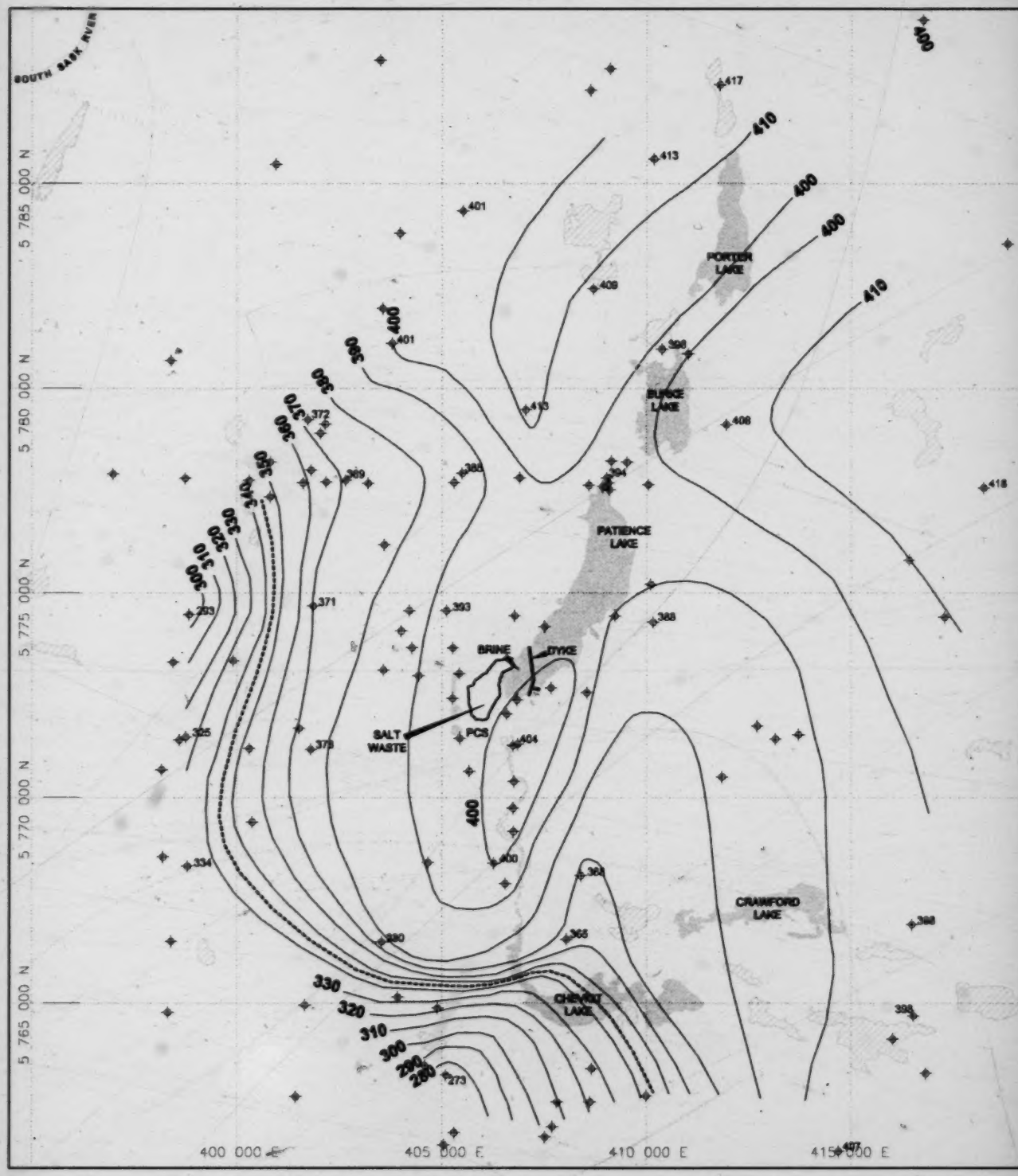
SOUTH SASK RIVER
PORTER LAKE
BURKE LAKE
PATIENCE LAKE
CRAWFORD LAKE
CHERNOT LAKE
BRINE
DYKE
SALT WASTE
PCS
5 785 000 N
5 780 000 N
5 775 000 N
5 770 000 N
5 765 000 N
400 000 E
405 000 E
410 000 E
415 000 E

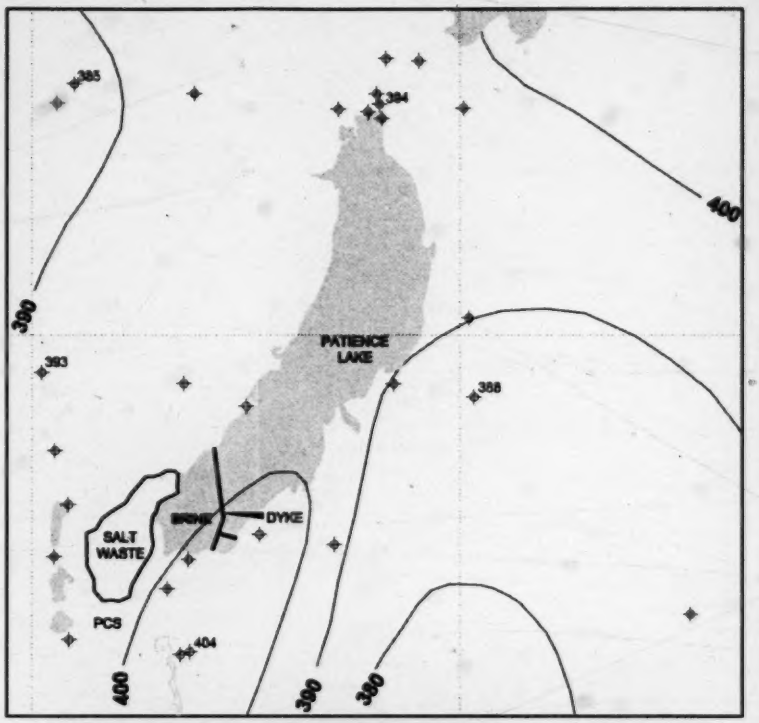

PATIENCE LAKE AND THE PATIENCE LAKE MINE SITE
SCALE 1 : 75 000

LEGEND

- SURFACE WATER, INTERMITTENT
- BOREHOLE LOCATION (FROM CHRISTIANSEN, 1999)
- 388 — LEA PARK FORMATION ELEVATION (masl)
- LEA PARK FORMATION ELEVATION CONTOURS (masl)
- INFERRED EXTENT OF SASKATOON LOW COLLAPSE FEATURE

0 1 2 3 4 5 km
SCALE 1 : 125,000

COORDINATES ARE UTM NAD27 ZONE 13.

MAP 2

LEA PARK FORMATION TOPOGRAPHY

DEPARTMENT OF EARTH AND ATMOSPHERIC SCIENCES
UNIVERSITY OF ALBERTA

DAN BORN | **2003**

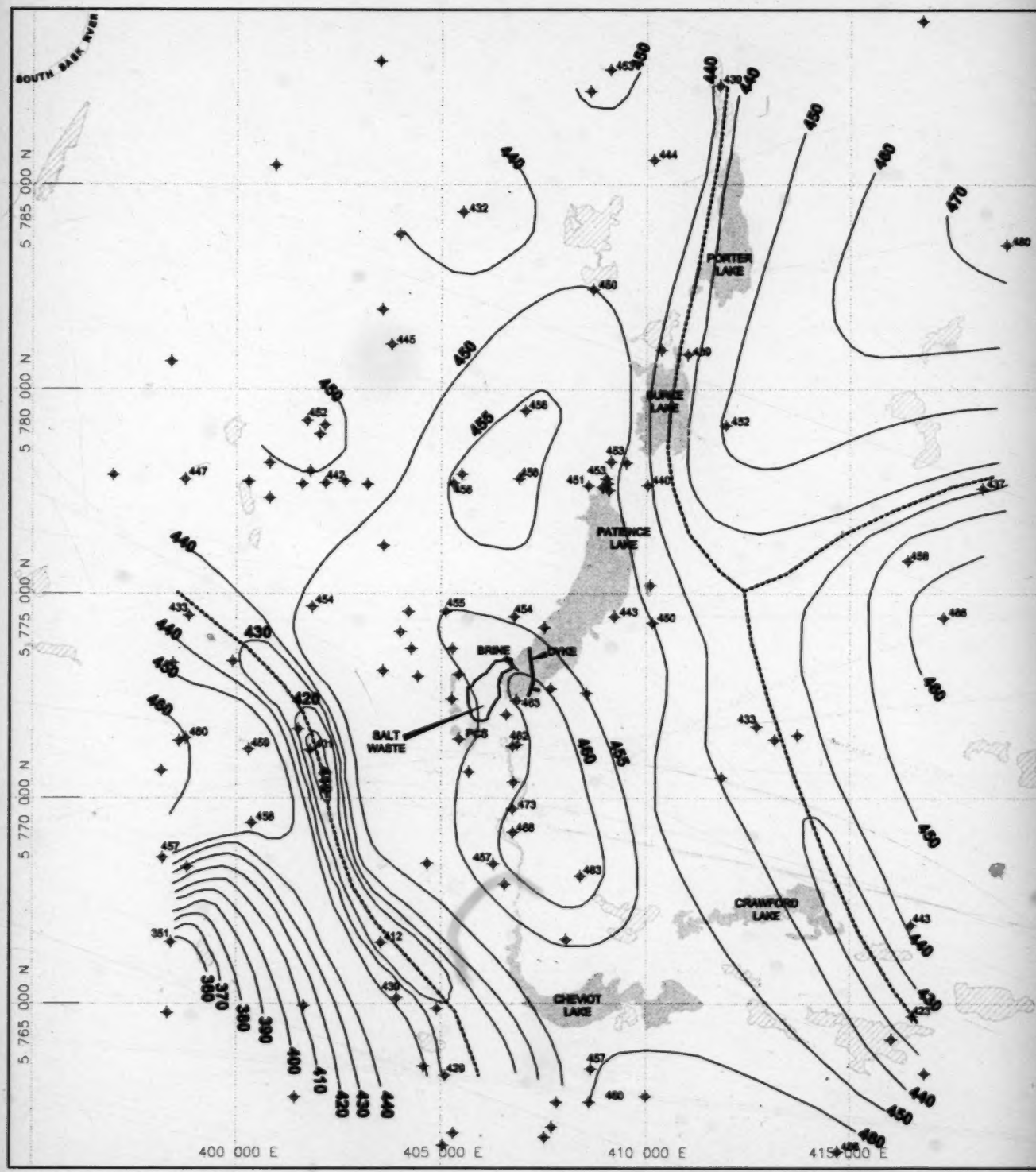
SOUTH SASK RIVER
PORTER LAKE
BURKE LAKE
PATIENCE LAKE
CRAWFORD LAKE
CHEVIOT LAKE
BRINE
DYKE
SALT WASTE
PGS
5 785 000 N
5 780 000 N
5 775 000 N
5 770 000 N
5 765 000 N
400 000 E
405 000 E
410 000 E
415 000 E

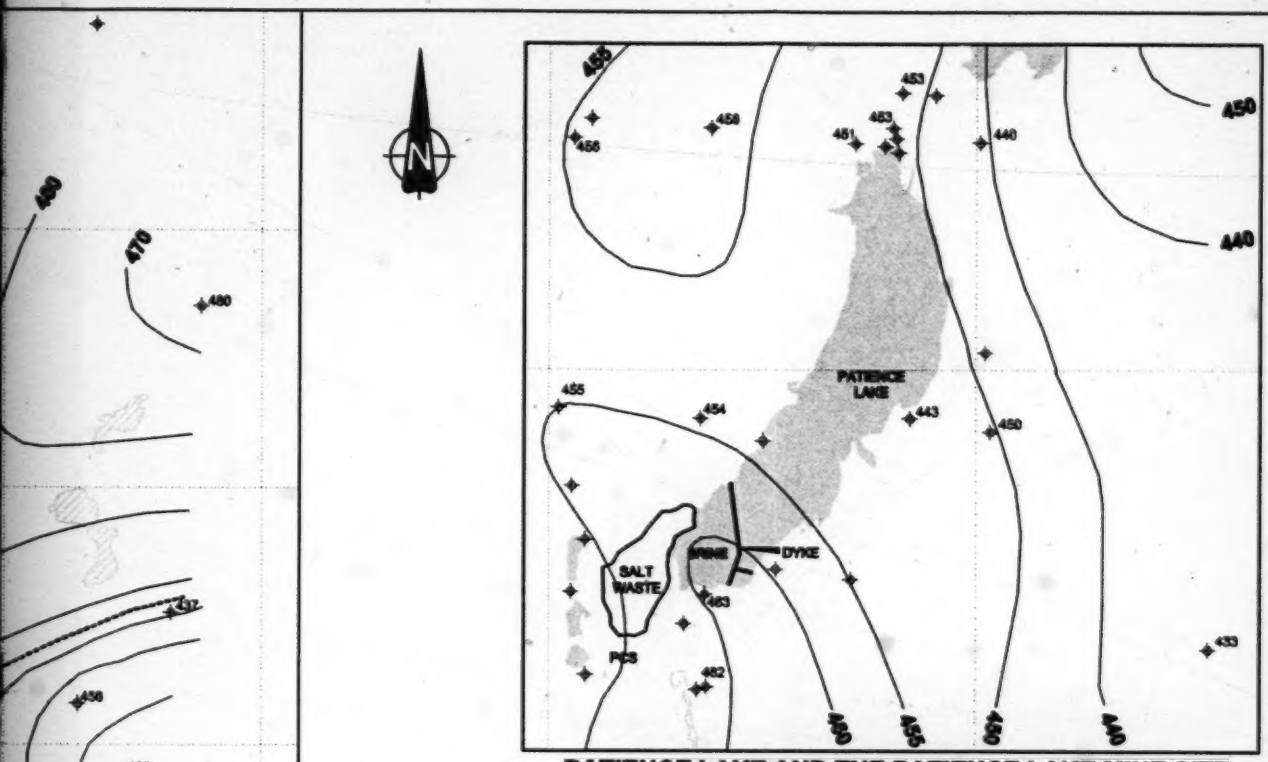

PATIENCE LAKE AND THE PATIENCE LAKE MINE SITE
SCALE 1 : 75 000

LEGEND

- SURFACE WATER, INTERMITTENT
- BOREHOLE LOCATION (FROM CHRISTIANSEN, 1999)
- 488 — BEARPAW FORMATION ELEVATION (masl)
- BEARPAW FORMATION ELEVATION CONTOURS (masl)
- INFERRED BEDROCK CHANNEL

0 1 2 3 4 5 km
SCALE 1 : 125,000

COORDINATES ARE UTM NAD27 ZONE 13.

MAP 3

BEARPAW FORMATION TOPOGRAPHY

DEPARTMENT OF EARTH AND ATMOSPHERIC SCIENCES
UNIVERSITY OF ALBERTA

DAN BORN | 2003

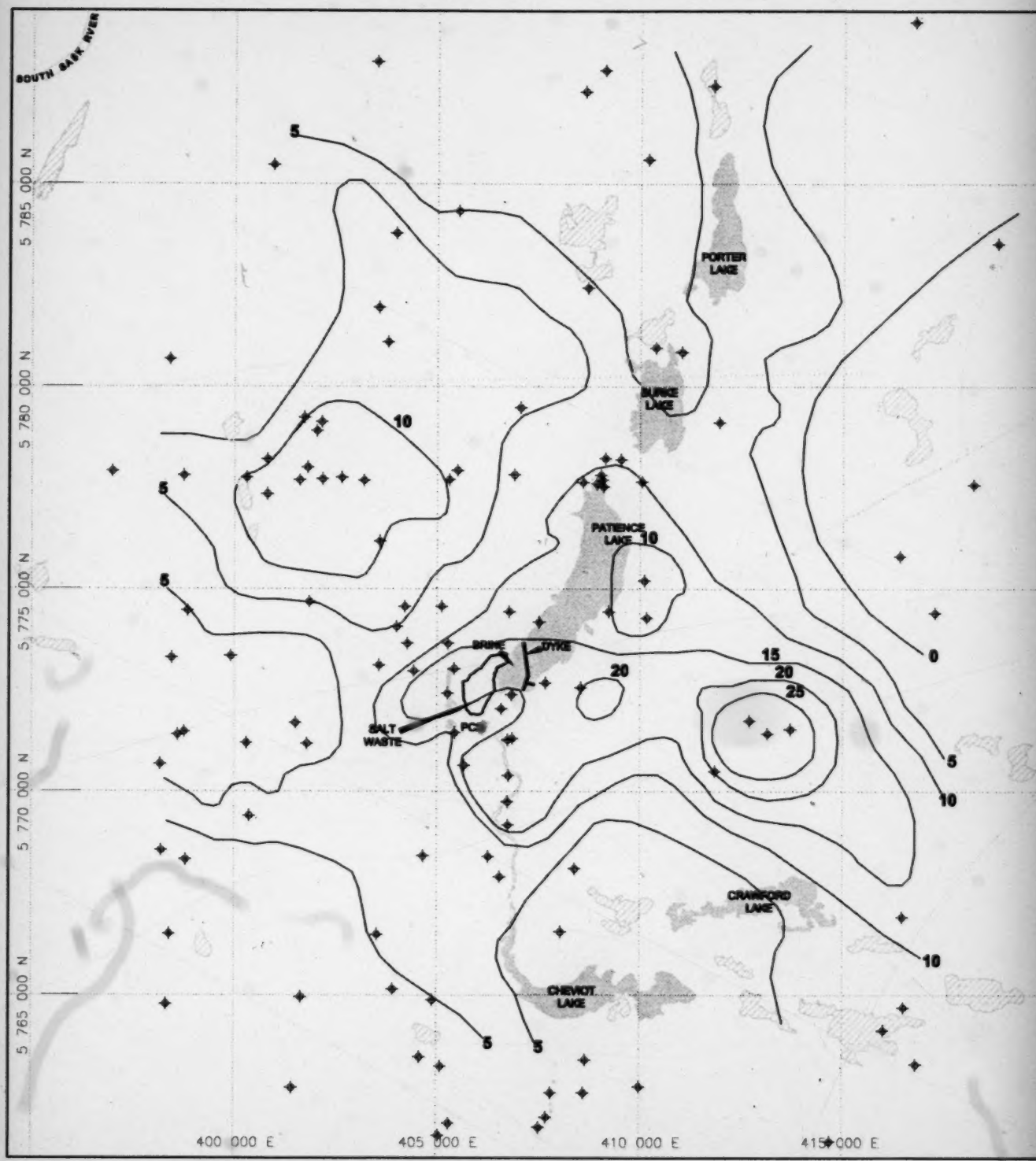
SOUTH BASIN RIVER
PORTER LAKE
BURKE LAKE
PATIENCE LAKE
BRINE
DYKE
SALT WASTE
PCS
CRAWFORD LAKE
CHEVIOT LAKE
5
10
15
20
25
0
5 785 000 N
5 780 000 N
5 775 000 N
5 770 000 N
5 765 000 N
400 000 E
405 000 E
410 000 E
415 000 E

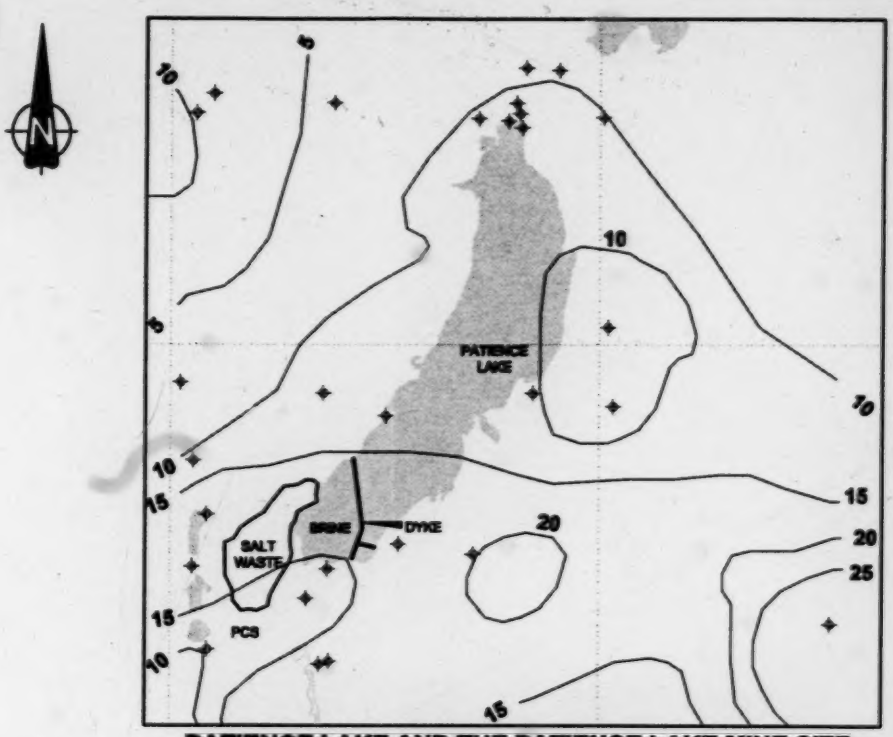

PATIENCE LAKE AND THE PATIENCE LAKE MINE SITE
SCALE 1 : 75 000

LEGEND

- SURFACE WATER, INTERMITTENT
- BOREHOLE LOCATION (FROM CHRISTIANSEN, 1999)
- FORESTRY FARM AQUIFER THICKNESS CONTOURS (m)

0 1 2 3 4 5 km
SCALE 1 : 125,000

COORDINATES ARE UTM NAD27 ZONE 13.

MAP 4

ISOPACH OF FORESTRY FARM AQUIFER

DEPARTMENT OF EARTH AND ATMOSPHERIC SCIENCES
UNIVERSITY OF ALBERTA

DAN BORN | **2003**

SOUTH BABE RIVER
PORTER LAKE
BURKE LAKE
PATENCE LAKE
0
5
10
15
20
10
BRINE
BRINE
SALT WASTE
PCS
CRAWFORD LAKE
CHEVROT LAKE
5 785 000 N
5 780 000 N
5 775 000 N
5 770 000 N
5 765 000 N
400 000 E
405 000 E
410 000 E
415 000 E

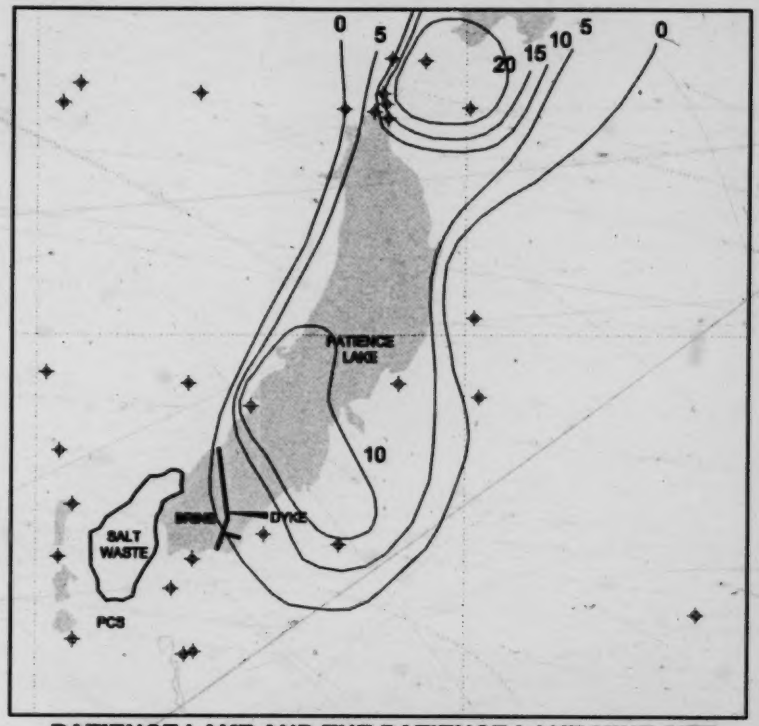

PATIENCE LAKE AND THE PATIENCE LAKE MINE SITE
SCALE 1 : 75 000

LEGEND

SURFACE WATER, INTERMITTENT

BOREHOLE LOCATION (FROM CHRISTIANSEN, 1999)

FLORAL SAND THICKNESS CONTOURS (m)

0 1 2 3 4 5 km
SCALE 1 : 125,000

COORDINATES ARE UTM NAD27 ZONE 13.

MAP 5

ISOPACH OF FLORAL SAND

DEPARTMENT OF EARTH AND ATMOSPHERIC SCIENCES
UNIVERSITY OF ALBERTA

DAN BORN | **2003**

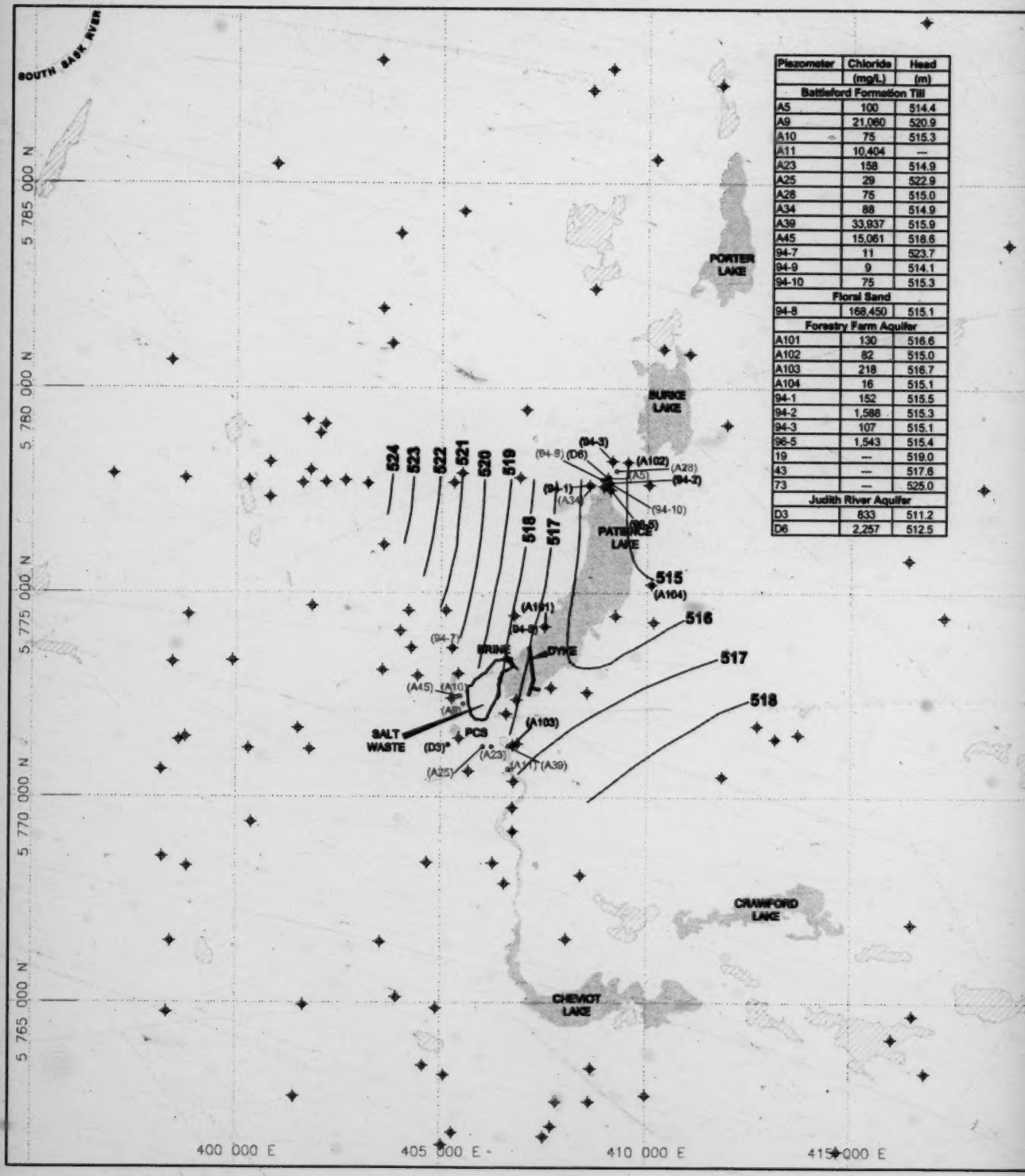

Piezometer	Chloride (mg/L)	Head (m)
Battleford Formation Till		
A5	100	514.4
A9	21,060	520.9
A10	75	515.3
A11	10,404	—
A23	158	514.9
A25	29	522.9
A28	75	515.0
A34	88	514.9
A39	33,937	515.9
A45	15,061	518.6
94-7	11	523.7
94-9	9	514.1
94-10	75	515.3
Floral Sand		
94-8	168,450	515.1
Forestry Farm Aquifer		
A101	130	516.6
A102	82	515.0
A103	218	516.7
A104	16	515.1
94-1	152	515.5
94-2	1,588	515.3
94-3	107	515.1
96-5	1,543	515.4
19	—	519.0
43	—	517.6
73	—	525.0
Judith River Aquifer		
D3	833	511.2
D6	2,257	512.5

Chloride (mg/L)	Head (m)
Formation Till	
100	514.4
1,060	520.9
75	515.3
0,404	—
158	514.9
29	522.9
75	515.0
88	514.9
3,937	515.9
5,061	518.6
11	523.7
9	514.1
75	515.3
l Sand	
8,450	515.1
rm Aquifer	
130	516.6
82	515.0
218	516.7
16	515.1
152	515.5
,586	515.3
107	515.1
,543	515.4
—	519.0
—	517.6
—	525.0
er Aquifer	
833	511.2
,257	512.5

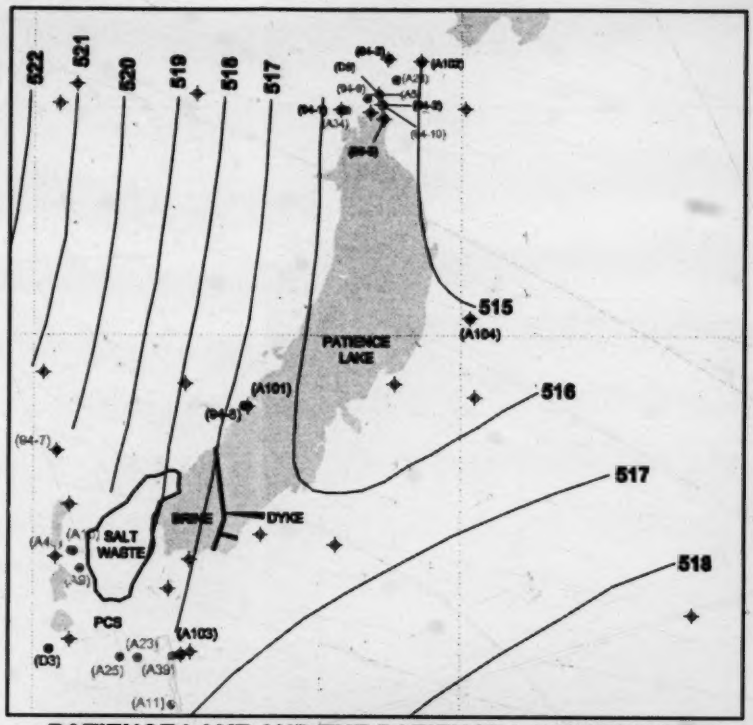

PATIENCE LAKE AND THE PATIENCE LAKE MINE SITE
SCALE 1 : 75 000

LEGEND

- SURFACE WATER, INTERMITTENT
- BOREHOLE LOCATION (FROM CHRISTIANSEN, 1999)
- 515 — GROUNDWATER SURFACE ELEVATION IN FORESTRY FARM AQUIFER (masl)

PIEZOMETERS

- BATTLEFORD FORMATION TILL
- FORESTRY FARM AQUIFER
- FLORAL SAND
- JUDITH RIVER AQUIFER

0 1 2 3 4 5 km
SCALE 1 : 125,000

COORDINATES ARE UTM NAD27 ZONE 13.

MAP 6

PIEZOMETER LOCATIONS, GEOCHEMISTRY AND OBSERVED HYDRAULIC HEAD DISTRIBUTION IN THE FORESTRY FARM AQUIFER

DEPARTMENT OF EARTH AND ATMOSPHERIC SCIENCES
UNIVERSITY OF ALBERTA

DAN BORN

2003

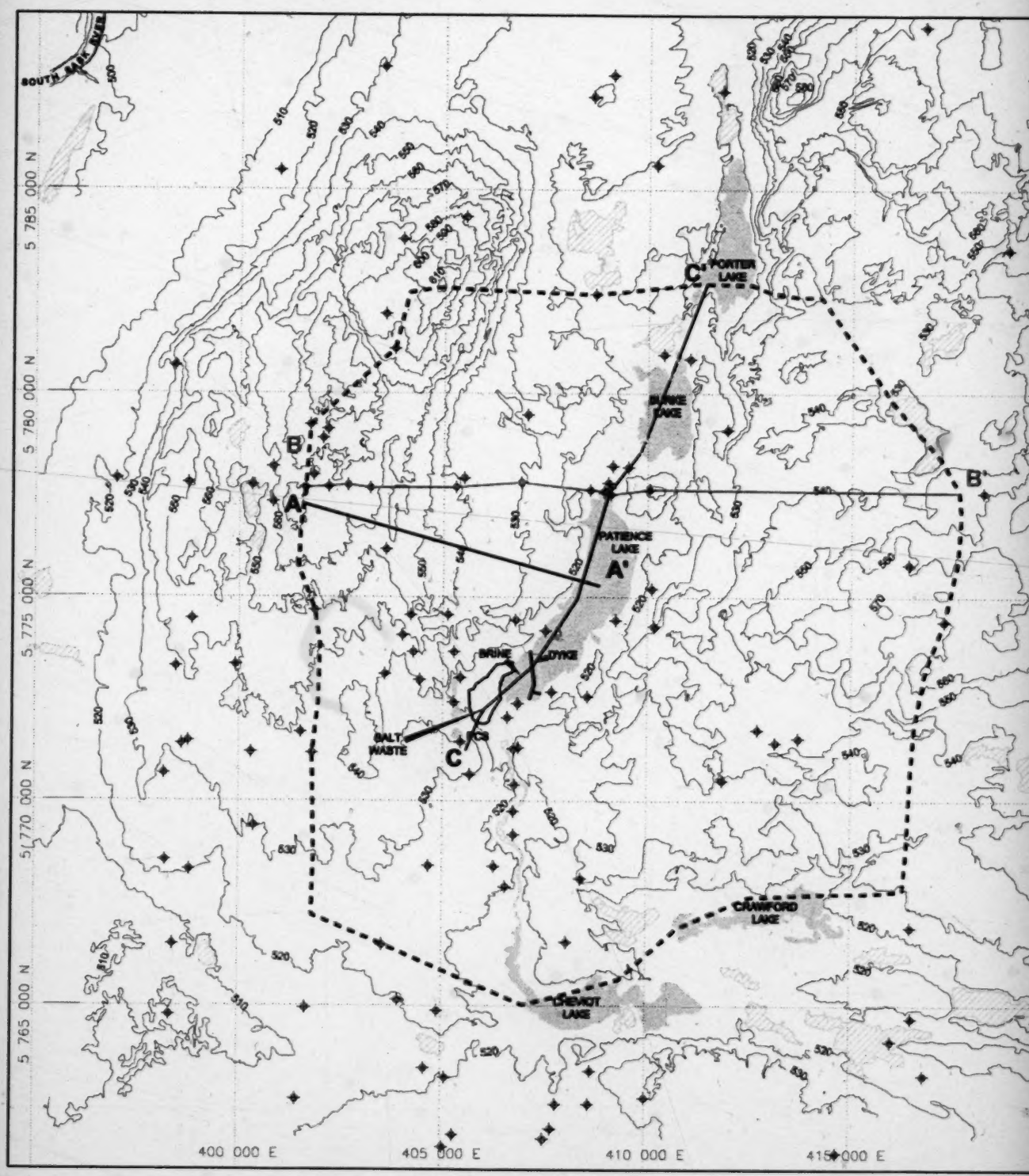
SOUTH BABE RIVER
PORTER LAKE
BURKE LAKE
PATIENCE LAKE
DYKE
BRINE
SALT WASTE
PCB
CRAWFORD LAKE
CHEVROT LAKE
A
A'
B
B'
C
C'
5 785 000 N
5 780 000 N
5 775 000 N
5 770 000 N
5 765 000 N
400 000 E
405 000 E
410 000 E
415 000 E

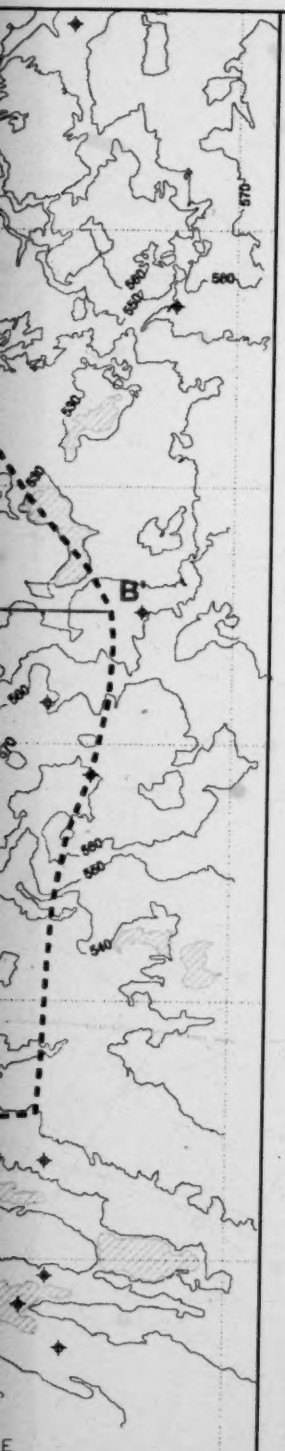

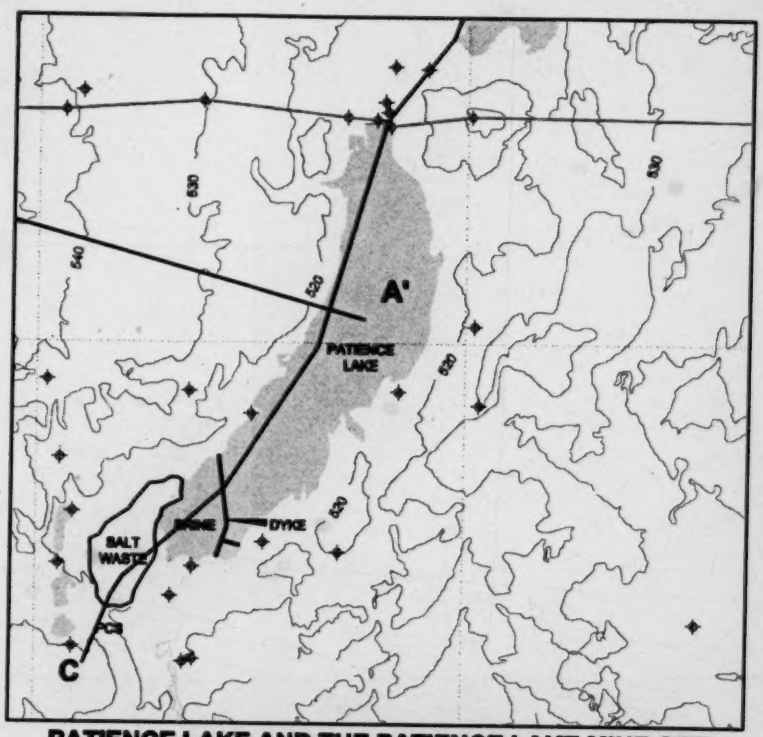

PATIENCE LAKE AND THE PATIENCE LAKE MINE SITE
SCALE 1 : 75 000

LEGEND

- SURFACE WATER, INTERMITTENT
- 520 — GROUND SURFACE ELEVATION CONTOUR (masl) (10 m CONTOUR INTERVAL)
- BOREHOLE LOCATION (FROM CHRISTIANSEN, 1999)
- 3D MODEL DOMAIN
- A—A', C—C' — 2D MODEL SECTION
- B—B' — HYDROSTRATIGRAPHIC SECTION

0 1 2 3 4 5 km
SCALE 1 : 125,000

COORDINATES ARE UTM NAD27 ZONE 13.

MAP 7

2D NUMERICAL MODEL CROSS SECTION LOCATIONS AND 3D NUMERICAL MODEL DOMAIN OUTLINE

DEPARTMENT OF EARTH AND ATMOSPHERIC SCIENCES
UNIVERSITY OF ALBERTA

DAN BORN | **2003**

Appendix B

SUTRA and SUTRA2D3D Numerical Formulation

Introduction

SUTRA is a numerical model that simulates density-dependent saturated or unsaturated groundwater flow and transport of either a single reactive solute or thermal energy (Voss, 1984). It has been used extensively to investigate the transport of dense, saline water for a variety of physical systems: seawater intrusion (Voss and Souza, 1987; Yechieli, 2000), brine transport in sedimentary basins (Lahm et al., 1998), flow to/from saline lakes (Rogers and Dreiss, 1995), and flow from irrigation water disposal basins (Simmons and Narayan, 1997, 1998). SUTRA was originally developed as a 2D model (Voss, 1984) and has since been updated (SUTRA2D3D) to include the third dimension (Voss and Provost, 2003). Both versions of the model are based on the same numerical formulation, the primary difference being the addition of a third spatial dimension. Therefore, although the following description focuses on the 2D formulation, it is general enough to represent both models. Major differences in the 2D and 3D formulations will be identified where necessary.

Numerical Formulation

Both the groundwater flow and transport equations in SUTRA are discretized using a combination of finite element (FE) and integrated finite difference (IFD) methods. The governing equation for fluid mass balance is:

$$\left(S_w \rho S_{op} + \varepsilon \rho \frac{\partial S_w}{\partial P}\right)\frac{\partial P}{\partial t} + \left(\varepsilon S_w \frac{\partial \rho}{\partial U}\right)\frac{\partial U}{\partial t} - \nabla\left[\left(\frac{k k_r \rho}{\mu}\right)(\nabla P - \rho g)\right]$$

$$-Q_p - \upsilon_p (P_{BC} - P) = 0 \qquad [1]$$

S_w is the fluid saturation, ρ is the fluid density, S_{op} is the specific pressure storativity, ε is the porosity, P is the pressure, U is the solute concentration, k is the saturated

permeability, k_r is the relative permeability, μ is the dynamic fluid viscosity, g is the acceleration due to gravity, Q_p is a fluid mass source, υ_p is a conductance and P_{BC} is an externally specified pressure. Discretization by elements, nodes and cells (described below) is used to approximate the governing equation. The Galerkin method of weighted residuals is used to minimize the associated global error.

The first and second terms (pressure and solute derivatives) in [1] are discretized cellwise (Figure B1), where each dependent variable is assigned a value at every node, and a linear basis function is used to interpolate over the area (or volume) of the cell.

The third term, containing Darcy's Law, represents the change in fluid mass due to fluid inflows or outflows. The permeability (k) is discretized elementwise, whereas pressure (P) is discretized nodewise (Figure B1). Relative permeability (k_r) and density (ρ, in the permeability term) are evaluated at each Gauss point (Figure B1), whereas viscosity remains constant over the entire mesh. Density in the gravity term is treated differently. To maintain consistency with the pressure term (∇P), the ρg term must be discretized similarly. Failure to do so would "result in spurious vertical velocities, especially in regions of sharp vertical changes in U" (Voss, 1984 p. 125). As Voss points out, a linear change in P across an element results in a *constant* ∇P whereas a linear change in U results in a *linear* change in ρ. Thus, within a single element (in the local ζ coordinate only), the resulting discretized pressure gradient is:

$$\frac{\partial P}{\partial \xi}(\xi,\eta)=\sum_{i=1}^{4} P_i \frac{\partial \Omega_i}{\partial \xi} \qquad [2]$$

where Ω_i is the basis function at node i. Therefore, the consistent discretization that follows for the ρg term is:

$$(\rho g)_\xi(\xi,\eta)=\sum_{i=1}^{4} \rho_i g_i \left|\frac{\partial \Omega_i}{\partial \xi}\right| \qquad [3]$$

For a more complete description, the reader is referred to Voss, 1984 p. 125.

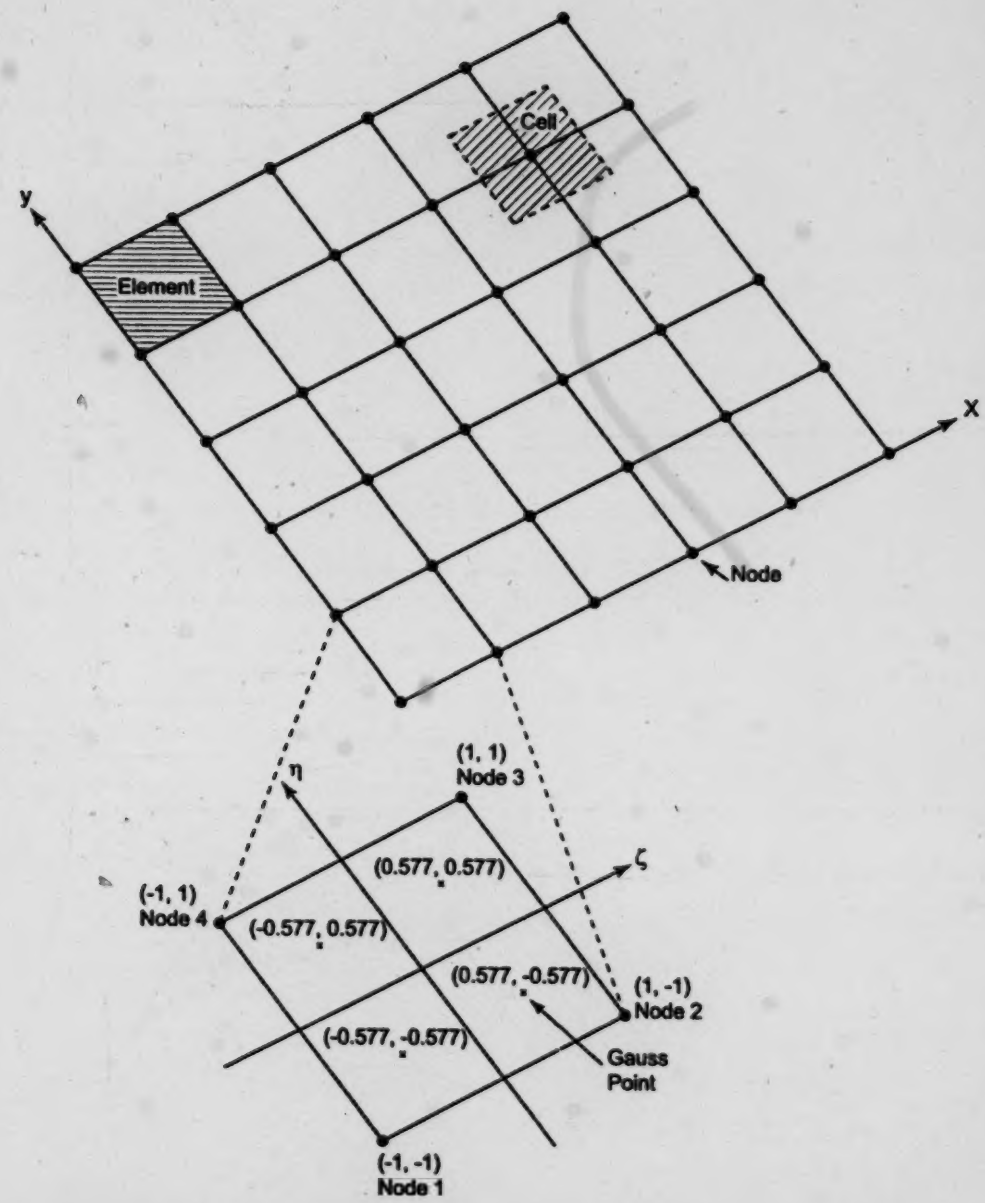

Figure B1. Two-dimensional representation of element-, cell- and nodewise spatial discretization implemented in SUTRA and SUTRA2D3D. x, y represent a global coordinate system whereas ζ, η represent an element's local coordinate system.

The final two terms in [1] (fluid mass source and specified pressure boundary conditions respectively) are discretized cellwise, incorporating a linear basis function.

The governing mass balance equation for transport of a conservative solute with no solute mass production/decay is:

$$[\varepsilon S_w \rho]\frac{\partial U}{\partial t} + \varepsilon S_w \rho \mathbf{v}\nabla U - \nabla\{\rho[\varepsilon S_w (D_m \mathbf{I} + \mathbf{D})]\nabla U\} - Q_p(U^* - U)$$

$$- Q_{PBC}(U_{BC} - U) = 0 \qquad [4]$$

$\mathbf{v}$ is the velocity vector, D_m is the molecular diffusivity of the solute, $\mathbf{I}$ is the identity tensor, $\mathbf{D}$ is the dispersion tensor, U^* is the solute concentration for a fluid source, Q_{PBC} is a source of fluid due to a specified pressure and U_{BC} is the solute concentration for fluid inflow at a point of specified pressure. As with the fluid mass balance equation, the residual for the discretized solute equation is minimized using the Galerkin method.

The individual terms in [4] are discretized in a similar manner as the fluid equation. The derivative of concentration with time and boundary condition terms are discretized cellwise and use a linear basis function (Figure B1). The velocity ($\mathbf{v}$) is determined from the solution to [1] and evaluated at each Gauss point. The dispersion tensor ($\mathbf{D}$) is also evaluated at each Gauss point, where the dispersivities are discretized elementwise, unless the media is anisotropic. In this case the longitudinal dispersivity is evaluated at each Gauss point.

All boundary conditions are applied to nodes and discretized cellwise. Type 1 (Dirichlet) specified pressure boundary conditions are actually incorporated as a flux of fluid. A large conductance (υ_p in [1]) is specified such that the flux of fluid calculated at the node results in a pressure very close to that specified. A Type 2 (Neumann) boundary condition specifies a flux or gradient at a particular node. The default condition at the edge of the model domain is a flux of zero, resulting in no flow across the boundary. Non-zero fluxes directly add or remove fluid mass to/from the model domain.

For solute, a Type 1 boundary condition specifies the solute concentration at a node. Solute mass is added or removed from the domain to replace solute transported away by advection. Type 2 conditions for solute can be implemented to represent dispersion. Solute mass can enter the domain via advection wherever a fluid source or pressure is specified (Type 3; Cauchy). A solute concentration must be assigned for any fluid entering the system. The resulting solute flux is equal to the fluid flux times the specified solute concentration. Where there is no fluid flux across a boundary, a specified solute flux (Type 2) represents solute transport due to diffusion and/or dispersion.

An iterative finite difference approximation is used to discretize the time derivatives in the governing equations. For any given time step, SUTRA begins by solving the fluid matrix equation [1] for pressure. All terms are evaluated at the new time step, except for the time derivative of U and the ρg term in Darcy's Law. These are lagged in time, using information from the previous time step. The resulting pressure solution is then used to solve the solute matrix equation [4] for U at the new time step. The solute concentrations, and resulting fluid densities are then updated, and the pressure solution is resolved. This iterative process is repeated until the maximum change in pressure and concentration at all nodes is less than a user-defined convergence criteria.

Several options are available to solve the matrix equations resulting from the discretization of [1] and [4]. The original SUTRA code (Voss, 1984), which is strictly two-dimensional, uses only banded Gaussian Elimination to solve the matrices directly. In SUTRA2D3D (Voss and Provost, 2003), several iterative methods are also available. The Incomplete Cholesky preconditioned Conjugate Gradient method (CG) is applicable to symmetric matrices (constant density, saturated flow). For asymmetric matrices (i.e., for transport), Incomplete Lower and Upper (ILU) preconditioned Generalized Minimal Residual (GMRES) and ILU ORTHOMIN solvers are available. For the transient problems investigated, GMRES was found to be faster and more robust than ORTHOMIN and was therefore used exclusively. CG was used to solve the flow equation for steady state, constant density problems.

References

Lahm, T. D., Bair, E. S. and VanderKwaak, J., 1998. Role of salinity-derived variable-density flow in the displacement of brine from a shallow, regionally extensive aquifer. Water Resources Research, 34 (6), 1469-1480.

Rogers, D. B. and Dreiss, S. J., 1995. Saline groundwater in Mono Basin, California 1. Distribution. Water Resources Research, 31 (12), 3131-3150.

Simmons, C. T. and Narayan, K. A., 1997. Mixed convection processes below a saline disposal basin. Journal of Hydrology, 194, 263-285.

Simmons, C. T. and Narayan, K. A., 1998. Modelling density-dependent flow and solute transport at the Lake Tutchewop saline disposal complex, Victoria. Journal of Hydrology, 206, 219-236.

Voss, C. I., 1984. SUTRA: a finite-element simulation model for saturated-unsaturated fluid-density-dependent ground-water flow with energy transport or chemically-reactive single-species solute transport. U. S. Geological Survey Water-Resources Investigations Report 84-4369, 409 p.

Voss, C.I. and Provost, A.M., 2003. SUTRA: a model for saturated-unsaturated, variable-density ground-water flow with solute or energy transport. 02-4231, U. S. Geological Survey Water-Resources Investigations.

Voss, C. I. and Souza, W. R., 1987. Variable density flow and solute transport simulation of regional aquifers containing a narrow freshwater-saltwater transition zone. Water Resources Research, 23 (10), 1851-1866.

Yechieli, Y., 2000. Fresh-saline ground water interface in the western Dead Sea area. Ground Water, 38 (4), 615-623.

Appendix C

SUTRA and SUTRA2D3D Model Verification

Introduction

An important part of a standard groundwater modelling protocol is to verify that the numerical model used for the analysis solves the governing equations correctly (Anderson and Woessner, 1992). Typically, numerical results are verified by comparing them to an analytical solution. However, since an analytical solution does not exist for density-dependent groundwater flow and solute transport, numerical results are often compared to the results of laboratory experiments and other numerical models.

Voss and Souza (1987) verified the SUTRA code (Voss, 1984) using Henry's seawater intrusion problem (Henry, 1964) and Elder's free convection problem (Elder, 1967). Kolditz et al. (1998) confirmed the results of Voss and Souza (1987) using FEFLOW, but also demonstrated that the solution to Elder's problem is sensitive to discretization.

Additional verification of SUTRA is necessary because the original code is modified slightly to (1) reformat model output and (2) enable time varying specified concentration boundary conditions. In addition, the code is recompiled for use on an UNIX platform. The SUTRA2D3D code used for transient modelling (Voss and Provost, 2003) is a pre-release version based on the original 2D code by Voss (1984). The governing equations and numerical discretization remain the same in the 3D model. However, significant changes to the code were necessary to incorporate the third dimension, including the addition of new matrix solvers. For this reason, it is necessary to verify the 3D model independently of the 2D model.

Elder's problem closely matches conditions at the Patience Lake mine site, and therefore it is considered the most appropriate test case for SUTRA and SUTRA2D3D verification. The problem considers an initially hydrostatic system where a more dense fluid is introduced over top of a less dense fluid. This hydrodynamically unstable system results in the downward convection of dense solute. Elder's original work considered

only a 2D system. However, Diersch and Kolditz (1998) developed a 3D extension to the original 2D problem and their results are used to help verify the SUTRA2D3D code.

SUTRA: Two Dimensional Model Verification

The solute analogue to the Elder (1967) thermal convection problem consists of a 600 m by 150 m rectangular cross section (Figure C1). The mesh is discretized into 100 elements horizontally and 50 elements vertically, similar to the discretization used by Kolditz et al. (1998). A 300 m, 1kg/kg solute source is centred along the top of the domain and the fluid density varies linearly as a function of solute concentration from 1000 kg/m^3 to 1200 kg/m^3. The base of the model has a specified concentration of zero and the remainder of the model boundary is considered no-flow with respect to the solute. The entire boundary of the domain is specified as no-flow with respect to the fluid, except at the top corners of the domain where the pressure is specified as 0 Pa. Initially, the pressure distribution is hydrostatic and the solute concentration is zero.

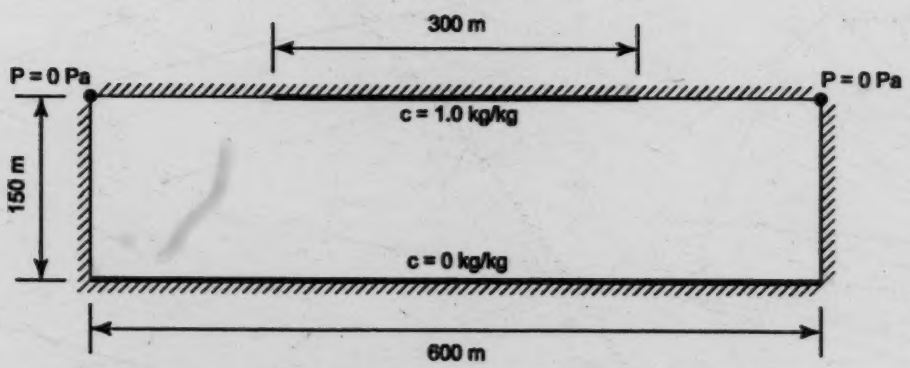

Figure C1. Model domain and boundary conditions for the 2D Elder problem.

A total of 20 years is simulated, where time steps are ramped linearly from 2 days to 1 month over a period of a year and then maintained constant for the remainder of the simulation. Model parameters match that of Voss and Souza (1987) (Table C1).

Table C1. Model parameters used in the 2D and 3D Elder problem model verification.

Parameter (units)	Value
Porosity (-)	0.1
Permeability (m^2)	4.845×10^{-13}
Dynamic Viscosity (kg/ms)	0.001
Diffusion Coefficient (m^2/s)	3.565×10^{-6}
Longitudinal Dispersivity (m)	0
Transverse Dispersivity (m)	0
Gravity (m/s^2)	9.81

The results of the 2D model verification are compared with the FEFLOW model results of Kolditz et al. (1998) who used a similar mesh discretization and the same model parameters (Figure C2). The SUTRA and FEFLOW codes produce very similar solute distributions both spatially and temporally. Initially, two convection cells (fingers) develop at the ends of the solute source. Upward flow adjacent to these fingers produces two additional cells, resulting in upward flow at the center of the source (Figure C2(c)). After 10 years, the convection cells converge into two dominant cells. These cells persist to the end of the simulation.

SUTRA2D3D: Three Dimensional Model Verification

The test case used to verify SUTRA2D3D (Voss and Provost, 2003) is based on the 3D Elder's analogue proposed by Diersch and Kolditz (1998). The symmetry of the original problem (Figure C2) is exploited to reduce the computational effort required and allow finer spatial discretization. The 3D domain consists of a 300 m x 300 m x 150 m block, which is nominally discretized into elements 10 m and 3 m in the horizontal and vertical directions respectively (Figure C3). In the top 9 m of the domain, the vertical discretization is refined to 1.5 m. Horizontal discretization is refined to 1.25 m at the edge of the solute source, producing elements with a maximum horizontal aspect ratio of 8. The resulting mesh has a total of 129,654 nodes and 122,112 elements. A 150 m x 150 m, 1 kg/kg solute source is applied areally to the top of the domain (Figure C3). Concentration at the base of the domain is specified as zero; elsewhere, the boundary of

the domain is considered no-flow with respect to the solute. Pressure is specified on the top perimeter along the two sides of the domain opposite the solute source and no-flow with respect to the fluid along the remainder of the model boundary. All other remaining model parameters are exactly the same as for the 2D Elder's problem (Table C1). Time steps are increased linearly from 0.25 days to 10 days over a period of 1 year and then maintained constant.

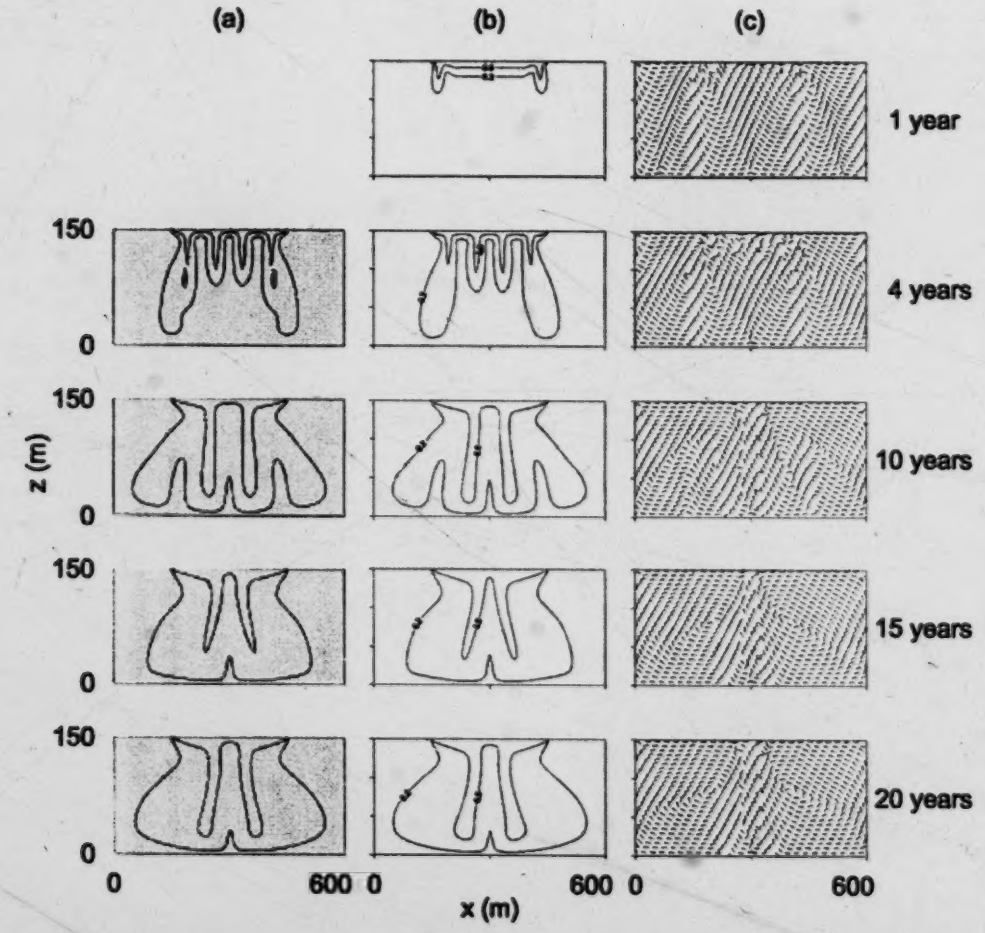

Figure C1. Results for the 2D Elder problem at 1, 4, 10, 15 and 20 years. (a) 0.2 and 0.6 relative concentration contours using FEFLOW (Kolditz et al., 1998); (b) 0.2 and 0.6 relative concentration contours using SUTRA; (c) SUTRA velocity vectors showing the direction of convecting fluid.

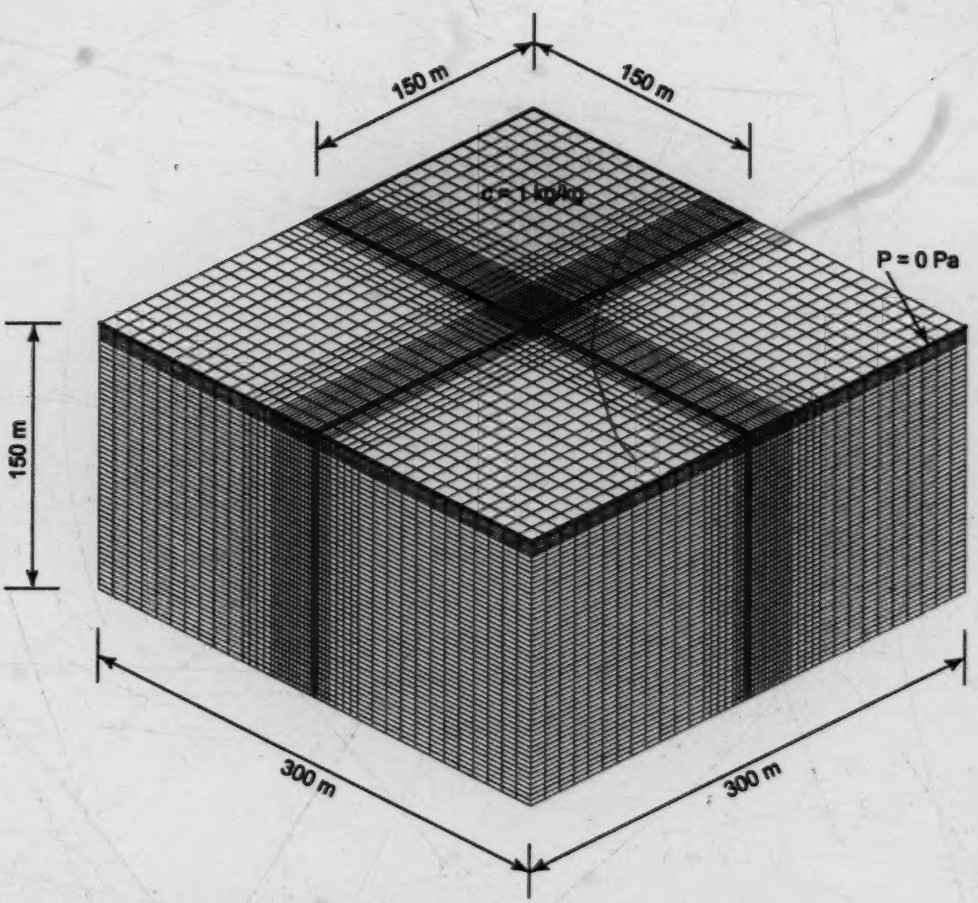

Figure C3. Model domain and boundary conditions for the 3D Elder problem.

Initially, the results of the 3D Elder's simulation are similar to the 2D verification. Convective fingers develop at the edge of the solute source and migrate uniformly into the subsurface (Figure C4(a-d)). After 5 years, the fingers migrate to the base of the model domain at the edges and corner of the solute source (Figure C4(e)), indicating stronger convection at these locations. In the 2D case, after 4 years, secondary finger development (Figure C2) causes upward flow at the center of the source. However, in the 3D case, upward flow is not observed. Secondary fingers propagate downward at the corner of the 3D source (Figure C4(e)), which would correspond to the centre of the 2D source. Kolditz et al. (1998) demonstrated, in the 2D Elder problem, changes in

mesh discretization can result in upward or downward flow at the center of the solute source.

The secondary finger propagates horizontally into the model domain at 45° and produces downward flow at the corner of the source zone (Figures C4(f) and C5(c)). As the simulation continues, the fingers originating from the inside edge of the solute source migrate beyond the base of the domain, resulting in a single cell where convection continues along the diagonal of the source zone (Figures C4(g-k) and C5(c-e)). After 20 years, the convection pattern stabilizes, resulting in downward convection at the outside corner of the model domain (Figures C4(k-l) and C5(f)).

The SUTRA2D3D simulations are verified by comparison to the FEFLOW results of Diersch and Kolditz (1998) in Figure C6. The model domain in Figures C3, C4 and C5 correspond to the cut-away view illustrated in Figure C6. The SUTRA2D3D and FEFLOW simulations agree, producing the same convection patterns both spatially and temporally. Small differences arise after approximately 15 years. The downward convection at the corner of the solute source propagates nearly vertical in the SUTRA2D3D verification (Figure C4(k)). Using FEFLOW, convection is deflected slightly from the vertical (Figure C6(e)). These small differences could arise from differences in mesh discretization, as demonstrated by Kolditz et al. (1998).

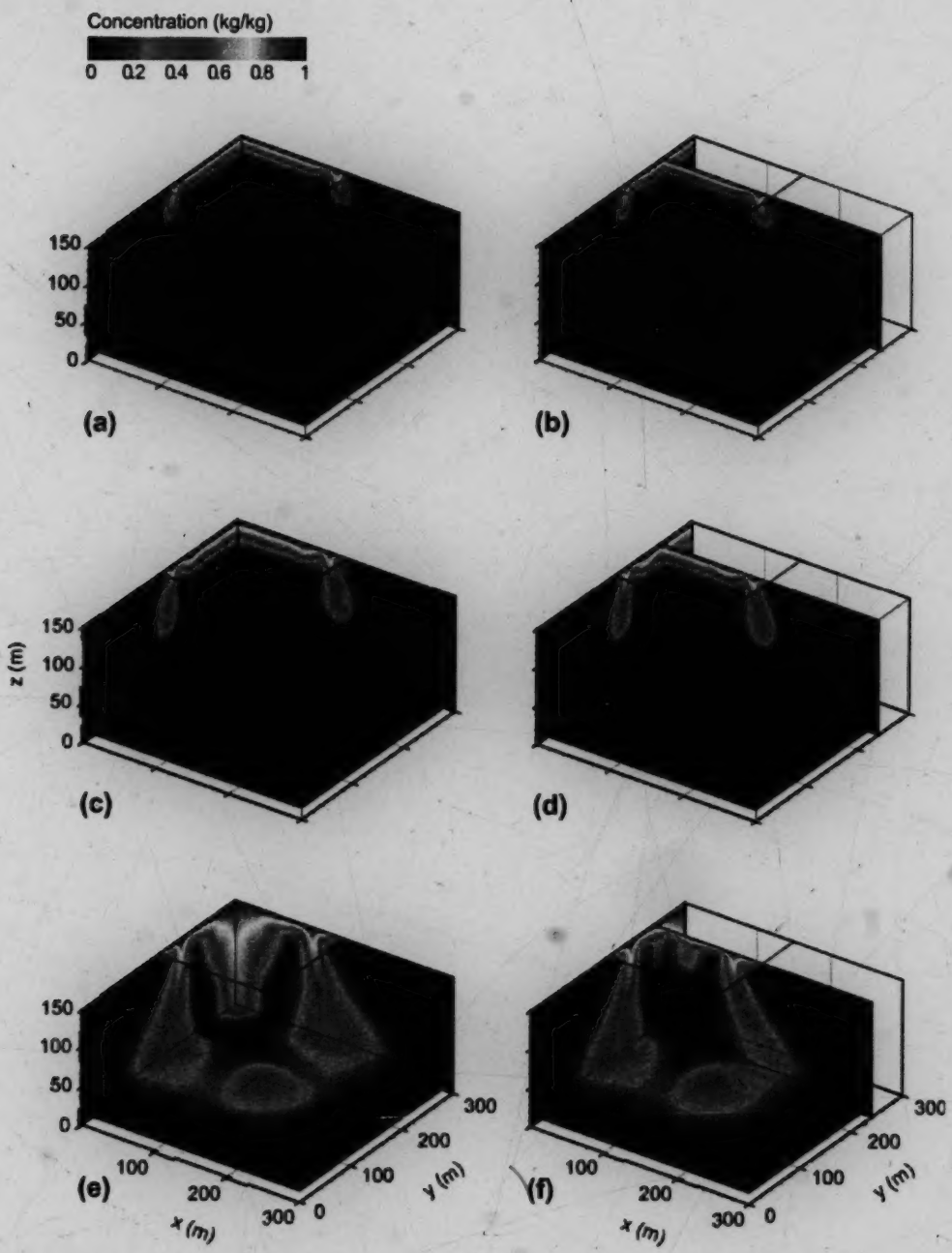

Figure C4. Results for the 3D Elder problem showing cut-away views at (0, 300, 15) on the left and (0, 240, 15) on the right. (a), (b) 1 yr; (c), (d) 2 yr; (e), (f) 5 yr.

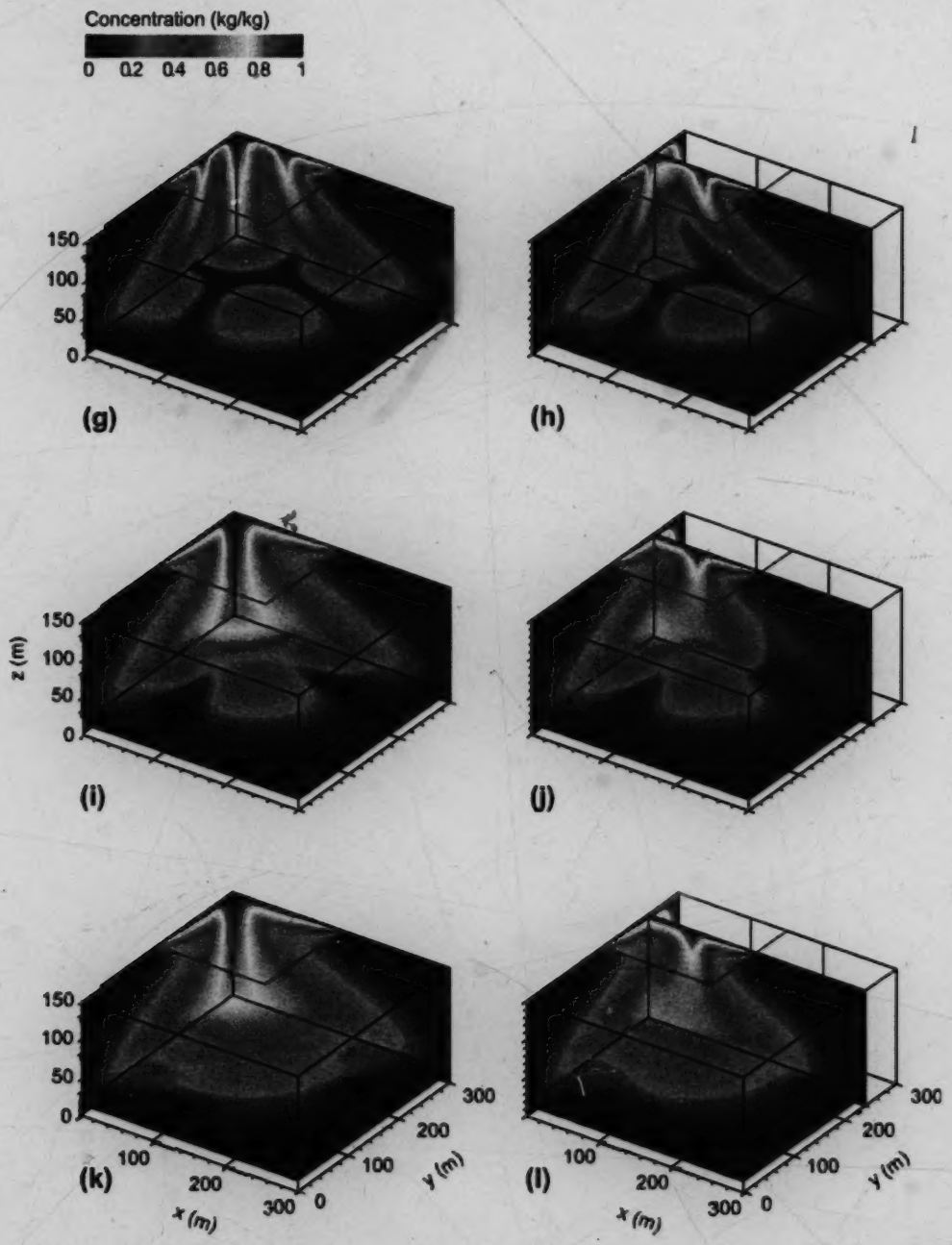

Figure C4. Results for the 3D Elder problem showing cut-away views at (0, 300, 15) on the left and (0, 240, 15) on the right. (g), (h) 10 yr; (i), (j) 15 yr; (k), (l) 20 yr.

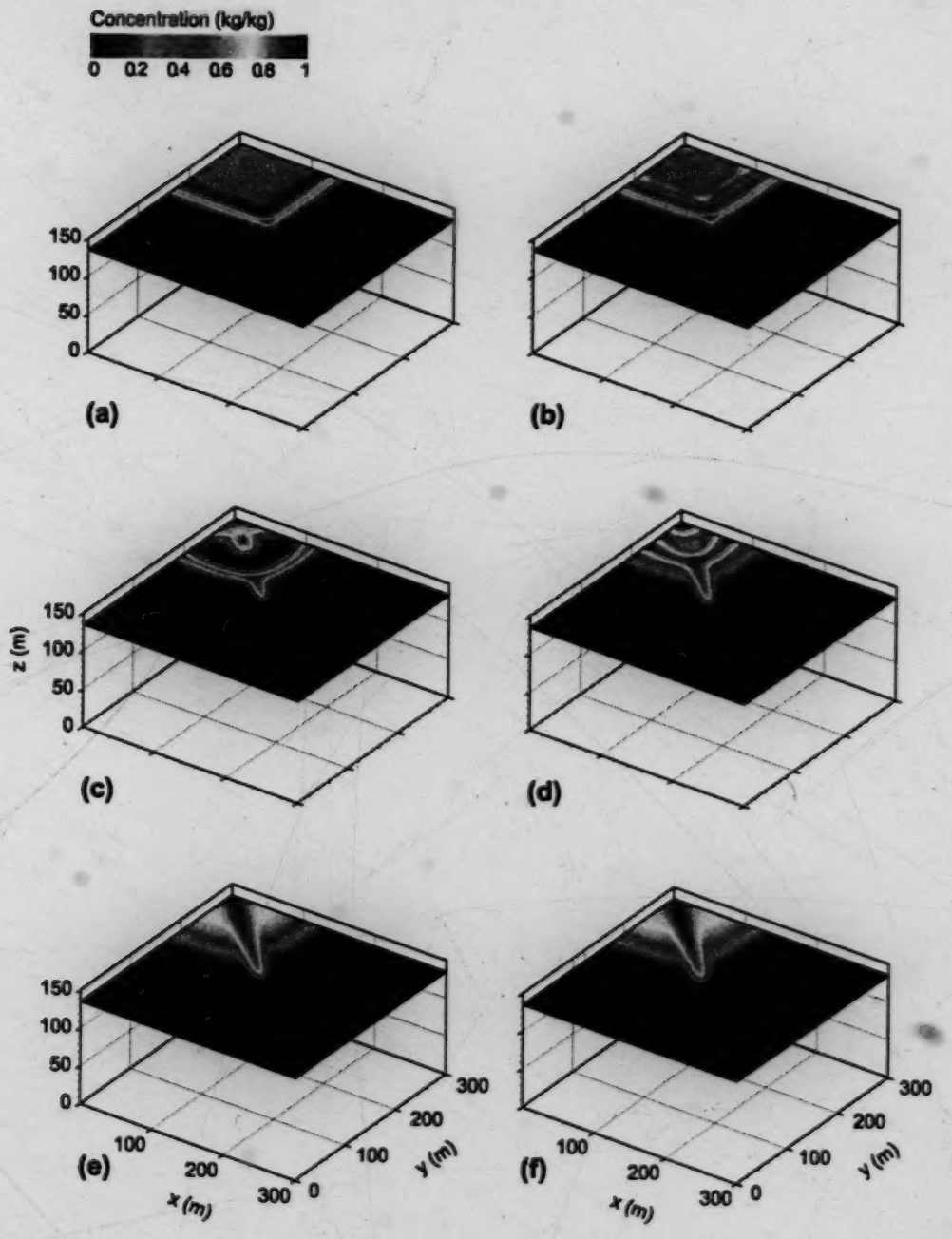

Figure C5. Results of the 3D Elder problem showing the concentration distribution for a 2D slice at z = 135 m. (a) 1 yr; (b) 2 yr; (c) 5 yr; (d) 10 yr; (e) 15 yr; (f) 20 yr.

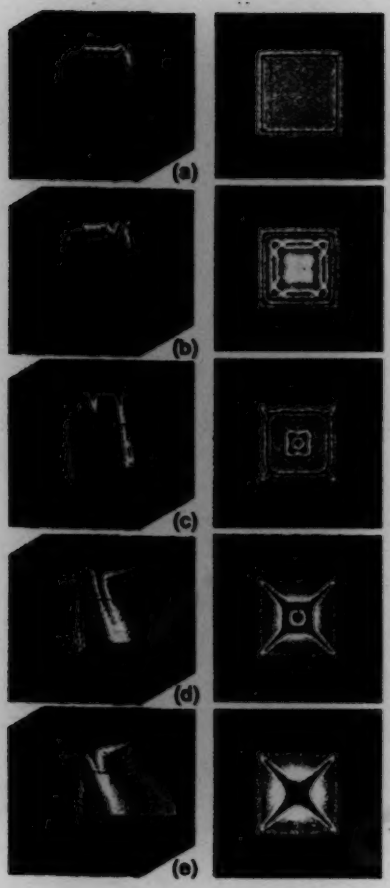

Figure C6. Solute distributions for the 3D Elder problem by Diersch and Kolditz (1998) at (a) 1 yr; (b) 2 yr; (c) 4 yr; (d) 10 yr; (e) 20 yr. Left is a cut-away view similar to Figure C4, right is a 2D slice at z = 135 m, similar to Figure C5.

References

Anderson, M.P. and Woessner, W.W., 1992. Applied groundwater modeling: simulation of flow and advective transport. Academic Press, San Diego, 381 pp.

Elder, J.W., 1967. Transient convection in porous medium. Journal of Fluid Mechanics, 24 (4), 823-843.

Diersch, H.G. and Kolditz, O., 1998. Coupled groundwater flow and transport: 2. Thermohaline and 3D convection systems. Advances in Water Resources, 21, 401-425.

Henry, H.R. 1964. Effects of dispersion on salt encroachment in coastal aquifers, U. S. Geological Survey Water Supply Paper, 1613 C, C71-C84.

Kolditz, O., Ratke, R., Diersch, H.G. and Zielke, W., 1998. Coupled groundwater flow and transport: 1. Verification of variable density flow and transport models. Advances in Water Resources, 21, 27-46.

Voss, C.,I., 1984. SUTRA: a finite-element simulation model for saturated-unsaturated fluid-density-dependent ground-water flow with energy transport or chemically-reactive single-species solute transport. U. S. Geological Survey Water-Resources Investigations Report 84-4369, 409 p.

Voss, C.I. and Provost, A.M., 2003. SUTRA: a model for saturated-unsaturated, variable-density ground-water flow with solute or energy transport. 02-4231, U. S. Geological Survey Water-Resources Investigations.

Voss, C.I. and Souza, W. R., 1987. Variable density flow and solute transport simulation of regional aquifers containing a narrow freshwater-saltwater transition zone. Water Resources Research, 23 (10), 1851-1866.